UNIVERSITÉ DE MONTRÉAL

SYNCHROPHASOR DATA ANALYTICS FOR CONTROL AND PROTECTION APPLICATIONS IN SMART GRIDS

SEYED YOUNES SEYEDI
DÉPARTEMENT DE GÉNIE ÉLECTRIQUE
ÉCOLE POLYTECHNIQUE DE MONTRÉAL

THÈSE PRÉSENTÉE EN VUE DE L'OBTENTION
DU DIPLÔME DE PHILOSOPIAE DOCTOR
(GÉNIE ÉLECTRIQUE)
JUIN 2017

UNIVERSITÉ DE MONTRÉAL

ÉCOLE POLYTECHNIQUE DE MONTRÉAL

Cette thèse intitulée :

SYNCHROPHASOR DATA ANALYTICS FOR CONTROL AND PROTECTION APPLICATIONS IN SMART GRIDS

présentée par : SEYEDI Seyed Younes
en vue de l'obtention du diplôme de : Philosophiae Doctor
a été dûment acceptée par le jury d'examen constitué de :

M. MAHSEREDJIAN Jean, Ph. D., président
M. KARIMI Houshang, Ph. D., membre et directeur de recherche
M. SHESHYEKANI Keyhan, Ph. D., membre
M. KAMWA Innocent, Ph. D., membre externe

DEDICATION

To my family

ACKNOWLEDGEMENTS

I would like to give my thanks to my professors: Dr. Houshang Karimi, and Dr. Jean Mahseredjian for their supervision, trust, and constant support of this PhD project. I would also like to express my gratitudes to all those at Polytechnique Montreal, and the jury members who have made this thesis possible: Dr. Innocent Kamwa and Dr. Keyhan Sheshyekani. Finally, with special thanks to Dr. Josep M. Guerrero and Dr. Santiago Grijalva who participated in this research, as the project would not have been thriving without their expertise.

Seyed Younes Seyedi, June, 2017.

RÉSUMÉ

Des réseaux intelligents sont des réseaux d'énergie fortement distribués où les technologies d'énergie et des services sont intégrés avec des informations, des communications et contrôlent des technologies. Puisque les sources d'énergie renouvelable deviennent plus efficaces et rentables, les réseaux intelligents peuvent livrer la puissance propre, durable, sécuritaire, et fiable aux consommateurs. Cependant, l'utilisation rapide de sources d'énergie renouvelable provoque des défis techniques en termes de surveillance, le contrôle et la protection des réseaux électriques. En fait, l'énergie renouvelable implique les phénomènes qui sont naturellement stochastiques comme la lumière du soleil et le vent. Donc, les réseaux intelligents devraient être capables de surveiller et répondre aux changements tant dans fournisseur d'énergie que dans la demande. L'évolution des réseaux électriques provoque aussi le déploiement de nombreuses unités de mesure sans précédent et d'intelligents appareils de mesure. En vertu des systèmes de communications, les signaux en temps réel et les données peuvent être échangés entre les composants des réseaux intelligents. Le flux de données en temps réel fournit une occasion unique pour des applications axées sur les données et des outils pour démultiplier la modernisation de réseaux et la résilience.

Les unités de mesure de phaseur sont les dispositifs spécialisés qui acquièrent le phaseur synchronisé (synchrophasor) des données des réseaux électriques. L'analytique de données Synchrophasor peut potentiellement étre plus performant que des méthodes traditionnelles en termes de prise de décisions. Spécifiquement, l'analytique de données est des approches qualitatives/quantitatives et les algorithmes qui rassemblent et traitent des données pour en fin de compte améliorer la conscience situationnelle dans des réseaux électriques. Motivé par ce fait, cette thèse présente des solutions viables pour l'analytique de données synchrophasor dans le but d'améliorer la surveillance, le contrôle et la protection de réseaux de distribution.

La thèse se concentre sur trois fonctionnalités qui sont portées de basé sur l'analytique de données synchrophasor: Détection de perturbation centralisée, surveillance de production décentralisée (PD) et la protection "backup" coordonnée. L'objectif de surveillance de perturbation est de réaliser la détection rapide et fiable de tension/des déviations de fréquence qui affectent la stabilité de réseau. La surveillance de PD est liée à la détection de la présence/absence de ressources énergétiques pour la gestion du flux de puissance. La perturbation et des outils de surveillance de PD fraient la voie pour la protection adaptative

de secours de réseaux de distribution actifs. Le plan de protection adaptatif de secours assure la stabilité de post-défaut en détectant des défauts de ligne dans un temps de tolérance permis. La coordination entre le contrôle et des systèmes de protection de secours mène à la récupération rapide de tension/la fréquence et minimise la panne de courant. L'efficacité et la fiabilité des méthodes développées et des algorithmes sont validées par des simulations informatiques vastes basées sur des différents benchmarks.

ABSTRACT

Smart grids are highly distributed energy networks where energy technologies and services are integrated with information, communications and control technologies. As renewable energy sources are becoming more efficient and cost–effective, the smart grids can deliver safe, clean, sustainable and reliable power to consumers. However, the rapid utilization of renewable energy sources brings about technical challenges in terms of monitoring, control, and protection of power systems. In fact, renewable energy involves phenomena which are naturally stochastic such as sunlight and wind. Therefore, the smart grids should be capable of monitoring and responding to changes in both power supply and demand. The evolution of the power systems also gives rise to deployment of unprecedented number of measurement units and smart meters. By virtue of communications systems, real-time signals and data can be exchanged between components of the smart grids. The flow of real-time data provides a unique opportunity for data-driven applications and tools to leverage grid modernization and resiliency.

Phasor measurement units are specialized devices that acquire synchronized phasor (synchrophasor) data from the power systems. Synchrophasor data analytics can potentially outperform traditional methods in terms of decision making. Specifically, data analytics are qualitative/quantitative approaches and algorithms that collect and process data to ultimately improve situational awareness in the power systems. Motivated by this fact, this thesis presents viable solutions for synchrophasor data analytics with the aim of improving monitoring, control and protection of power distribution grids.

The thesis focuses on three functionalities that are carried out based on synchrophasor data analytics: Centralized disturbance detection, monitoring of distributed generation (DG) systems, and coordinated backup protection. The objective of disturbance monitoring is to achieve fast and reliable detection of voltage/frequency deviations that affect the network stability. The DG monitoring is concerned with detecting presence/absence of energy resources for management of the flow of power. Disturbance and DG monitoring tools pave the way for adaptive backup protection of active distribution networks. The adaptive backup protection scheme ensures the post-fault stability by detecting line faults within a permissible tolerance time. The coordination between control and backup protection systems leads to fast recovery of voltage/frequency and minimizes power outage. The efficacy and reliability of the developed methods and algorithms are validated by extensive computer simulations based on different benchmarks.

TABLE OF CONTENTS

LIST OF TABLES

LIST OF FIGURES

LIST OF SYMBOLS AND ABBREVIATIONS

AC	Alternating Current
ADN	Active Distribution Network
CDF	Cumulative Distribution Function
DC	Direct Current
DG	Distributed Generation
DS	Distributed Storage
EMTP	ElectroMagnetic Transients Program
EPLL	Enhanced Phase Locked Loop
FACTS	Flexible AC Transmission System
FPS	Frames per Second
GOOSE	Generic Object Oriented Substation Event
GPS	Global Positioning System
IED	Intelligent Electronic Device
IEEE	Institute of Electrical and Electronics Engineers
LOF	Local Outlier Factor
LOP	Local Outlier Probability
MGCC	Microgrid Central Controller
NaN	Not a Number
PCC	Point of Common Coupling
PDC	Phasor Data Concentrator
PDF	Probability Density Function
PLL	Phase Locked Loop
PMU	Phasor Measurement Unit
PV	Photovoltaic
PLOF	Probabilistic Local Outlier Factor
RES	Renewable Energy Source
ROCOF	Rate of Change of Frequency
SC	Secondary Controller
SCADA	Supervisory Control And Data Acquisition
TCP	Transmission Control Protocol
UDP	User Datagram Protocol
UTSP	Unified Three-phase Signal Processor
VSC	Voltage Source Converter

CHAPTER 1 INTRODUCTION

1.1 The Vision for Future Power Grids

In future power grids, a vast number of distributed generation (DG) systems will be deployed in power grids where renewable energy sources (RESs) such as wind and solar will play an indispensable role. As illustrated in Fig. 1.1, *smart grid* is a vision for future power grids that encompass a broad range of information, communications, control, and energy technologies. In such power grids, DG, distributed storage (DS) units, and consumers are interconnected with the power plants and transmission systems through microgrids and active distribution networks (ADNs). Microgrids and ADNs are advanced power systems which are composed of DG/DS systems, lines, loads, transformers, metering and intelligent electronic devices (IEDs). These autonomous systems enhance the grid resiliency and mitigate the power outage since they can supply energy in the absence of the utility grid.

Electric vehicles and smart homes are among the other conspicuous features of modern power grids. In fact, smart grids will provide the infrastructure necessary for enabling the efficient use of electric vehicles. Electric vehicles will interact with the utility grids by serving as mobile DS units, a concept which is called "vehicle-to-grid" in the smart grid terminology. Smart meters and home energy management systems allow for automated and bidirectional exchange of information between smart homes and the utility grids. A smart home equipped with an energy management system facilitates tracking of energy consumption and thus reduces electricity bills.

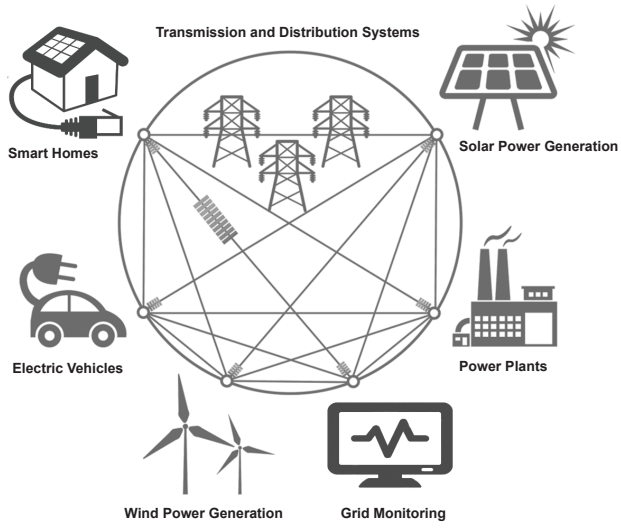

Figure 1.1 Different technologies involved in smart and modern power grids

1.2 The Era of Big Data in Smart Grids

In light of advanced control and communication technologies, smart grids are able to provide consumers with safe, clean, sustainable and reliable energy. However, smart grids, as large-scale and heterogeneous energy networks, will face challenging issues regarding management, control, reliability, and power quality. Moreover, time-varying RESs, advanced controllers, and communication systems give rise to increasing complexity of modern power grids where the role of information and data analytics is indispensable. It is expected that, with the evolution of power systems, planning and operation of grids rely on different types of real-time and offline data.

As power grids incorporate more RESs, an unprecedented number of sensors, controllers, and actuators will inevitably emerge in the grid. A sensor can be envisaged as a device/system which provides specific types of data/information depending on the desired functionality. In the context of smart grid, most of the sensors belong to the following categories:

- Phasor measurement units (PMUs)
- Phasor data concentrators (PDCs)
- IEDs and protective relays
- Frequency disturbance recorders (FDRs)
- Supervisory control and data acquisition (SCADA) systems
- Smart meters
- Geographic information systems
- Weather forecast data
- Electricity market information

An actuator which is responsible for applying a control action, can be thought of as a switch, protective device, DG system, DS unit, etc. Moreover, the sensors, the controllers and the actuators can be spatially separated and thus communication systems are required for transfer of the measurements, signals, and control data.

Among the aforementioned categories, PMUs and PDCs are generally regarded as high-rate sources of data in power grids. These devices can provide samples of voltage/current phasors,

instantaneous frequency, real/reactive power, and other pertinent data in real-time. It turns out that deployment of such devices leads to a large variety of data at a high granularity and volume: a fact which ultimately brings about the concept of *Big Data* in power grids. Big data in power grids can be characterized by three remarkable features:

- Large volume: extended time horizon for processing and archiving data, mainly due to extensive deployment of high-rate sensors such as PMUs, PDCs, and smart meters
- High velocity: faster temporal variations, mainly due to time-varying RESs and high penetration of DG systems
- Increasing variety: Different types of data stem from many sensors/sources that did not exist in conventional power grids

In the era of big data, data-driven applications and tools play a crucial role for a modernized, reliable, and secure operation of power grids. Data-driven approaches improve decision making and can potentially outperform traditional model-based tools. Motivated by this fact, the focus of this thesis is on data analytics and data-driven approaches with the aim of improving situational awareness in modern power grids.

1.3 Statement of the Problem

In 2011, the president of North American Electric Reliability Corporation (NERC) wrote to the members [4]:

"Almost all of the major network failures, excluding those emanating from severe weather conditions, have malfunctioning of relays or automatic control systems as a factor that contributes to the aggravation of the failure. Relays may operate when not needed, or fail to operate when needed for several reasons. Generally speaking, relays may fail to operate correctly due to incorrect settings, bad coordination with other devices, ineffective commissioning and maintenance, failure of communications channels, or power supplies."

Basically, data-driven applications rely on exchange of information/data between different devices and power system components. Therefore, it is important to account for possible impairments that may be imposed on data during data acquisition and transmission. Noise, delay, and unpredictable loss of data are deemed to be the harmful impairments that deteriorate the performance of the data-driven applications. Such impairments in data may stem from the following phenomena:

- Imperfect or defective communication devices

- Congestion and severe background traffic in shared communication links
- Sensor failures
- Measurement noise
- Interference caused by lightning, harmonics and subharmonics

Such data impairments increase uncertainty in information and have deleterious effects on the reliability and robustness of the aforementioned applications. Therefore, use of a reliable and accurate data processing framework is deemed to be indispensable for these real-time applications. In this regard, lack of an elaborate data processing framework tailored to smart distribution grids is noticeable. The challenge is that real-time algorithms and mechanisms are required that collect, analyze, and transform real-time data with the primary goal of reliable decision making. The methods and algorithms not only should cope with noisy, delayed and intermittent arrival of information but also they should improve performance of data-driven control and protection applications.

1.4 Thesis Objectives

With the availability of low-cost and accurate measurement devices along with fast and efficient processors, it is anticipated that new control and protection applications will be developed for future power grids. There is no doubt that the performance of these applications depends on how the data are obtained and processed in real-time. Here an important question arises: Can a data processing framework improve control and protection of modern distribution grids while being able to coexist with conventional systems?

The main objective of this thesis is to develop algorithms and mechanisms for synchrophasor data acquisition/processing tailored to monitoring, control and protection applications in smart microgrids and ADNs. The data acquisition and processing tasks are analyzed under noisy and intermittent data conditions when developing disturbance monitoring structure. The other objective of this thesis is the analysis of fault/event detection in the presence of synchrophasor data delays. The data acquisition task deals with methods and protocols for extraction of information and transmission to a centralized control unit. If carefully designed, it can also diminish the deleterious impacts of data impairments. The data processing task, however, corresponds with algorithms for detection, monitoring, and decision making. Moreover, qualified performance metrics are required in order to evaluate reliability and efficiency of the proposed methods and mechanisms for control and protection purposes.

The primary outcome of this study is a reliable and effective data processing framework to assist control and protection applications in smart microgrids and ADNs. Among the other objectives of this thesis are data-driven methods that yield:

- More resilient ADNs
- Enhanced automation and planning of power systems
- Ease of network reconfiguration and resource management
- Improved situational awareness
- More reliable smart grid infrastructure

Ultimately, the resulting data-driven methods leverage reliable and secure operation of power grids that widely utilize DG technology and RESs. The end users of the proposed data processing framework can be high-level controllers, protection systems, monitoring systems, and even operators of the utility grid.

1.5 Methodology

A reliable data processing framework paves the way for a broad range of applications from resource management and economic operation to situational awareness in modern power systems. At the system level, our proposed data processing framework relies on:

1. Distributed sources of data
2. Hierarchical control and protection structure
3. Time-critical event detection

Distributed data acquisition is accomplished by using communication systems and measurement devices in the smart grid infrastructure. The measurement diversity is achieved by collecting necessary information from several nodes. The measurement diversity improves the robustness of monitoring applications against unpredictable loss of data by taking advantage of spatial and temporal correlations inherent in large datasets. Information transmission reduces reconfiguration cost and maintenance time, hence, the investment in new metering devices and communication systems can be justified. The hierarchical structure is a promising paradigm for systematic control and protection of different components in large-scale power systems. The hierarchical structure also facilitates scalability of the data processing by designating computational tasks to different processors and devices. In this setting, the low-level applications aid the applications in upper layers in terms of data management and

processing. Finally, unforeseen events in power systems (e.g., disturbances, faults, etc.) must be detected and accommodated for in a timely manner due to the fact that control and protective actions are essentially time-critical.

Fig. 1.2 illustrates the adopted methodology in this study. As shown in this figure, the developed data processing framework consists of three functionalities: Data acquisition, data analytics, and data-driven applications. These constituent functionalities will be discussed later in the next subsections.

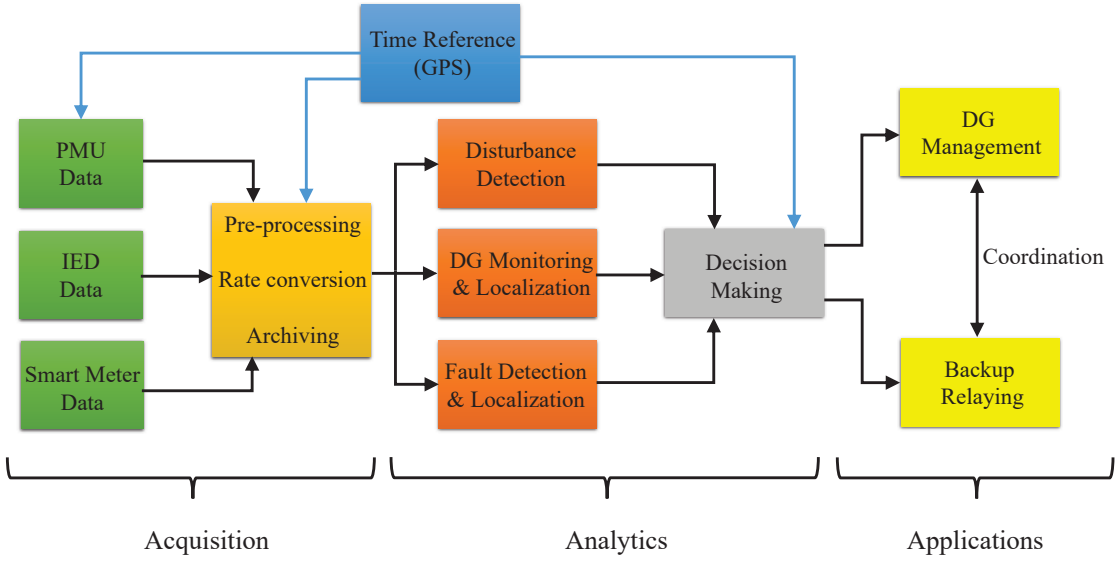

Figure 1.2 The functional block diagram of the proposed data processing framework

Extensive time-domain and statistical computer simulations are required to investigate the applicability of the aforementioned data analytics. The computer simulations mostly involve system-level simulations where very detailed implementation of power system components are not necessarily helpful. In this study, Electro-Magnetic Transients Program (EMTP-RV) [5] and Simulink [6] are used for simulating the electrical part of the grid and the PMUs. The extracted signals and PMU data are then fed to MATLAB modules for analysis of datasets. The MATLAB modules may also simulate some data impairments, e.g., data noise and random data losses. The superiority of the developed data processing framework can be demonstrated by numerical assessment of the performance metrics.

1.5.1 Data Acquisition

Data, signals, and behavioral messages are extracted from different nodes in the microgrid/ADN. In this research, the primary sources of data include PMUs, IEDs, and smart

meters. The PMU data (also referred to as synchrophasor data) are usually streamed to a PDC (within a central unit) with a fixed reporting rate. The IED data and other protective messages are exchanged if either an event is locally detected or a request message from an upper layer unit is received. The smart meter data which carry useful information about real-time power consumption are also collected in fixed periods.

At the central unit, the PMU data streams are collected and pre-processed. The PMU data streams should be archived since decision making algorithms may require access to past data. Moreover, the received data can be decimated in order to meet the sampling requirement of specific control and protection applications.

1.5.2 Data Analytics

In the context of this thesis, data analytics refers to qualitative/quantitative techniques and algorithms that improve performance of hierarchical control and protection applications. Centralized disturbance detection, monitoring of DG connection/disconnection events, and fault identification are the main functionalities that can be carried out based on data analytics. Microgrids and ADNs are subject to network-wide disturbances such as voltage/frequency deviations when they become isolated from the utility grid. Local and droop-based controllers may fail in suppressing such disturbances. The data processing algorithms should reliably detect such deviations and trigger a restoration process if necessary. In order to evaluate detection of subtle deviations, it is crucial to assess the performance of disturbance monitoring under noisy and intermittent data conditions.

The presence and absence of DG systems in distribution networks can change over the time. In practice, a DG system may become disconnected from the rest of the network due to, for example, a temporary fault, and then reconnect with the network. The data processing algorithms should identify how many DG systems are actually operational and determine the location of DG connection/disconnection events within the network. Moreover, the presence and absence of DG systems and loads can affect the interval during which a line fault can be tolerated without compromising the post-fault stability of voltage/frequency. Hence, data analysis method should be devised to ensure that all faults are reliably detected and isolated in a permissible time.

1.5.3 Control and Protection Applications

The previously mentioned data analytics can substantially improve performance of control and protection applications in smart microgrids and ADNs. They not only facilitate opti-

mal/economic operation but also enhance the performance of secondary/tertiary control, and increase reliability of grid protection.

Once a network-wide disturbance is detected, a decision making algorithm verifies the sources of disturbances. If an islanding event is confirmed as the source of the disturbance, then the secondary control application can trigger the voltage/frequency control mode. Islanding events can be confirmed by using remote methods which are based on communications between microgrid and the utility grid. Remote methods monitor the status of circuit breakers immediately. Remote methods present small or even zero non-detection zone and have no impact on the power quality. Remote methods are very effective in multiple-inverter systems, but they need large investment and may not be economic in small systems. If a steady-state disturbance is observed while the network operates under the islanded mode, then the secondary control application updates the reference values of voltage/frequency based on the droop-based control concept.

Once a DG disconnection/connection event is detected, a DG management mechanism determines new setpoints of operational DG systems and updates the values of fault tolerance time. A backup protection mechanism constantly supervises local protection systems. It clears line faults if local protective devices fail in detecting faults within the permissible time. Moreover, as depicted in Fig. 1.2, the DG management mechanism must be synchronized with the backup protection mechanism. The fault clearance entails abrupt changes in the network topology that directly affect both local and secondary control applications. Therefore, coordination between DG management and protection mechanisms is important.

1.6 Thesis Contributions

The smart grid reliability and resiliency can be improved by utilizing data-driven control and protection application. Moreover, such applications depend on a framework to obtain and process different types of data about real-time behavior of the power system. This is a big challenge since the data processing framework interacts with different integrated technologies including communications, control, generation, and storage systems. To overcome this challenge, the focus of this thesis is on developing a novel data processing framework that improves decision making for intelligent control and protection applications. The preeminent contributions of this thesis are effective data analytics including:

1) Detection of network-wide voltage/frequency disturbances [1]. Unlike conventional monitoring systems, our proposed approach relies on several PMUs in order to detect subtle

disturbances as fast and reliable as possible. In particular, detection time and probability of false alarm are analyzed under noisy and intermittent synchrophasor data conditions. This contribution increases accuracy of voltage/frequency monitoring and is useful for bumpless transfer to islanded mode. It is also important for centralized control when the network is in the islanded operation mode.

2) Detection of presence/absence of DG systems and localization of connection/disconnection events within the network [2], [7]. DG systems are important resources in microgrids and ADNs and their presence/absence may change over the time. We propose an online detection mechanism that relies on current symmetrical components reported from the main point of common coupling in order to estimate the number of operational DG systems. This contribution is not only conducive to secondary control functionalities but also vital for reliable operation of backup protection applications.

3) Adaptive Backup protection coordinated with centralized DG management [3]. The increasing penetration of DG systems may significantly change the short-circuit currents. This phenomenon adversely affects the performance of line protection systems that operate based on over-current relaying concept. We propose a method that detects line faults within the per-determined tolerance time which is crucial for successful backup protection. Since the connection/disconnection of DG systems are tracked over the time, the secondary controller is able to update the critical value of fault isolation time. Hence, using our approach, the post-fault stability of islanded zone is assured. Moreover, upon fault isolation, the central controller updates the setpoints of DG systems in order to facilitate voltage/frequency recovery in the islanded zone.

1.7 Thesis Outline

This thesis includes six chapters which are briefly explained in the sequel:

- CHAPTER 1: Introduction: This chapter introduces the smart grid technology and explains how data-driven control and protection applications emerge in modern power grids. Moreover, an overview of the objectives, proposed methods and contributions of this thesis is given in this chapter.
- CHAPTER 2: A review on the synchrophasor technology: The second chapter is dedicated to the components of synchrophasor networks and hierarchical control systems in smart grids. Moreover, Chapter 2 reviews existing methods that address power system state-estimation, monitoring, and protection based on synchrophasor data.

- CHAPTER 3: Centralized disturbance detection: This chapter addresses reliable detection of voltage/frequency disturbances based on processing of noisy synchrophasor data that are subject to delay. Noise-delay tradeoff in synchrophasor data acquisition is explained, and average detection time and probability of false detections are numerically evaluated.

- CHAPTER 4: Monitoring of DG systems: Detection methods for estimation of the number of operational DG systems and localization of DG connection/disconnection events are developed in Chapter 4. The secondary DG monitoring unit processes the datasets of current symmetrical components at the main PCC and local nodes of the network. The robustness of the monitoring approach is evaluated in the presence of solar energy variations and sudden load changes.

- CHAPTER 5: Coordinated protection and secondary control: Detection of line faults within the critical fault tolerance time is the main subject of this chapter. The fault detection triggers a decision making algorithm that finds the optimal setpoints of DG systems for the islanded operation. The response time of the protective devices, DG capacities, and the communications delays are taken into account in the simulations.

- CHAPTER 6: Conclusion and recommendations: The last chapter presents a summary of the results and important remarks which can be drawn from this PhD thesis. Chapter 6 ends with suggestion of new research topics that can be addressed in future studies.

CHAPTER 2 A REVIEW ON THE SYNCHROPHASOR TECHNOLOGY

Microgrids and ADNs are the key elements of a modern power grid. Such networks are inherently exposed to diverse operating conditions due to prevalence of DG systems and DS units [8]. One of the major issues regarding the operation of microgrids and ADNs with high penetration of RESs is related to the voltage/frequency control and power flow management [9]. For instance, the variability of photovoltaic (PV) generation results in voltage fluctuations which can be detrimental to voltage regulation in distribution networks. To achieve reliable and secure operation in smart grids, new and sophisticated infrastructures have been proposed [10]. In fact, by employing communication and intelligent control systems, modern distribution networks can effectively harness RESs to improve the network performance in terms of power quality, reliability, efficiency, cost, and sustainability. In this section, we first briefly review the recent contributions to the field of intelligent and hierarchical control in modern power systems. Then, we proceed by discussing synchrophasor networks and how synchrophasor data play a pivotal role in high-level control and protection applications.

2.1 Networked Control Methodology in Smart Grids

Networked control in smart grids relies on digital communication systems for transfer of information and control signals between different components of the power system. Networked control methodology offers several advantages and is gaining a broad range of applications in smart grids. For example, information can be easily shared among multiple distributed controllers and different monitoring systems [11]. Moreover, new sensors and actuators can be easily augmented to the power system. Above all, the configuration and maintenance costs can be significantly reduced.

It is worth noting that, the interconnection of digital communication systems to the control and power systems results in new challenges. The digital communication systems are inherently discrete, i.e., signals must be measured, quantized, and transmitted over communication links. The communication links have limited and costly capacity, and if the number of nodes increases, then the communication links may fail in delivering the critical information. Furthermore, digital communication systems may induce packet delay and packet losses.

2.2 Hierarchical and Droop-Based Control in Smart Grids

The union for the coordination of transmission of electricity (UCTE) has developed a hierarchical structure for control of large-scale power systems [12]. In modern power systems,

the hierarchical structure is regraded as an effective paradigm for control of power system components [13, 12]. Moreover, attempts are made toward standardization of this control structure for smart grids with high penetration of DG systems [14].

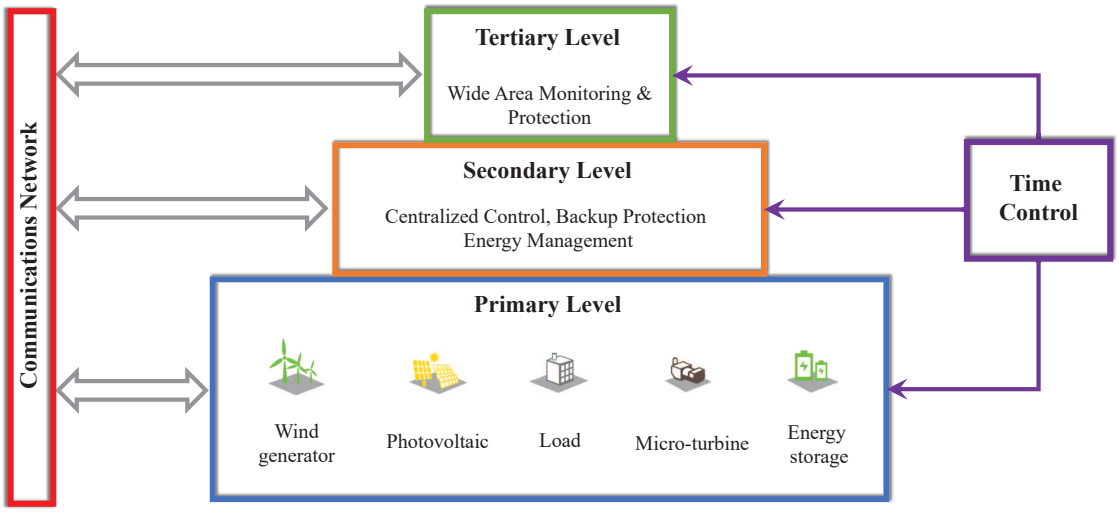

Figure 2.1 The three levels of the hierarchical control structure

Fig. 2.1 illustrates the general schematic of hierarchical control framework. As shown in this figure, most of the power system studies consider three levels for hierarchical control of microgrids and ADNs. A communications network is required for transfer of the control signals and data between different layers. It should be highlighted that, the control and protection applications at the higher layers do not necessarily require high-rate data. At the primary level of this structure, local (also known as primary) controllers are responsible for decentralized control of current/power or voltage/frequency [15]. To this aim, each operating DG system requires high-rate information about the instantaneous voltage and current at its local point of common coupling (PCC) [16, 14].

When connecting two or more DG systems to the network, the DG systems should use the well-known P/Q droop control method to mimic the behavior of synchronous generators and supply the time-varying loads. In droop control with inductive lines, the relationships between real/reactive powers and voltage/frequency are determined by [13]

$$\omega_o = \omega^* - K_P(s)(P_o - P^*) \tag{2.1}$$

$$V_o = V^* - K_Q(s)(Q_o - Q^*) \tag{2.2}$$

where ω^* and V^* denote the reference values for frequency and voltage amplitude, respectively. ω_o and V_o correspond to the measured frequency and voltage amplitude of the DG system, respectively. P_o and Q_o are the measured real and reactive powers, while P^* and Q^* are their reference values, respectively. The parameters $K_P(s)$ and $K_Q(s)$ are the droop transfer functions that can be designed based on the control-synthesis techniques and the steady-state performance criteria. In their simplest form, the droop transfer functions become constant gains that keep the entire system within the voltage-stability limits [14].

At the second layer of the hierarchical structure, a secondary controller is responsible for the reliable and economical operation of entire network in either grid-connected or islanded mode. The secondary controller also performs power sharing, power management, and Load shedding. If the network under study is a microgrid, then the secondary controller may be called microgrid central controller (MGCC). When a new DG system is connected to a node or a malfunctioning unit is disconnected from the network, the primary control level may fail in controlling the frequency/voltage thus the overall microgrid is disturbed [16]. Moreover, if the load's real and reactive powers change, then the amplitude and frequency at the local PCCs will deviate from their reference values. For example, Eqs. (2.1) and (2.2) indicate that a change in the local load results in steady deviations in the output frequency and voltage amplitude. Therefore, the secondary controller must monitor and restore such deviations by sending new values of ω^* and V^* to DG systems. Throughout this thesis, the point of connection of DG systems is called a local PCC. Power sharing between several DG units is another important functionality of the secondary controller [13]. To this aim, the secondary controller should determine and send the values of P^* and Q^* based on the capacities and rated powers of DG systems. Finally, it is worth noting that similar functionalities regarding control of DS units can be assigned to the secondary controller.

At the highest level of the hierarchical structure, the tertiary control layer regulates the power flow between the microgrid and the utility grid at the main PCC [12]. Moreover, a tertiary controller is responsible for coordination between multiple microgrids interacting with each other within an ADN [13]. The tertiary controller can also determine the optimal operating points of microgrids depending on the requirements of the utility grid.

It should be noted that the primary controllers are designed to operate instantaneously and in a decentralized manner. While the primary control layer does not require any communication link, the second and third control layers are inherently based on communication links and operate similar to networked control methods. The main advantage of hierarchical control is

improved robustness against disturbances and load changes which may not be settled by the local controllers.

Time synchronization is of crucial importance in proper operation of hierarchical control and protection applications. In realistic scenarios, the controllers receive the samples of voltage/frequency from distributed local PCCs. As a consequence of communication impairments, these information may arrive at a high-level controller without order or with unequal time delays. In many real-time applications such as disturbance and fault detection, the deviation of a parameter from the desired value is important for decision making. This implies that, the hierarchical control and protection applications requires synchronized (time-aligned) data that are comparable over the entire network domain. Such synchronized information can be extracted based on global positioning system (GPS) clock signals as will be discussed later in this chapter.

2.3 Synchrophasor Networks

Basically, synchrophasor networks consist of three fundamental components [17]:

1. Phasor measurement unit (PMU): for synchronized extraction of voltage/current phasors and other relevant information

2. Phasor data concentrator (PDC): for effective collection, pre-processing, and management of synchrophasor datasets

3. Communication links: for transfer of synchrophasor data packets

Fig. 2.2 illustrates the generic architecture of synchrophasor networks. In the data acquisition layer, the PMUs extract synchrophasor data at distributed nodes in the grid. The synchrophasor data are then delivered to PDCs which facilitate data management by collecting different data streams and constructing synchrophasor datasets. Finally, the PDCs provide the synchrophasor datasets for different applications in the application layer.

Currently, cost is the main issue that affects widespread deployment of synchrophaosr networks in power systems. The cost of the installation, commissioning, and the communication infrastructure are important economical factors. Substations that are equipped with digital relays or IEDs already have the necessary communication backbone. Moreover, the IEC 61850 standard allows transfer of synchrophasor data via the same protocols and messaging structure that handle IED information [18]. As the cost of PMUs decreases and more IEDs

are being deployed in power systems we anticipate a gradual migration towards full utilization of synchrophasor networks in power grids.

As far as distribution networks are concerned, low-cost and high-precision PMUs, also known as micro-PMUs, have been commercialized in the recent years. This type of PMU is suitable for distributed phasor data acquisition at the distribution level due to precise measurements and highly accurate time stamps [19, 20, 21]. The size of circuit boards in micro-PMUs is very small and they can be installed in almost every bus of distribution grids. A micro-PMU is capable of measuring voltage/current phase angles with a resolution of 0.001 deg, and magnitudes with a resolution of 0.0002%. State-of-the-art micro-PMUs can report synchrophasor data up to 120 frames/sec which makes them a qualified candidate for modern intelligent protection systems [22].

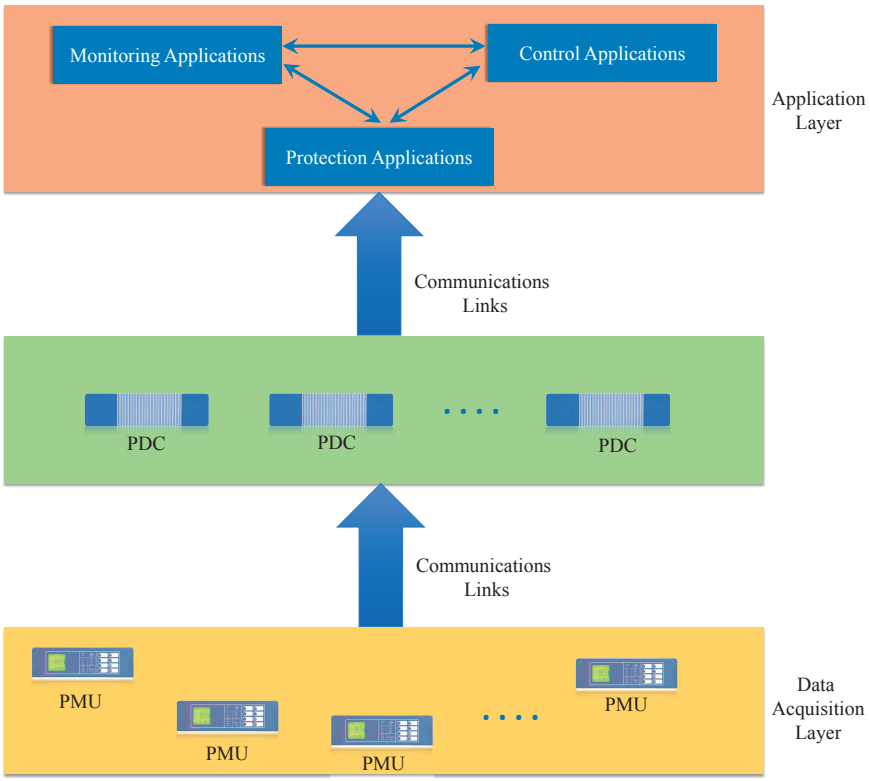

Figure 2.2 The generic architecture of synchrophasor networks

2.3.1 Synchrophasor Data Acquisition

It is known that the hierarchical control applications require time-aligned data for proper decision making. With the advent of reliable and accurate PMUs [23], a feasible data ac-

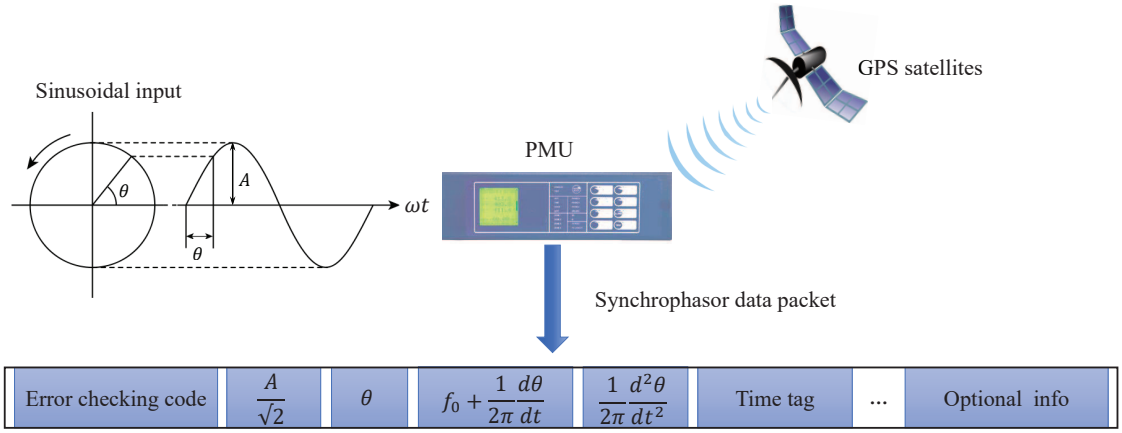

Figure 2.3 The extraction of synchrophasor data packets in power systems

quisition method is to locally measure the voltage/current phasors and then transmit the extracted data to the high-level applications. According to the IEEE standard C37.118-2011 [24], PMU is a device which extracts phasor magnitude, phase angle, frequency, and rate of change frequency (ROCOF) from the signals given at its input terminal, as illustrated in Fig. 2.3. The PMUs are equipped with transmitters which send the synchrophasor data packets to the desired destination via communication links.

In light of precise time stamps provided by PMUs, control, monitoring, and protection applications have access to synchronized and comparable data streams in real-time [23]. Commercial PMUs support a broad range of reporting rate, from 10 reports/sec up to 240 reports/sec for 60 Hz power systems [24]. The core of any PMU is a parameter estimator which extracts the synchrophasor data. The electrical signals appearing at the input terminals of PMUs may become corrupted by harmonics and additive noises. Hence, due to presence of noise in the input signals, the reported synchrophasor data may carry noisy values of the true parameters. The accuracy of synchrophasr data is thus dependent on the performance of the parameter estimator and the noise level. In what follows, we briefly review some of the techniques that are commonly used for parameter estimation:

- Discrete Fourier Transform (DFT) [25, 26]: The fast Fourier transform (FFT) applies to a window of input signal samples. Depending on the sampling frequency and length of the window, DFT-based algorithms are classified into fractional-cycle, one-cycle, and multi-cycle methods. The accuracy of DFT-based methods is liable errors emanated from aliasing and spectral leakage.

- Phase-Locked Loop (PLL) [27], [28]: Synchronous reference-frame phase-locked loop

(SRF-PLL), also known as dq0-PLL, is widely used for estimation of magnitude, frequency and phase angle of the positive sequence component of three-phase signals. Three independent enhanced PLLs (EPLLs) are required to estimate phasors of each phase of the three-phase signals. The accuracy of PLL-based methods can be affected by the presence of dc component, severe unbalancedness, and magnitude uncertainty in the input signals.

- Unified Three-phase Signal Processor (UTSP) [29]: The UTSP is basically an enhanced three-phase PLL which not only estimates the phasors and frequency of the sequence components but also synthesizes the signals in the time-domain. Similar to other PLL-based techniques, the UTSP shows longer transient times than those based on the DFT. However, the UTSP shows very good robustness against the measurement noise.

- Kalman Filter [30]: Basically, a Kalman filter can be configured to estimate the phasors similar to DFT-based methods. An adaptive Kalman filtering approach, also referred to as extended Kalman filter, however, depends on accurate frequency estimation. It can be thought of as a filter bank with arbitrary center frequencies. The main advantage of this approach is that it can effectively track the fundamental frequency along with its harmonics and specified inter-harmonics.

It is worth noting that, the aforementioned techniques differ in terms of robustness against measurement noise, response time, and computational aspects. Apart from the above methods, other techniques such as wavelet-based algorithms [31], signal subspace and adaptive filtering methods [32, 33] can be found in the literature.

2.3.2 Synchrophasor Data Communications

The IEEE standard C37.118.1-2011 defines a data frame as a set of phasor, frequency, and ROCOF samples that correspond to the same measurement time tag [24]. The reporting rate of synchrophasor data by PMUs is usually measured in frames per second (fps). The reporting rate is usually much smaller than the internal sampling rate of voltage/current waveforms. Therefore, a downsampling and delay compensation is normally required before transmission of data frames via communication links. There are two common protocols that may be used in synchrophasor data communication: transport layer protocol (TCP) and user datagram protocol (UDP).

In realistic scenarios, smart grids need effective mechanisms and protocols in order to ensure reliable data transmission and handling. The IEEE standards C37.118.2-2011 and C37.244-

2013 aim to address some issues regarding synchronization, processing, and real-time access to phasor data streams [34, 35]. These standards also define PDC as a unit that gathers phasor data, time stamps and other parameters from several PMUs (or other PDCs), and transmits the collected data to other devices. According to the this definition, a PDC can be thought of as an elaborate algorithm which can be integrated into other devices. In addition to data concentration, a PDC may fulfill other objectives such as data archiving, conditioning and validation [36]. PDCs are particularly helpful in intelligent applications such as situational awareness. In this study, we elaborate on PDCs as powerful data pre-processing tools for intelligent and hierarchical control/protection applications in smart grids.

2.4 Existing Trends and Applications

This section discusses some of the recent control and protection methods that rely on synchrophasor data processing. The existing methods are concisely reviewed from the perspective of high-level control and protection applications that are pertinent to this research.

2.4.1 Control Methods Based on Data Communications

Zheng et al. propose a centralized networked controller for a power system with parallel DG units connected with a single load [37]. They only consider the impact of communication delay in transferring the measured voltage and the reference values. The proposed schemes are applicable to scenarios where all inverters have access to a common communication link, hence, spatially distributed inverters are not considered.

The authors in [38] propose a robust networked control scheme that complies with the hierarchical structure. Specifically, they propose a distributed secondary control strategy where each DG system collects amplitude/frequency data from all operational systems and then calculates and broadcasts their average values using the communication network. This secondary control scheme can take into account spatially separated DG systems. However, its performance is liable to large errors due to DG failures in providing the true information under measurement noise.

Network control schemes for stabilizing the inter-area oscillations in power systems are discussed in [39] and [40]. These works only deal with the impact of packet loss on the stability margin of interconnected power systems. The effect of measurement noise and the procedure for estimation of power system states are not discussed. Moreover, the application is confined to oscillatory stability of wide-are power systems.

Networked control of power systems based on wide area measurements is discussed in [41] and [42]. The work presented in [41] accounts for the communication delay and packet dropout and aims to design a robust controller using wide area data as feedback signals. The adverse effects of limited bandwidth availability on the flexible AC transmission system (FACTS) controllers are explained in [42]. The underlying idea is to approximate the actual behavior of power system during the intervals when data from PMUs are not available. However, this work does not deal with packet loss and communication delays.

The work presented in [43] uses a networked control scheme for accurate and optimized power sharing in hybrid AC/DC microgrids. In this work, a centralized controller is implemented in an interconnecting voltage source converter (VSC) in order to optimally exchange power between the ac and dc sub-grids. The impact of a constant communication delay on the performance of interconnecting VSC is also investigated. However, most of modern networking technologies are based on packets for data transfer and thus variable communication delays and random losses are inevitable.

2.4.2 State Estimation Applications

The high reporting rate of PMUs basically allows control applications to effectively estimate the power system states in real-time. The authors in [44] propose a two-stage Kalman filtering approach for simultaneous estimation of both static and dynamic states in power systems, i.e., voltage magnitudes/phase angles and generator rotor angles/speeds. They also consider networked control of multiple inverters which are connected to a common bus and share a high speed communication link. Moreover, a data analyzer is proposed to determine the quality of data for power sharing. Specifically, their proposed data analyzer investigates the communication link failure and the abnormal values of power data. In [45] a distributed state estimation algorithm is proposed based on information exchanges with immediate neighboring nodes in large-scale power grids. The proposed state estimation algorithm incorporates the data obtained by both the SCADA system and PMUs to avoid the observability problem. Ghahremani and Kamwa propose a decentralized PDC-based state estimation method of the generators in large-scale power systems [46]. Their Kalman filtering technique processes PMU data extracted from the generator buses in order to estimate the rotor angle and speed of generators. In [47], a PMU-based robust state estimation method is proposed where synchrophasor data are used as priori information in a modified weighted least square estimation algorithm.

It is known that, the number of deployed PMUs and their locations in power grids affect the

observability of static and dynamic states. Finding an optimal PMU placement strategy to minimize uncertainty in state estimation is addressed by several researchers [48, 49, 50, 51, 52]. The authors in [48] discuss an important trade-off between the accuracy of the state estimation and the number of PMUs/smart meters in distribution grids. The genetic algorithm is used to solve an optimization problem in order to reach an optimal measurement infrastructure. The method proposed in [49] is basically a two-stage state estimation scheme which decomposes state vectors into observable and unobservable parts. A linear estimator receives PMU measurements to estimate the observable states variables. The resulting estimates are then used in a reduced-order state estimator to obtain the PMU unobservable state variables. In [50], a unified method is proposed for finding the minimum number and locations of PMUs such that all the state variables can be estimated. Their proposed approach yields the least infrastructure cost while preserves the grid observability. The methodology proposed in [51] aims at finding the optimal placement for both observability and detection of bad PMU data in critical measurements. According to their proposed approach, bad data in critical measurements are detected and subsequently converted to non-critical measurements through appropriate PMU placement. The ultimate advantage of their unified approach is that the robustness of the state estimation can be improved. In a paper written by Qi et al. [52], the empirical observability concept is applied to quantify the degree of observability of the dynamic power system states. The optimal PMU placement is formulated as an optimization problem which maximizes the determinant of the empirical observability Gramian.

2.4.3 Monitoring Applications

An important aspect of synchrophasor data is related to monitoring applications and situational awareness in smart grids. In fact, the PMU is deemed to be one of the most effective measurement devices in power system monitoring. According to the IEEE standard C37.118.1-2011, two operation classes are defined for PMUs, namely M class and P class. The M class is usually adopted in applications where high data accuracy is required while larger delays in data acquisition can be tolerated. Hence, most of monitoring applications may necessitate hiring PMUs that operate in the M class.

The authors in [53] propose a data-driven method for monitoring of short-term voltage stability in smart grids. In this approach, the time-series data reported by PMUs are used for the calculation of finite time Lyapunov exponents. They also address the impact of some data impairments (such as measurement noise, communication delay, and the length of measurement window) on the stability prediction. In [54], the authors improve the quality of PMU data by developing a state estimator for high-voltage buses. Their approach relies

on redundant PMU data in order to compute the power flows for disturbance and stability monitoring. An effective method for stability margin monitoring is proposed in [55]. In this method, first the generator angles are measured by PMUs and then then the phase angle difference between critical buses are calculated. An alarm is issued uppon detection of a disturbance which may violate the system transient stability.

The paper written by Kaci et al. proposes a comprehensive approach to monitor the power system stability based on the synchrophasor data streams [56]. Their approach is basically a data baselining method which relates PMU measurements with the grid performance measures under normal operating conditions. It combines conventional descriptive statistics with predictive data mining by means of a big database of power system information. Such a huge database comprises both load flow and dynamic data which can be collected over a time span of several years.

2.4.4 Protection Applications

Most of commercially available PMUs can operate according to the P class specifications. System designers may choose the P class for protection applications where a fast synchrophasor reporting is required [57]. A high data rate (which means more information in a shorter time period) comes at the cost of lower data accuracy. The accuracy of synchrophasor data, however, is of lower importance in protection applications.

Use of synchrophasor data for protection of power transmission lines is discussed by several papers [58, 59, 60, 61]. In this class of protection schemes, the main objective is to find the accurate location of faults independent of fault type/resistance, source impedance, and power flows. The fault detection and localization for high-voltage parallel transmission lines are well investigated in the paper written by Chen et al. [58]. They use two PMUs to measure voltage and current phasors at the two ends of transmission lines. An eigenvalue-based method is applied to decouple the mutual coupling effects between the parallel lines. The authors also propose an adaptive line parameter estimation algorithm for transposed and untransposed parallel lines. They employ ElectroMagnetic Transients Program (EMTP) simulations to show that their PMU-based protection scheme responds accurately to faults under the actual power system conditions. The authors in [59] propose a new method for backup distance protection of transmission lines. Similar to the method given in [58], their method relies on the use of the voltage and current phasors at both ends of the transmission lines. A system protection center receives the phasor data and eliminates the infeed effect (which increases the apparent impedance seen by the distance relays). The numerical results presented in [59]

show that this backup protection scheme has a good performance with different values of the fault resistance.

Current differential relaying for protection of transmission lines with PMU data is discussed in [60]. This paper also analyzes the sensitivity of the differential protection method for different values of fault resistance, location, and inception angle. The authors also evaluate the impact of communication delay on the performance of the differential protection scheme. An adaptive backup protection scheme for transmission lines is developed in [61]. In this paper, the linear least squares method is used to obtain a closed-form and non-iterative solution for the fault identification problem. The authors also propose an optimization model in order to minimize the number of required PMUs and alleviate the related issues such as data storage limitation and communications burden.

Synchrophasor data can also improve wide-area and backup protection in power systems [62, 63, 64, 65]. The authors in [62] point out that event detection and identification based on synchrophasor data play an important role in verifying the operation of relays. A fast variant of discrete S-transform is used for time-frequency analysis of voltage and frequency data reported by PMUs. Afterward, a set of features are derived from the time-frequency representation of data that are relevant to the characteristics of disturbances. Finally, the calculated features are fed into a multi-class extreme learning machine classifier that identifies the power system disturbances. Zare et al. propose a wide-area backup protection scheme that relies on communication systems to obtain synchrophasor data over a large power system [63]. The advantages of the proposed method is that it requires phasors of positive-sequence and identifies different types of faults under both normal and stressed conditions. The authors have also investigated the effect of communications/PMU failures on the applicability of their proposed scheme.

Intelligent protection algorithms can process PMU data in order to automatically generate early alarms before a voltage collapse occurs [64]. In [64], a method is presented for filtering synchrophasors with the aim of attenuating unwanted perturbations and removing the bad PMU data. The filtered synchrophasor data are subsequently used to calculate the sensitivity parameters by differentiating bus voltages with respect to the real/reactive powers transfered between buses. A warning alarm is generated before these sensitivities abruptly possess a large positive value (comparison with a threshold).

Hyder et al. [65] put forward a predictive protection framework based on adaptive syn-

chrophasor data communications. In their proposed framework, the maximum loadability and voltage instability point of the power system are periodically estimated by employing synchrophasor data and a curve-fitting technique. The curve fitting technique yields an optimization problem which is solved by using a convex programming tool. Moreover, the authors propose an adaptive scheme in order to dynamically increase the efficiency of communications links. This is achieved by switching between normal and fast data rates based on the outputs of a predictive algorithm.

2.4.5 Big Data Learning

Widespread usage of PMUs will eventually result in expansion of the volume of data. Dynamic phasor data are inherently stochastic, correlated in time and space which indicates more complexity [66]. It is anticipated that utilities will face challenges in terms of data management as well as data processing. Big Data in power systems is characterized by:

1) Large volume: extended time horizon for archiving data
2) High velocity: temporal constraints on collecting, processing and analyzing data
3) Increasing variety: data come from many sources that did not exist in conventional grids

Big data technology has been successfully applied to quantum, financial and biological systems. Data analytics facilitates improved situational awareness and secure grid operation Powerful data-driven tools are deemed to outperform traditional model-based tools [67]. Basically, data-driven approaches improve decision making about network disturbances such as faults, dynamic events, intermittent power from renewable sources, etc.

The authors in [68] review different applications of big data in the energy industry. It is shown that, big data can enhance the smart grid operation and management at higher levels. The study presented in [69] reveals that load modeling and load forecasting are two main big data intelligence applications in smart grids. Load modeling is related to the characterization of the behavior of different consumers and the grid to achieve optimal power management. Load forecasting is pertinent to predictions of power exchange in both short and long terms. A new method based on the random matrix theory is proposed in [70] which enables a feasible architecture for big data analysis in smart grids. The proposed method is shown to be a promising tool for anomaly detection in power systems.

CHAPTER 3 CENTRALIZED DISTURBANCE DETECTION

Modern power systems are shifting toward large scale grids that comprise multitude of interconnected microgrids. A microgrid is a localized system of DG systems, DS units, loads, and smart measurement devices and is capable of bi-directional exchange of power [71]. Such active networks give rise to several challenges in regard to control, stability, reliable operation, and power quality [13]. Moreover, microgrids are prone to issues such as voltage and frequency disturbances. Detection of such disturbances by control systems is therefore necessary for improving the operation of entire system.

This chapter develops a new structure for the centralized detection of voltage/frequency disturbances with noisy synchrophasor data that are subject to delay. We first present the analysis of noise-delay tradeoff in synchrophasor data acquisition, and then develop a new PDC for compensation of data losses. The performance metrics for the detector are numerically evaluated in the case of microgrid islanding. The results corroborate that the proposed structure counteracts the data noise and reduces the disturbance detection time. Moreover, numerical results show that the proposed algorithm lowers the probability of false detection and it can achieve the lower bound of average detection time. This study helps microgrid experts with assessing the performance of synchrophasor networks through which voltage/frequency disturbances are detected.

3.1 Introduction

The hierarchical control structure is considered as an effective methodology for control of large-scale power systems with multitude of DG systems and RESs [13]. Local controllers belong to the first layer of the hierarchical structure and carry out decentralized control of voltage, current, and frequency [15]. Each DG system requires high rate samples of the instantaneous voltage, current, and frequency at its local PCC [16, 72]. The MGCC belongs to the second layer of the hierarchical structure and is responsible for networked control of microgrid. The advantage of using the MGCC is improved robustness of control system against disturbances that are settled by the primary layer of the structure. The MGCC gathers the data from dispersed local PCCs. This means that the MGCC needs synchronized data that can be extracted using PMUs [24, 34, 73, 23].

3.1.1 Disturbances in Microgrids

In the context of microgrids, disturbance refers to deviations in voltage or system frequency which may result in reliability, control or safety issues. Modern microgrids can operate in both grid-connected and islanded modes. Transitions from the grid-connected mode to the stand-alone mode is a source of voltage/frequency disturbances [74, 75]. For instance, to assure the proper operation of the microgrid, the MGCC can supervise DG systems upon detection and confirmation of islanding. The control commands sent from the MGCC can be a change in real/reactive power setpoints, disconnection of DG, or switching to another controller [76]. The other type of network-wide disturbances is observed when the microgrid operates in the islanded mode based on a droop control strategy. In a droop-controlled microgrid, change of load or generation results in changes in the steady-state values of voltage/frequency [38]. Under such circumstances, the MGCC initiates the restoration process whenever a deviation in steady-state values of voltage/frequency is detected.

3.1.2 Existing Methods

Applications of phasor data for detection, monitoring and control purposes in power systems are addressed in the literature, refer to subsection 2.4.3 in Chapter 2 and references [77, 78]. The previous methods attempt to monitor voltage/frequency states and their transitions assuming that the synchrophasors are reported from a single node without loss of information or delays. In real-world microgrids, however, the phasor data are subject to impairments such as noise and random data losses.

Fast detection of disturbances is vital for time-critical control applications. A shortcoming of existing methods is that concerns regarding the detection time are not addressed. In fact, they assume that deviations in the system frequency or voltage can be immediately detected by the central controller. This implies a detection time equal to zero which may not be plausible in realistic scenarios. It can be concluded that the centralized disturbance detection using noisy and intermittent synchrophasor data has not been fully investigated. Monitoring of voltage/frequency states based on different measurement units invokes a rigorous analysis of reliability and robustness of the detection process. The MGCC relies on communication links in order to supervise DG systems in regard to power control and mitigation of disturbances [71]. Centralized detection of disturbances is achievable at a very low cost as long as the control structure conforms to a hierarchical form. However, a robust detection mechanism is required to compensate for data impairments that can potentially affect the secondary and tertiary levels of the hierarchical structure.

3.1.3 Contributions

This chapter proposes a new paradigm for reliable detection of voltage/frequency disturbances with noisy and intermittent synchrophasor data. A data concentration algorithm is proposed that compensates for data losses in communications between PMUs and the MGCC. This structure achieves a robust and reliable detection by mitigating the measurement noise which in turn reduces the probability of false detection. Moreover, the use of multiple PMUs decreases the average detection time. The islanding of a residential microgrid is simulated to evaluate the performance of the proposed structure. The simulation results indicate that the lower bound of average detection time can be achieved for a broad range of packet dropout rates. This study aids engineers in developing data acquisition systems for reliable and robust secondary control applications. Centralized control methods in islanded microgrids depend on fast detection of voltage/frequency deviations. In this chapter, an islanding event is simulated to create the voltage/frequency disturbances. It should be noted that, islanding detection is not a goal of this chapter since there is a wealth of islanding detection methods in the literature [79] and [75]. Moreover, most of the passive islanding detection methods assume that ideal voltage magnitude/frequency data are available and do not consider loss of data. Our proposed detector can be envisage as an auxiliary function which sends an alarm to local islanding detection systems for taking remedial actions. Control functionalities which restore voltage/frequency of droop-controlled microgrids can also take advantage the proposed detection structure.

3.1.4 List of Symbols

Table 3.1 lists the symbols and their descriptions which are used throughout this chapter.

3.2 Synchrophasor Data Acquisition in Smart Microgrids

3.2.1 Parameter Estimation

Centralized disturbance detection by means of L PMUs is illustrated in Fig. 3.1. The PMUs estimate phasor parameters at the local PCCs of L DG systems. The variable $v_l(t)$ denotes the voltage signal of the l^{th} local PCC at time t [1]:

$$v_l(t) = A_l(t)\sin\Big(2\pi f_0 t + \theta_l(t)\Big), \quad 1 \leq l \leq L, \tag{3.1}$$

Table 3.1 List of symbols in disturbance detection system

Symbol	Description
t	time
k	Discrete time index
L	Total number of PMUs
f_0	Nominal power system frequency
$\varepsilon_l(t)$	Additive noise in the input signals
F_s	Sampling rate of analog signals
N	Size of window
D	Decimation factor
F_t	Reporting rate of PMU
w	Vector of window coefficients
τ_p	PMU processing time
τ_p	Data acquisition delay
$\tau_{l,k}$	Communication delay at time index k from lth PMU
$r_{l,k}$	Binary indicator for delivery of data at time k from lth PMU
$p_{d,l}$	Packet drop probability from lth PMU
$\beta_{x,k}$	Normalized sum of deviation for parameter x at time index k
ζ_k	Binary indicator for the actual state of microgrid
$\tilde{\zeta}_k$	Binary indicator for the detected state of microgrid
Γ_x	Disturbance detection threshold for parameter x
T_d	Average detection time (overall)
τ_e	Average detection delay (at the controller)

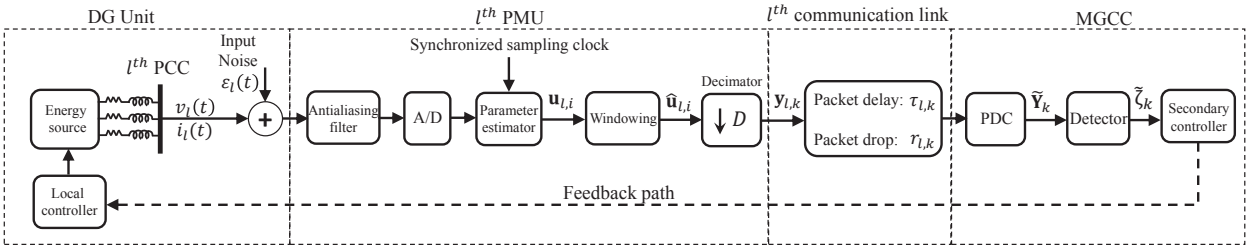

Figure 3.1 Disturbance detection with noisy and intermittent synchrophasor data [1]

where f_0 denotes the nominal power system frequency. This signal is expressed by a phasor as follows [1]

$$V_l(t) = \frac{A_l(t)}{\sqrt{2}} e^{j\theta_l(t)}. \tag{3.2}$$

In general, the PMUs report the measurement time tags along with the estimates of phasor magnitude, phase angle, frequency, and ROCOF of voltage/current signals. The input sig-

nals are corrupted by additive noise, which is denoted by $\varepsilon_l(t)$. The generic procedure for synchronized phasor estimation is also given in Fig. 3.1. A low-pass filtering is applied on the input signal to attenuate components above the Nyquist frequency of the sampling process. An analog-to-digital (A/D) converter samples the filtered signal according to the rate F_s samples/sec. Now, let $t = i/F_s$, where $i = 0, 1, 2, ...$ The parameter estimator extracts the phasor magnitude $A_{l,i}$ and the phase angle $\theta_{l,i}$ which lies in the interval $[-\pi, \pi]$.

The estimator can be realized using either of the techniques that are explained in subsection 2.3.1. In this chapter, we adopt the UTSP to obtain synchrophasor data. One advantage of the UTSP is that it can estimate the phasor information with good immunity to noise and fast response time [29, 80]. The UTSP parameters are seven real positive gains which are tuned to yield the desired speed of estimation. A detailed design procedure of these gains are discussed in [29].

Due to presence of the measurement noise in the process of phasor extraction, the phasor data are noisy versions of the true values. Suppose that, $n_{l,A,i}$ and $n_{l,\theta,i}$ represent the additive noises in the measurement of magnitude and phase angle, respectively. It follows that [1]

$$A_{l,i} = A_l(\frac{i}{F_s}) + n_{l,A,i}, \qquad \theta_{l,i} = \theta_l(\frac{i}{F_s}) + n_{l,\theta,i}. \tag{3.3}$$

The parameter estimator also extracts the instantaneous frequency, $f_{l,i}$, and the ROCOF, $\delta_{l,i}$, as [1]

$$f_l(t) = f_0 + \frac{1}{2\pi}\frac{d}{dt}\theta_l(t), \qquad \delta_l(t) = \frac{d}{dt}f_l(t), \tag{3.4}$$

and

$$f_{l,i} = f_l(\frac{i}{F_s}) + n_{l,f,i}, \qquad \delta_{l,i} = \delta_l(\frac{i}{F_s}) + n_{l,\delta,i}, \tag{3.5}$$

where $n_{l,f,i}$ and $n_{l,\delta,i}$ are the additive noises in the acquisition of frequency and ROCOF samples, respectively.

Now assume that $\mathbf{s}_l(t)$ denotes the vector of the true parameters [1]:

$$\mathbf{s}_l(t) = [A_l(t)\ \theta_l(t)\ f_l(t)\ \delta_l(t)]^T \tag{3.6}$$

and define the vector of the estimation noise as [1]:

$$\mathbf{n}_{l,i} = [n_{l,A,i}\ n_{l,\theta,i}\ n_{l,f,i}\ n_{l,\delta,i}]^T \tag{3.7}$$

The output of the phasor estimator is obtained as [1]:

$$\mathbf{u}_{l,i} = [A_{l,i}\ \theta_{l,i}\ f_{l,i}\ \delta_{l,i}]^T = \mathbf{s}_l\Big(\frac{i}{F_s}\Big) + \mathbf{n}_{l,i}. \tag{3.8}$$

Our studies based on the UTSP results and the Kolmogorov-Smirnov test verify that the noise in the output data fits well to the Gaussian distribution. For instance, Fig. 3.2 compares the empirical cumulative distribution functions (CDF) of the noise in estimated phase angle with the Gaussian CDF. In this figure, the internal sampling rate for the UTSP is $F_s = 900$ samples/sec and the input SNR is 20 dB. The theoretical CDF is plotted with mean equal to 0 and standard deviation equal to 2.1 deg. The excellent match between the empirical and the theoretical CDFs confirms the assumption of Gaussian distribution. Based on the obtained results, we assume that the elements of the random vectors $\mathbf{n}_{l,i}$ follow a Gaussian distribution.

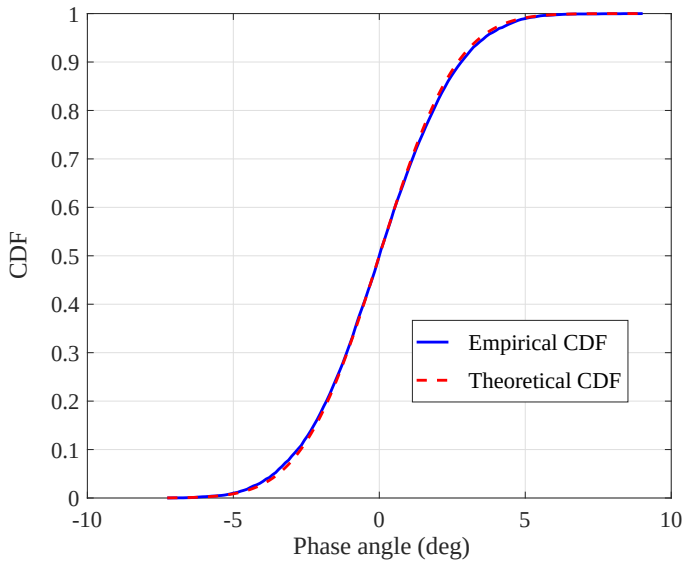

Figure 3.2 The CDF of the noise in the phase angle data for the positive-sequence component reported by the UTSP

Windowing and decimation operations are applied on the output of the parameter estimator to produce a frame of synchrophasor data which is suitable for transmission over communication links. According to the IEEE standard C37.118.1-2011 [24], a data frame is a set of

phasor, frequency, and ROCOF samples that are measured at the same measurement times. Since the sampling rate of input signals is high, the decimator downsamples the extracted information to decrease the cost of communications. Note that windowing is basically a low-pass filtering operation that offers several advantages:

- Mitigate the adverse measurement noise
- Attenuating abrupt transients due to interfering signals and sudden switching
- Removing the aliasing effect in the downsampling process

The sample vectors $\mathbf{u}_{l,i}$ are filtered by a window of size $N+1$. In fact, $N+1$ shows the number of consecutive sample vectors that are used in the windowing process. We assume that N is even number, hence, the following vector relationship is written [1]

$$\hat{\mathbf{u}}_{l,i} = \frac{1}{W} \sum_{m=-N/2}^{N/2} w_m \ \mathbf{u}_{l,i+m} \tag{3.9}$$

where,

$$W \triangleq \sum_{m=-N/2}^{N/2} w_m \tag{3.10}$$

w_m are the real coefficients of the window. The reported time tags must be determined according to the center of the window, and compensation for any preceding delays is necessary. The decimated signals are reported to the MGCC at the rate F_t fps. Let D denote the integer decimation factor, i.e.,

$$D = F_s/F_t \tag{3.11}$$

The k^{th} data frame reported by the l^{th} PMU is the vector [1]

$$\mathbf{y}_{l,k} = \hat{\mathbf{u}}_{l,kD}, \quad k = 0, 1, 2, ..., \ 1 \leq l \leq L. \tag{3.12}$$

The coefficients for commonly used windows are given as [81]:

$$\text{Rectangular:} \ \ w_m = \begin{cases} 1, & -N/2 \leq m \leq N/2 \\ 0, & \text{o.w.} \end{cases}$$

$$\text{Triangular:}\quad w_m = \begin{cases} 1+\frac{2m}{N}, & -N/2 \le m \le 0 \\ 1-\frac{2m}{N}, & 0 \le m \le N/2 \\ 0, & \text{o.w.} \end{cases}$$

$$\text{Hamming:}\quad w_m = \begin{cases} 0.54 - 0.46\cos\Big(2\pi m/N + \pi\Big), & -N/2 \le m \le N/2 \\ 0, & \text{o.w.} \end{cases}$$

3.2.2 Noise-Delay Tradeoff in Synchrophasor Data Acquisition

The phasor estimation errors are related to the elements of the vector $\mathbf{n}_{l,i}$. Basically, the average power of $\varepsilon_l(t)$ directly affects the statistics of the data noise vector. Due to structural complexity of the parameter estimator, explicit analysis of the statistics of the data noise is not a mathematically tractable problem. To be more specific, the UTSP includes several feedback loops which are coupled. Hence, not only the elements of the estimation noise vector are correlated but also the noise samples (for each parameter) become correlated in time.

It is crucial to assess the *effective noise* in synchrophasor data frames. Suppose that the noise that enters the l^{th} estimator is a white Gaussian noise with zero mean and fixed variance σ_l^2. Let $\hat{\mathbf{n}}_{l,k}$ represent the effective noise vector (after the windowing) in the k^{th} data frame. From Eqs. (3.8)-(3.12) it is concluded that [1]

$$\hat{\mathbf{n}}_{l,k} = \frac{1}{W}\bar{\mathbf{n}}_{l,kD}\mathbf{w}, \tag{3.13}$$

where $\bar{\mathbf{n}}_{l,kD}$ is the noise matrix obtained by stacking the estimation noise vectors as [1]:

$$\bar{\mathbf{n}}_{l,kD} = [\mathbf{n}_{l,kD-N/2} \cdots \mathbf{n}_{l,kD} \cdots \mathbf{n}_{l,kD+N/2}] \tag{3.14}$$

and $\mathbf{w}$ represents the vector of the window coefficients [1]:

$$\mathbf{w} = [w_{-N/2} \cdots w_0 \cdots w_{N/2}]^T \tag{3.15}$$

The correlation matrix of the effective noise is thus expressed as [1]

$$\mathbf{R}_l = \mathbb{E}\Big\{\hat{\mathbf{n}}_{l,k}\hat{\mathbf{n}}_{l,k}^T\Big\} = \frac{1}{W^2}\mathbb{E}\Big\{\bar{\mathbf{n}}_{l,kD}\mathbf{w}\mathbf{w}^T\bar{\mathbf{n}}_{l,kD}^T\Big\} \tag{3.16}$$

If the input noise is stationary within the estimation interval, then the elements of the matrix $\mathbf{R}_l$ does not vary over the time. For the rest of our analysis, the variable x represents a parameter that belongs to the set $\mathcal{P}$ given as [1]:

$$x \in \mathcal{P} = \{A, \theta, f, \delta\} \tag{3.17}$$

The autocorrelation of the noise in the generic parameter x is given by [1]

$$R_{l,x}(i,j) = \mathbb{E}\Big\{n_{l,x,i} n_{l,x,j}\Big\} \tag{3.18}$$

The variance of the effective data noise is an important quantity for detection and monitoring systems. This quantity should be evaluated under the ideal conditions of the power system, i.e., the input voltage/current signal is not in a disturbed or transient condition. The variance of the effective noise in each parameter can be assessed by [1]:

$$\hat{\sigma}^2_{l,x} = \frac{1}{W^2}\left[\mathbf{w}^T\mathbf{w}\sigma^2_{l,x} + \sum_{\substack{i=-N/2 \\ i\neq j}}^{N/2}\sum_{j=-N/2}^{N/2} w_i w_j R_{l,x}(i,j)\right] \tag{3.19}$$

where

$$\sigma^2_{l,x} = \mathbb{E}\Big\{n^2_{l,x,i}\Big\} \tag{3.20}$$

represents the noise variance in parameter x at the l^{th} PMU (before windowing). The value of $\sigma^2_{l,x}$ depends on the input noise variance, σ^2_l, and the structure of the parameter estimator. Our studies indicate that, the effective noise in each estimated parameter is correlation q-dependent [82]. In other words, a positive number q exists which satisfies the following equation [1]:

$$R_{l,x}(i,j) = 0, \qquad |i-j| > q, \quad \forall x \in \mathcal{P}.$$

The values of q is a function of the internal sampling frequency, F_s. Fig. 3.3 shows an example of the autocorrelation of noise in frequency data estimated by the UTSP. In this case, the input is a balanced 60 Hz voltage signal corrupted by Gaussian noise and the internal sampling rate is $F_s = 900$ samples/sec. In can be seen that $R_{l,f}(i,j) \approx 0$ for $|i-j| > 40$.

A prevalent post-estimation filter is realized by a rectangular window with $\mathbf{w} = \mathbf{1}_{N+1}$. Assuming that a rectangular window with $N \geq q$ is applied on the estimated parameters Eq.

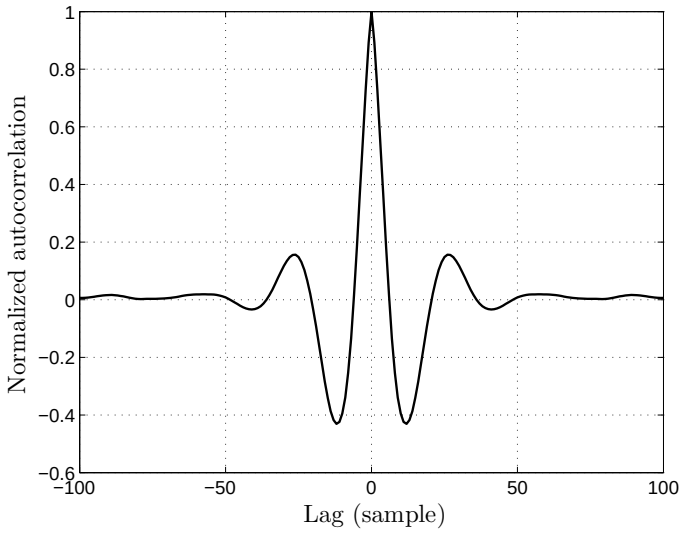

Figure 3.3 The autocorrelation of the noise in frequency data estimated by the UTSP

(3.19) yields [1]

$$\hat{\sigma}_{l,x}^2 = \frac{1}{N+1}\sigma_{l,x}^2 + \frac{1}{(N+1)^2}K_{l,x} \tag{3.21}$$

where the constant $K_{l,x}$ is given by [1]

$$K_{l,x} = \sum_{\substack{i=-q/2 \\ i\neq j}}^{q/2} \sum_{j=-q/2}^{q/2} R_{l,x}(i,j) \tag{3.22}$$

Eq. (3.21) shows that the variance of the effective data noise depends on $\sigma_{l,x}$, N, and the structure of the estimator (through the parameter $K_{l,x}$).

As a result of windowing, a non-trivial group delay is inevitably imposed on the synchrophasor data. The data acquisition delay is given by [1]

$$\tau_{pmu} = \frac{N}{2F_s} + \tau_p. \tag{3.23}$$

The first term in the above equation indicates the group delay and the second term, τ_p, is called the PMU processing time. The PMU processing time involves all pre-estimation delays emanating from anti-aliasing filtering and the parameter estimator. According to Eq. (3.21) the variance of the effective noise decreases by a factor $1/(N+1)$. Nevertheless, the data

acquisition delay is proportional to N. The tradeoff between the variance of the effective noise and the data delay affects the accuracy and latency of disturbance detection. An example of the noise-delay tradeoff for frequency data is shown in Fig. 3.4. In this figure, the left and right vertical axes show the values of the effective noise variance and the data acquisition delay, respectively.

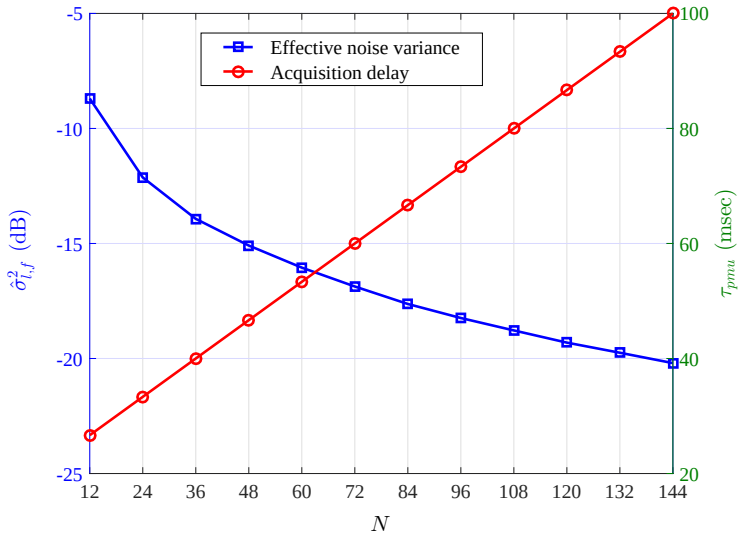

Figure 3.4 Noise-delay tradeoff in the acquisition of frequency data: $\sigma_l^2 = 0.05$, $F_s = 900$ samples/sec and $\tau_p = 20$ msec

3.3 Data Communications

The performance of centralized detection and control applications depends on the service quality provided by communications networks [38]. In light of PMUs, the phasor information at distributed nodes can be acquired in a synchronized manner. However, communications systems may introduce data losses [37] and thus the actual synchrophasor data received by the PDC/MGCC may be intermittent.

The transmission control protocol (TCP) and user datagram protocol (UDP) [34] are two common protocols for transmission of data packets. In the TCP, if an erroneous packet is detected, then the receiver side of the link requests retransmission of the packet. However, by using the UDP, the erroneous packets are dropped at the receiver side. Therefore, the subsequent data packets which are waiting for transmission do not tolerate further delays. Digital communications systems utilize error detection coding, e.g., cyclic redundancy codes, to identify erroneous data packets [34]. In the TCP, the inevitable delay in the request and

reply process [83] has adverse effect on time-critical applications. It can be concluded that, the UDP is an efficient protocol for transmission of data from PMUs to the MGCC, whereas the TCP is suitable for sending commands to DG systems and local controllers. For the rest of our analysis, the transmission of synchrophasor data packets is based on the UDP.

The service quality of communications systems can vary over the time. From the vantage point of detection applications, it usually suffices to model the l^{th} communications link by a delay variable, $\tau_{l,k}$, and a binary variable $r_{l,k}$ (refer to Fig. 3.1). $\tau_{l,k}$ represents the aggregated communication delay imposed on the k^{th} data packet transmitted from the l^{th} PMU. The value of $\tau_{l,k}$ depends on the size of data packets, data rate, channel access time, coding time, etc. In some practical scenarios a communication medium, e.g., a wireless channel, is shared among different PMUs. In that case, the total communication delay is affected by the network congestion, hence, $\tau_{l,k}$ is a random variable. Detailed characterization of communication systems is beyond the scope of this thesis. It should be highlighted that by virtue of time tags provided in synchrophasor networks, the values of $r_{l,k}$ and $\tau_{l,k}$ can be found by the MGCC.

The binary random variable $r_{l,k}$ represents delivery of the k^{th} data packet. $r_{l,k} = 0$ is assigned to the dropped/erroneous data packet at time index k. The delivered data packet at time k is associated with $r_{l,k} = 1$ and is assumed to be error-free. The Bernoulli distribution characterizes the packet dropouts in communications links [1]:

$$\Pr\{r_{l,k} = 0\} = p_{d,l}, \tag{3.24}$$

$$\Pr\{r_{l,k} = 1\} = 1 - p_{d,l}, \tag{3.25}$$

In (3.25), $p_{d,l}$ shows the probability of packet dropout in the communications between the l^{th} PMU and the MGCC. This parameter is basically a gauge of the service quality of lossy communications links.

At the MGCC, first a PDC collects the reported synchrophasor data [35]. Considering delay requirements of detection and control applications, the PDC is not allowed to wait for a long time in order to collect data. Under such circumstances, the PDC uses a waiting interval [34] and constructs a dataset of the data delivered in this interval. A synchrophasor dataset for time index k is denoted by $\tilde{\mathbf{Y}}_k$. $\tilde{\mathbf{Y}}_k$ is basically a $4 \times L$ matrix formed by concatenation of synchrophasor data reported by different PMUs.

As a common practice, the PMUs report their data frames at an integer rate F_t fps. Suppose that the reporting instants are uniformly spaced over the time. In a one-second period each PMU reports F_t phasor samples and the transmission of the first sample begins with the second rollover [24]. The PDC is synchronized with the PMUs and under ideal conditions it receives L data packets from L PMUs in $1/F_t$ seconds period. In this regime, the acquisition, transmission, and collection of data are carried out in a synchronized manner. Therefore, it is plausible to assume that the PDC waiting time is equal to the interval between two successive samples, i.e., $1/F_t$.

3.4 Centralized Disturbance Detection

3.4.1 Data Concentration Algorithm

Loss of synchrophasor data due to delayed arrival/dropout of data packets should be taken into account in PDC design. A conventional method is to insert an invalid data indicator (e.g., NaN) in place of lost data elements, as declared by the IEEE standard for synchrophasor data transfer [34]. However, indicators do not facilitate decision making and render conventional PDCs inefficient for monitoring and detection applications. In light of measurement diversity provided by multiple PMUs, PDCs can use received data frames to estimate elements of the lost data frames.

Upon dropout of a data packet from a PMU, parameters $x \in \mathcal{P}$ for that PMU can be estimated by the PDC. The set of the received data can be used to reconstruct the lost data. Suppose that the vector $\mathbf{y}_{l,k}$ denotes the data reported at the k^{th} time index [1]:

$$\mathbf{y}_{l,k} = [y_{l,A,k}\ y_{l,\theta,k}\ y_{l,f,k}\ y_{l,\delta,k}]^T \tag{3.26}$$

and let $\tilde{\mathbf{y}}_{l,k}$ be the data at the output of the PDC [1]:

$$\tilde{\mathbf{y}}_{l,k} = [\tilde{y}_{l,A,k}\ \tilde{y}_{l,\theta,k}\ \tilde{y}_{l,f,k}\ \tilde{y}_{l,\delta,k}]^T \tag{3.27}$$

Algorithm 3.1 explains the procedure of synchrophasor data concentration by assuming that the PDC waiting time is equal to one reporting interval. Algorithm 3.1 is recursive in terms of the local information (phasors) but interpolative for the global information (frequency and ROCOF).

Algorithm 3.1: Interpolative/Recursive Data Concentration [1]:

1. Construct the set of PMU indices that their data have been received successfully:

$$\mathcal{L}_k \triangleq \Big\{ l \mid r_{l,k} = 1, \tau_{l,k} \leq 1/F_t \Big\} \tag{3.28}$$

2. If $|\mathcal{L}_k| = 0$, then proceed to step 3, otherwise go to step 4.

3. Recursive Concentration: Set $\tilde{y}_{l,x,k} = \tilde{y}_{l,x,k-1}, l = 1, 2, ..., L, \forall x \in \mathcal{P}$.
   Go to step 1 with time index $k + 1$.

4. For $l = 1, 2, ..., L$:
   If $l \in \mathcal{L}_k$, then set $\tilde{y}_{l,x,k} = y_{l,x,k}, \forall x \in \mathcal{P}$.
   If $l \notin \mathcal{L}_k$, then set $\tilde{y}_{l,A,k} = \tilde{y}_{l,A,k-1}$, $\tilde{y}_{l,\theta,k} = \tilde{y}_{l,\theta,k-1}$ proceed to step 5.

5. Interpolative Concentration: For the parameters $x \in \{f, \delta\}$, if $\sigma_{l,x}$ are *a priori* known, then use Eq. (3.29), otherwise use Eq. (3.30)*:

$$\tilde{y}_{l,x,k} = \left(\sum_{j \in \mathcal{L}_k} 1/\sigma_{j,x}^2 \right)^{-1} \sum_{j \in \mathcal{L}_k} \frac{y_{j,x,k}}{\sigma_{j,x}^2}, \tag{3.29}$$

$$\tilde{y}_{l,x,k} = \frac{1}{|\mathcal{L}_k|} \sum_{j \in \mathcal{L}_k} y_{j,x,k}, \tag{3.30}$$

   Go to step 1 with time index $k + 1$.

---

*$|\mathcal{S}|$ shows the cardinality of the set $\mathcal{S}$.

In Algorithm 3.1, the successfully received data packets are immediately used to construct the output dataset. In case of a data loss or excessive delay, the unknown phasor amplitude and phase angle are replaced by their most recent samples but the frequency and the ROCOF are interpolated. Eq. (3.29) is the maximum likelihood estimator of unknown data while Eq. (3.30) is the arithmetic mean of the received data. In low-voltage and residential microgrids where the line impedance is both inductive and resistive, the amplitude and phase angle data may vary among different local PCCs. However, the system frequency and the ROCOF are independent of the location of PMUs and the line impedance. If all communications links fail to deliver data packets, then step 3 is carried out that implies a recursive PDC.

In lossy synchrophasor networks where delivery of data can be intermittent, a detector which employs on an interpolative/recursive PDC is faster than the one which relies a conventional

PDC. The sample estimators in Algorithm 3.1 also improve the immunity of synchrophasor datasets to measurement noise and PMU failures. Fig. 3.5 illustrates how sample estimators are used for extracting the unknown frequency samples. In this figure, only the communications between the fourth PMU and the PDC encounter packet dropout.

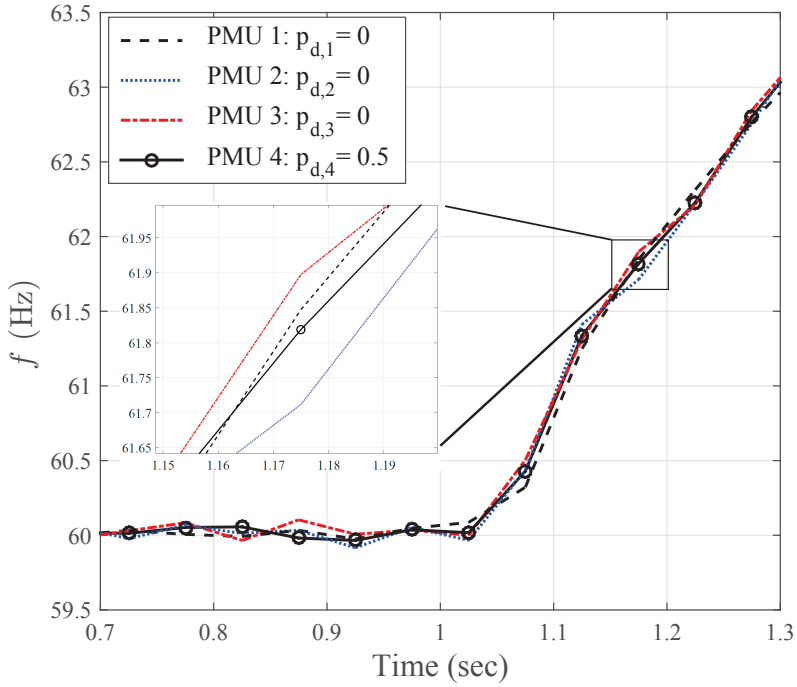

Figure 3.5 A snapshot of spatial interpolation under a ramp of system frequency for a microgrid with 4 PMUs. The circles indicate interpolated data samples [1]

3.4.2 Central Disturbance Detector

In general, a disturbance can be envisaged as a perturbation or deviation in phasor/frequency of local PCCs. As discussed in previous subsections, the synchrophasor data that convey phasor/frequency deviations undergo impairments over the time. The central detector relies on real-time datasets (which are produced by Algorithm 3.1) in order to make decision about the status of the microgrid. For the time index k, the detector finds the normalized sum of deviations in the parameter of interest [1]:

$$\beta_{x,k} = \frac{1}{L}\sum_{l=1}^{L}(\tilde{y}_{l,x,k} - x_0), \tag{3.31}$$

In Eq. (3.31), x_0 is the nominal value of the parameter x and is known *a priori*. Suppose that ζ and $\tilde{\zeta}$ are binary variables that represent the true and the detected states of the

microgrid, respectively. If the microgrid undergoes a network-wide disturbance, then $\zeta = 1$, otherwise $\zeta = 0$. In detection applications, $\tilde{\zeta} = 1$ indicates that a disturbance is detected and a secondary control mechanism should be triggered immediately. $\tilde{\zeta} = 0$ shows that the normal or non-disturbed condition of the microgrid is detected and the secondary control should not be applied. $\tilde{\zeta}$ goes from 0 to 1 whenever the normalized sum of deviations exceeds a predetermined threshold [1]:

$$\tilde{\zeta}_k = \begin{cases} 1, & \text{if } |\beta_{x,k}| > \Gamma_x \\ 0, & \text{otherwise} \end{cases} \tag{3.32}$$

The threshold Γ_x in (3.32) shows the normalized deviation in the parameter x beyond which the microgrid is considered to be disturbed. As will be shown later in this chapter, the central detector outperforms local detection methods that rely on single PMU data.

3.4.3 Performance Evaluation of the Central Detector

From a monitoring/control perspective it is important to assure fast and accurate detection of voltage/frequency disturbances. With UDP-based communications, the synchrophasor networks (including acquisition and transmission) are inherently stochastic. Since data are subject to random noise, delay, and unpredictable losses, it is necessary to have a statistical method for performance evaluation of the central detector.

By using stochastic synchrophasor networks, the random detection delay may lead to harmful transients or even stability issues. To further investigate the random delays, the average detection time, denoted by T_d is analyzed. T_d represents the expected value of the time interval between the disturbance occurrence and the detection instant. The average detection time is expressed in (3.33) [1]:

$$T_d = \tau_{pmu} + \frac{1}{2F_t} + \tau_e. \tag{3.33}$$

In the Eq. (3.33), the first term is the data acquisition delay and the second term is the expected value of waiting time for the transmission. The third term, τ_e, is the average value of the detection delay. τ_e shows how fast the disturbances are detected after the instant of data transmission. The value of τ_e depends on the likelihood of packet dropouts and degree of communications delays. In our proposed structure, the following inequality holds [1]:

$$\tau_e \geq \tau_{pdc} + \frac{1}{F_t} \tag{3.34}$$

and the lower bound for the average detection time is derived [1]

$$T_{d,LB} = \tau_{pmu} + \tau_{pdc} + \frac{3}{2F_t}, \tag{3.35}$$

where τ_{pdc} represents the PDC processing time as explained in [35].

In real-world scenarios, measurement noise and sudden load changes may result in false detections (alarms) [84]. Under such circumstances, the probability of false detection should be evaluated [1]:

$$p_{FD} = \Pr\left\{\tilde{\zeta} = 1 | \zeta = 0\right\}, \tag{3.36}$$

where $\Pr\{.|.\}$ is the operator of the conditional probability. If PMUs encounter a large timing error during the phasor estimation process, then bad PMU data can be reported. Bad PMU data should be detected and ignored before they are used by the detector otherwise, they aggrandize the false detections [36, 44]. The proposed detection structure should be augmented by a real-time identifier which prevents bad data from entering the detector. The augmented structure counteracts delay, measurement noise, and bad PMU data and lowers the probability of false detection.

The performance of the proposed structure can be assessed based on the values of the aforementioned metrics. It should be underscored that, these statistical metrics do not impose constraints on the method or complexity of the detector. In fact, they can be applied to any monitoring/detection system which relies on synchrophasor networks. A smaller p_{FD} implies a more reliable disturbance detector. Moreover, a smaller T_d indicates a faster data acquisition system and higher robustness against loss of synchrophasor information. The MGCC determines the control commands based on the type of disturbances, the microgrid parameters, and the capacities of DG systems. Control links are used to transfer the control signals from the MGCC to the local controllers belonging to the microgrid (refer to Fig. 3.1).

3.5 Numerical Results

3.5.1 Network Simulation Procedure

The test microgrid is a low-voltage residential network with circuit diagram illustrated in Fig. 3.6. The proposed disturbance detection scheme is implemented in this microgrid that incorporates DG systems and household loads. A PMU is deployed at each local PCC and the two feeders have the same number of DG systems/loads, i.e., L is an even number. Sim-

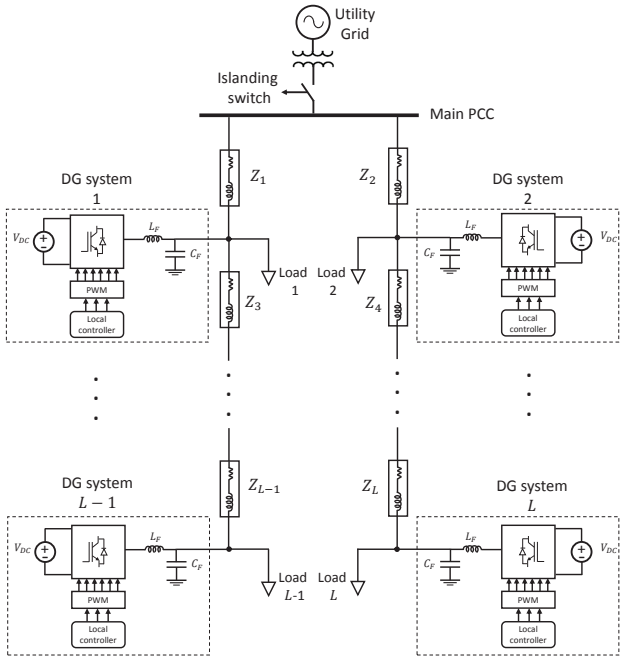

Figure 3.6 The single-line schematic of a microgrid with a radial structure and residential loads [1]

ilar to most of PV-based networks [85], the DG systems employ three-phase voltage-sourced converters (VSCs) and current controllers (at the primary level). The nominal values of system frequency and voltage are 60 Hz and 380 V, respectively. In order to account for variations of energy consumption, the household consumers are modeled by random PQ loads. Specifically, the real and reactive powers of loads are independent uniformly distributed over $[0, 10]$ kW and $[0, 2]$ kVAR, respectively.

In the grid-connected mode, the DG systems can deliver a certain amount of real power under unity power factor, i.e., $Q^* = 0$ [75]. Therefore, the reactive power demanded by the loads must be provided by the utility grid. At the secondary control level, the MGCC matches the real power of DG systems to the average value of the consumed real power by setting the setpoint of each DG system to $P^* = 5$ kW. In Fig. 3.6, Z_l represents the model of low-voltage line segments between adjacent local PCCs. The distance between neighboring local PCCs is 40 m and the segment impedance is 0.64 Ω/Km. The DC voltage produced by the energy sources that supply DG systems is fixed at $V_{DC} = 700$ V. The inductance and capacitance of the output LC filter are $L_F = 15$ mH and $C_F = 10$ μF, respectively. The UTSP gains are as follows: $\mu_1 = \mu_2 = \mu_3 = 67, \mu_4 = 20000, \mu_5 = 130, \mu_6 = 433, \mu_7 = 1333$. These values are chosen such that the response time of the PMU becomes less than one cycle.

The internal sampling rate of PMUs is $F_s = 2000$ samples/sec and the rectangular window with size $N = 120$ is employed for windowing of estimated phasors. The extracted data are transmitted at the rate of $F_t = 20$ fps, i.e., one frame every three cycles. The PMU and PDC processing times are $\tau_p = 20$ msec and $\tau_{pdc} = 0$, respectively.

The disturbances are significant deviations of system frequency or voltage magnitude from their nominal values that occur after islanding of the test microgrid at the time instant $t = 1$ sec. The nominal values of the frequency and magnitude are $f_0 = 60$ Hz, and $A_0 = 1$ pu. Monte Carlo simulation method is adopted for statistical performance assessment of the proposed disturbance detection structure. According to this simulation procedure, first random loads are realized and the developed algorithms are sequentially executed. Afterward, the results of the detector are captured and the values of the performance metrics are computed. Whenever the value of the parameter $\tilde{\zeta}$ changes from 0 to 1 before time $t = 1$ sec, then a false detection is recorded. We suppose that only errors due to the measurement noise result in a false detection. Moreover, all PMUs operate under the same input SNR, and the communications links have identical packet dropout rates. We also suppose that the MGCC does not have *a priori* knowledge of the parameters $\sigma_{l,x}$ and thus Eq. (3.30) is used for frequency interpolations in case of data loss. The data communications delays are much smaller than the reporting interval, i.e., $\tau_{l,k} \ll 1/F_t$. The simulation step time for the detection and decision making at the secondary control level is set to 1 msec.

3.5.2 Discussion of the Numerical Results

Fig. 3.7 shows time-domain simulation results for two cases of fast and slow detections with $L = 4$ PMUs. The input SNR of PMUs and the frequency disturbance threshold are 19 dB and $\Gamma_f = 0.1$ Hz, respectively. Fig. 3.7 (a) reveals that, the loss of synchrophasor data in case of severe packet dropouts is such that the data concentration algorithm cannot update $\beta_{f,k}$ over a long period. As depicted in Fig. 3.7 (b), the detection time in the slow case is slightly longer than 24 cycles. The slow detection of disturbances can significantly affect the monitoring and centralized control applications. In the case of fast detection, however, the detection time is equal to $T_{d,LB}$. Note that in this network the detection time has a lower bound equal to $T_{d,LB} = 125$ msec.

Fig. 3.8 illustrates the reliability of the proposed structure in terms of probability of false detection for different values of L. This simulation result shows that monitoring systems can benefit from measurement diversity inherent in synchrophasor datasets. Moreover, in order to maintain a constant p_{FD}, the required input SNR of PMUs decreases by increasing the

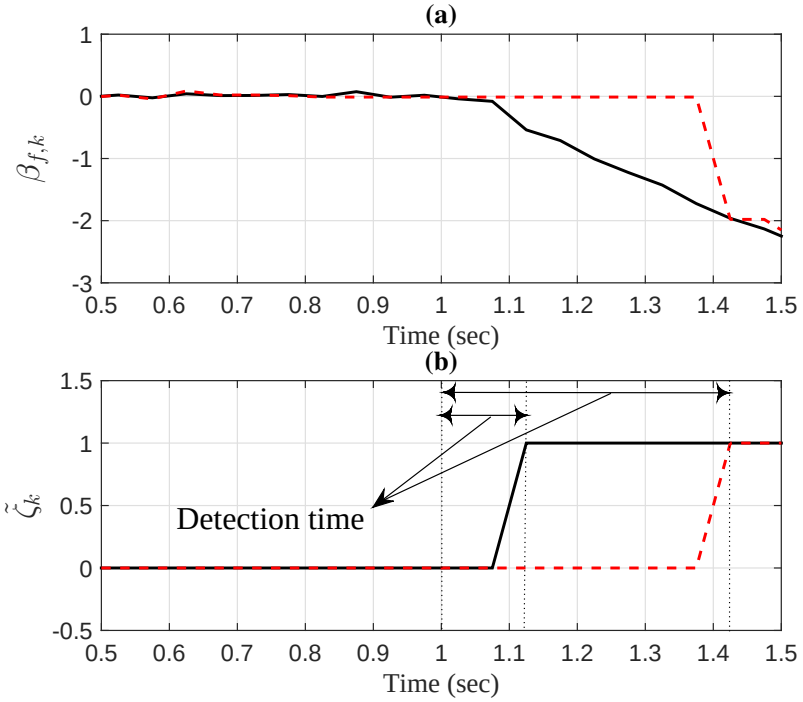

Figure 3.7 Cases of fast (solid curves) and slow (dashed curves) detection under packet dropouts. (a): The normalized sum of deviations, (b): The detected state [1]

number of PMUs. By doubling L, the required SNR reduces 3 dB in the low-SNR region.

The simulation results shown in Fig. 3.9 demonstrate the performance of local detection methods for the test microgrid. According to local detection methods, each DG system constantly monitors the phasor information obtained at its local PCCs. The absolute value of deviations in locally estimated frequency/amplitude data is compared with a threshold. If the deviations exceed their thresholds, then the DG system sends a disturbance alarm to the central control unit. In this figure, p_{FD} shows the probability that at least one DG system sends an alarm signal which happens if the absolute value of frequency deviation exceeds 0.1 Hz or magnitude deviation surpasses 0.1 pu. The concluding remark is that the local detection methodologies have a high likelihood of false alarm in the low and moderate SNR regions.

Comparisons of the simulation results presented in Figs. 3.8 and 3.9 demonstrate the advantage of the proposed structure. The MGCC can reliably monitor voltage/frequency disturbances when $\sigma_l^2 \leq -25$ dB. In this SNR region the probability of false detection is smaller than 10^{-6}. In low to moderate SNR region, the centralized detector has a better performance compared with local detection methods. This result substantiates the advantage of using the

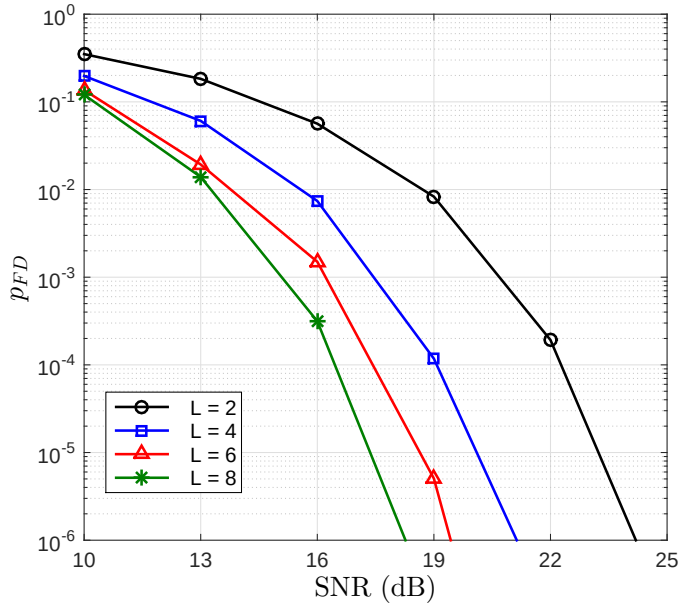

Figure 3.8 Probability of false detection in the central detection [1]

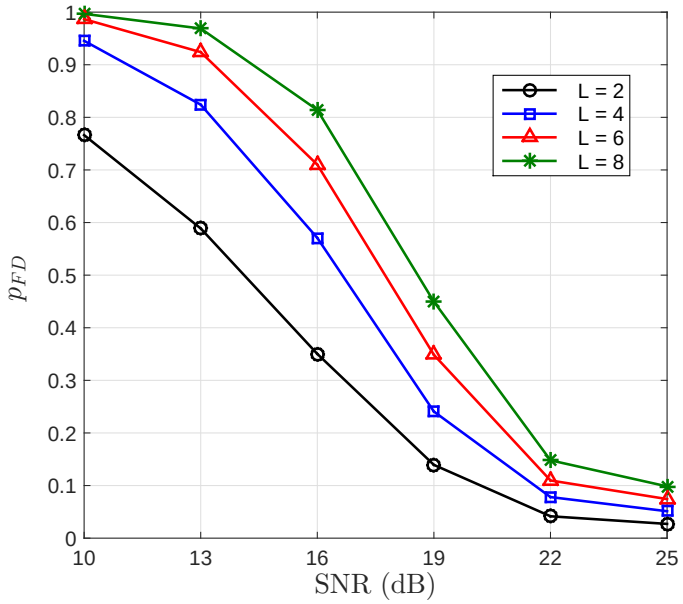

Figure 3.9 Probability of false detection in the local detection [1]

central detection structure for reliable monitoring and secondary control of DG systems.

The results of conventional and interpolative PDCs with $L = 8$ PMUs are given in Fig. 3.10.

It can be seen that, the time required for detection of frequency disturbances increases by increasing the dropout rate regardless of the data concentration method. By means of the interpolative PDC, the disturbances are detected faster on average specially under severe packet dropouts. For example, for a packet drop rate equal to 0.8, the interpolative PDC results in 8 msec reduction of the detection time. However, the difference between detection times is in excess of 39 msec for a dropout rate equal to 0.96.

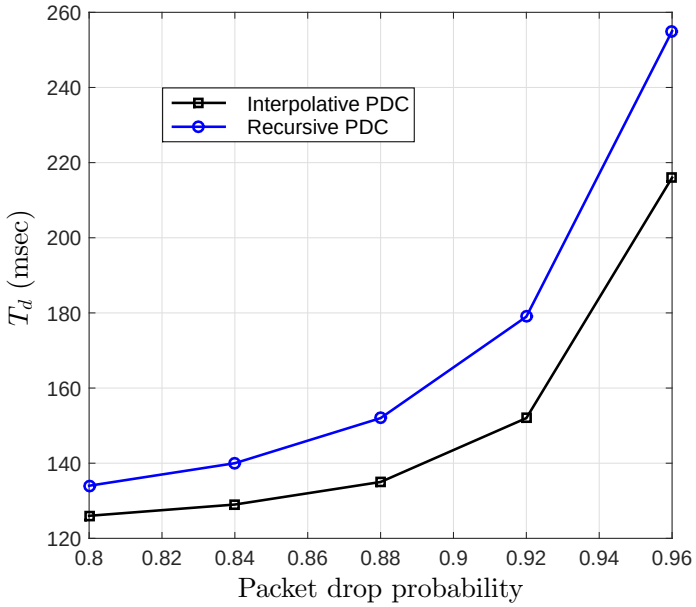

Figure 3.10 Performance comparison of interpolative and recursive PDC algorithms, $\Gamma_f = 0.5$ Hz, input SNR = 19 dB [1]

Fig. 3.11 demonstrates that a higher detection time results in a lower probability of false detection and vice versa. In fact, a smaller p_{FD} is achieved at the cost of a larger T_d for a fixed input SNR. It can be concluded that, for a given probability of false alarm, the detection time can be decreased by increasing the number of PMUs in the microgrid. This simulation result clearly shows the noise-delay tradeoff in synchrophasor-based monitoring applications.

Fig. 3.12 demonstrates the performance of the proposed structure in terms of the average detection time. The synergy of the proposed disturbance detector with the interpolative PDC increases robustness of monitoring applications against loss of synchrophasor data. For the case of $L = 8$ PMUs, the average detection time is very close to its lower bound given by Eq. (3.35). If the packet dropouts rate goes beyond 0.8, the detection time is expected to rise gradually. The worst detection happens with $L = 2$ PMUs since in this case the data concentration algorithm does not perform interpolation upon loss of synchrophasor data.

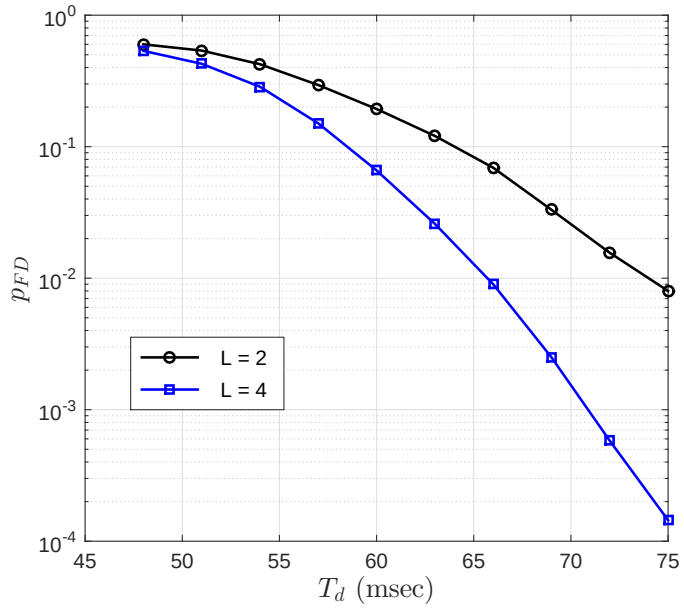

Figure 3.11 Probability of false detection vs. average detection time: $\sigma_l^2 = -19$ dB, $p_{d,l} = 10\%$ [1]

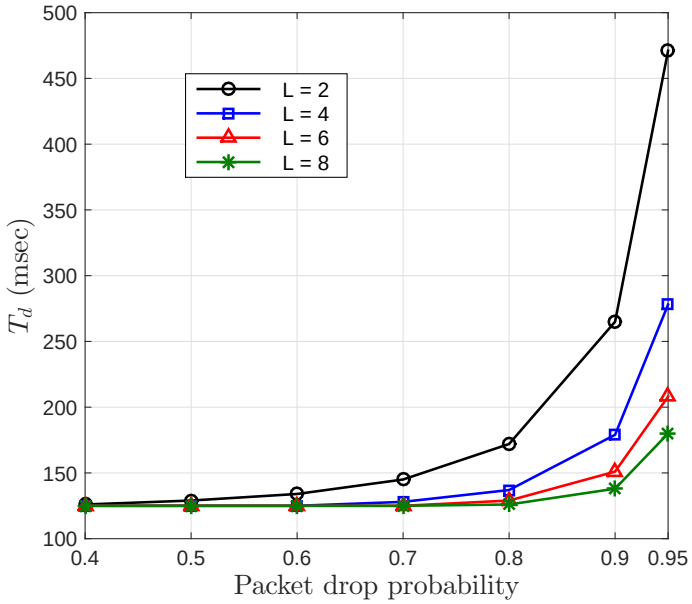

Figure 3.12 The average detection time vs. packet dropout rate, $\Gamma_f = 0.1$ Hz, $\Gamma_A = 0.1$ pu, input SNR = 16 dB [1]

3.6 Conclusion

This chapter elaborates on a new structure for reliable and centralized detection of voltage/frequency disturbances in microgrids which utilize noisy and intermittent synchrophasor data. It is verified that monitoring systems can use interpolative data concentration algorithms in order to counteract severe noise and data losses in communications links. The overall detection structure can even decrease the average detection time by using more PMUs. It is also shown that the proposed detection structure is robust against the measurement noise that enters PMUs. In the presence of noise, the reliability of the developed detection structure is assessed in terms of the probability of false detection. In particular, in the low and mediate SNR regions, the performance of the proposed detection system is superior when compared with that of local threshold-based detectors. It turned out that false detections can be further suppressed at the expense of larger average detection time.

CHAPTER 4 MONITORING OF DISTRIBUTED GENERATION SYSTEMS

Hierarchical control/protection applications in smart grids require knowledge of the real-time status of DG systems. Lack or failure of communications with the secondary control layer significantly undermine the performance of such applications. Under such circumstances, the control/protection applications cannot determine the operational energy sources. The high-level control applications require a secondary monitoring method to track presence/absence of DG systems in the network.

This chapter proposes a new monitoring approach that empowers the MGCC to estimate the number of operational DG systems, determine the total generation capacity, and localize the DG events. First, a parameter estimator is used to estimate an autoregressive model for the synchrophasors of current symmetrical components (CSC) that flow into the main PCC. Afterwards, an adaptive algorithm identifies sudden changes in DG status by inspecting the norm of the forward prediction error. The received synchrophasor data from spatially distributed nodes are used to construct local datasets. The local outlier probability (LOP) method is applied on each local dataset in order to localize the DG events within the microgrid. The simulation results confirm that the secondary monitoring and localization methods are robust against sudden load changes.

4.1 Introduction

Microgrids and ADNs are subject to diverse operating conditions due to prevalence of DG systems as well as DS units [86]. In recent years, intelligent control architectures and data-centric tools are under development [10, 87]. Smart microgrids and ADNs use intelligent control methods to enhance the network performance in terms of reliability, efficiency, and autonomous operation [13, 88, 89].

In general, different DG systems may exist in the network and their operating conditions can change over the time. Power sharing and frequency/voltage restoration are possible if DG systems are capable of communicating with the secondary controllers. DG systems that rely on RESs usually employ a maximum power point tracking (MPPT) controller which determines the reference for real power without any communications. Since DG systems contribute to the flow of power, their presence or absence affects power transfer between the network and the utility grid. The presence or absence of DG systems can also affect short

circuit currents in case of line faults [90]. Hence, IEDs and other protection schemes should be adapted to the new DG conditions [91], [92].

In conventional distribution grids, connection/disconnection of DG systems cannot be identified in real-time. Hence, inaccurate functionalities render the operation and protection of entire network susceptible to disturbances and failures. To overcome these challenges, microgrids and ADNs need a secondary mechanism to follow the presence or absence of DG systems based on the information extracted by PMUs. In light of monitoring mechanisms, the high-level control applications improve the reliability and autonomous operation of the network.

In smart microgrids, a secondary monitoring and localization system empowers the MGCC to determine active DG systems. To accomplish DG monitoring, the following DG events must be detected:

1. Disconnection event: a DG system is disconnected from the network, e.g., due to a locally detected islanding, malfunction of the DG's primary controller, or unwanted opening of the inter-connection circuit breaker.

2. Connection event: an operational DG system connects with the network, e.g., after closing the inter-connection circuit breaker.

We prove that the phasors of the CSC that are obtained at the main PCC can be modeled as complex Gaussian random processes. Basically, the flow of power at the main PCC includes contributions of numerous loads and sources. A parameter estimator is used to obtain a time-series model for the CSC based on the least-squares estimation method. The time-series model is then used by a monitoring algorithm which distinguishes between changes in generation from load changes by inspecting the norm of the forward prediction error. Moreover, the LOP method is applied to different local datasets of CSC in order to identify the location of the DG events. The performance of the secondary monitoring algorithm is assessed by numerical analysis of the probability of non-detection and also the probability of false detection.

4.1.1 Literature Review

Monitoring of DG systems is envisaged as a necessity for autonomous and reliable operation of smart grids [93, 94]. The authors in [93] and [95] propose a new monitoring approach that uses state estimation and geometric methods to detect the operational status of DG systems. This methodology aims at identifying active DG systems under both balanced and

unbalanced conditions, and requires two kinds of measurements: real-time information that can be obtained from the SCADA system, and pseudo-measurements extracted from load forecast systems. In [96], the authors discuss that online monitoring based on communications between controllers, smart switches and meters enhance the reliability and stability of microgrids. In [94], the authors deal with an optimal sensor selection strategy which employs principal component analysis (PCA) method for monitoring of energy sources in wind farms. Careful inspection of the previous works reveals that, the performance and efficiency of DG monitoring where microgrids are subject to sudden load changes and renewable energy variations are not fully addressed.

4.1.2 Contributions

The contributions of this chapter are mentioned as follows:

1. Use of fixed detection criteria (that are extracted based on offline information) is not an efficient methodology under random load/source variations. In this chapter, We first obtain an online estimator that adaptively derives a time-series model for the synchrophasors of CSC. In contrast with our approach, previous methods that deal with filtering and state estimation only use the positive sequence component of voltage signals at different buses [97, 98]. According to this approach, the transition matrix of voltage states becomes *a priori* known, and the process noise is assumed to be zero-mean. Our secondary DG monitoring method is basically a single-node but multi-component analyzer. It is based on all sequence components (positive, negative, and zero) of currents that flow into the main PCC of the microgrid.

2. Our secondary DG monitoring method depends on a PMU to obtain synchrophasors of CSC and transmission of data to the MGCC. Hence, the complexity and data communications overhead remain unchanged with changing the topology of the microgrid. Furthermore, it depends only on online data to adaptively determine the criterion for event detection and localization.

3. Unlike the existing methods [93, 94], we adopt a statistical metric to evaluate the performance of the secondary DG monitoring under random fluctuations of RESs. The numerical results indicate that, the secondary monitoring method has very good robustness against sudden load changes.

4.1.3 List of Symbols

Table 4.1 lists the symbols and their descriptions which are used throughout this chapter.

Table 4.1 List of symbols in DG monitoring system

Symbol	Description
t	time
k	Discrete time index
x	Either of the symmetrical components p, n, z
$\mathbf{p}$	Vector of aggregated real power at the main PCC
$\mathbf{q}$	Vector of aggregated reactive power at the main PCC
$\mathbf{x}(k)$	Vector of the actual phasors of the x-sequences of currents
$\mathbf{w}(k)$	Process noise vector
$\mathbf{e}(k)$	Data noise vector
$\mathbf{A}$	Transition matrix
$\mathbf{m}$	Mean vector of process noise
$\mathbf{Q}$	Covariance matrix of process noise
$\mathbf{R}$	Covariance matrix of data noise
T	Dataset update time
N	Size of estimation dataset for the main PCC
$\mathcal{D}(k)$	Estimation dataset for the main PCC
$\ell(k)$	Operational number of microgrid
N_{DG}	Number of DG systems in microgrid
Γ	Deviation coefficient for event detection
N_{PMU}	Number of PMUs deployed within microgrid
N_L	Size of local datasets
$\mathcal{D}(k; b_\nu)$	Local dataset of the node b_ν at time k
λ	Significance level for event localization
m	Nearest neighbor number
$\beta(k; b_\nu)$	LOP of the node b_ν at time k

4.2 Stochastic Analysis of the Phasors of CSC at the Main PCC

Suppose that the voltage and the current waveforms at the main PCC are expressed as [2]

$$v_{abc} = \begin{pmatrix} V_a \sin(\omega t + \theta_a) \\ V_b \sin(\omega t + \theta_b) \\ V_c \sin(\omega t + \theta_c) \end{pmatrix} \tag{4.1}$$

$$i_{abc} = \begin{pmatrix} A_a \sin(\omega t + \delta_a) \\ A_b \sin(\omega t + \delta_b) \\ A_c \sin(\omega t + \delta_c) \end{pmatrix} \tag{4.2}$$

Note that, the voltage in the above equation can generally show balanced and unbalanced three-phase signals. The main PCC's current signal is decomposed into the symmetrical components as [99]:

$$I_{abc} = I_p + I_n + I_z \tag{4.3}$$

with the subscripts p, n, and z representing the positive-, negative-, and zero-sequence components, respectively. For the rest of our analysis, the variable x represents either of these components:

$$x \in \{p, n, z\}$$

Besides, the time variable, t, is removed from the mathematical expressions. The phasors of the x-sequences of the current at the main PCC are written as [2]

$$I_x = A_x \exp(j\delta_x) = I_{x,r} + jI_{x,i}. \tag{4.4}$$

Suppose that a large number of loads and energy sources are connected to each phase of the microgrid. Under this supposition, the central limit theorem states that the algebraic sum of the powers (flowing into the main PCC) follows a Gaussian distribution [82]. In fact, many studies show that the Gaussian distribution can fairly describe the random behavior of aggregated power in distribution grids [98, 100, 101, 102, 103].

Suppose that the aggregated real and reactive powers at the main PCC of the microgrid are denoted by the vectors $\mathbf{p}$, and $\mathbf{q}$, respectively. We define these vectors as [2]

$$\mathbf{p} \triangleq [P_a \ P_b \ P_c]^T = \begin{bmatrix} A_a V_a \cos(\theta_a - \delta_a) \\ A_b V_b \cos(\theta_b - \delta_b) \\ A_c V_c \cos(\theta_c - \delta_c) \end{bmatrix} \tag{4.5}$$

$$\mathbf{q} \triangleq [Q_a \ Q_b \ Q_c]^T = \begin{bmatrix} A_a V_a \sin(\theta_a - \delta_a) \\ A_b V_b \sin(\theta_b - \delta_b) \\ A_c V_c \sin(\theta_c - \delta_c) \end{bmatrix} \tag{4.6}$$

The aggregated real and reactive powers are statistically modeled by the mean vectors and

the covariance matrices, i.e., $\mathbf{p} \sim \mathcal{N}(\bar{\mathbf{p}}, \mathbf{C}_P),\ \mathbf{q} \sim \mathcal{N}(\bar{\mathbf{q}}, \mathbf{C}_Q)$ where [2]

$$\bar{\mathbf{p}} = \mathbb{E}\{\mathbf{p}\} = [\mu_{P,a}\ \mu_{P,b}\ \mu_{P,c}]^T \tag{4.7}$$

$$\bar{\mathbf{q}} = \mathbb{E}\{\mathbf{q}\} = [\mu_{Q,a}\ \mu_{Q,b}\ \mu_{Q,c}]^T \tag{4.8}$$

$$\mathbf{C}_P = \mathbb{E}\{(\mathbf{p} - \bar{\mathbf{p}})(\mathbf{p} - \bar{\mathbf{p}})^T\} \tag{4.9}$$

$$\mathbf{C}_Q = \mathbb{E}\{(\mathbf{q} - \bar{\mathbf{q}})(\mathbf{q} - \bar{\mathbf{q}})^T\} \tag{4.10}$$

Microgrids may have three-phase loads, different types of transformer connections, and non-transposed lines. Under these conditions, the real/reactive power that flows in one phase becomes correlated with the real/reactive power in the other phases. Hence, the covariance matrices $\mathbf{C}_P$ and $\mathbf{C}_Q$ are not necessarily diagonal. It is also known that, the real power of loads can be interrelated with their reactive powers. Hence, the cross-covariance matrix is also used for statistical characterization of the random aggregated power at the main PCC [2]:

$$\mathbf{C}_{PQ} = \mathbb{E}\Big\{(\mathbf{p} - \bar{\mathbf{p}})(\mathbf{q} - \bar{\mathbf{q}})^T\Big\} \tag{4.11}$$

Now, let $\Phi = (\varphi_1, \varphi_2, \varphi_3)$ represent the set of arbitrary angles. The following trigonometric vector functions are then constructed [2]:

$$\mathbf{c}_z(\Phi) \triangleq [\cos\varphi_1\ \ \cos\varphi_2\ \ \cos\varphi_3]^T \tag{4.12}$$

$$\mathbf{c}_p(\Phi) \triangleq [\cos\varphi_1\ \ \cos(\varphi_2 + 2\pi/3)\ \ \cos(\varphi_3 - 2\pi/3)]^T \tag{4.13}$$

$$\mathbf{c}_n(\Phi) \triangleq [\cos\varphi_1\ \ \cos(\varphi_2 - 2\pi/3)\ \ \cos(\varphi_3 + 2\pi/3)]^T \tag{4.14}$$

$$\mathbf{s}_z(\Phi) \triangleq [\sin\varphi_1\ \ \sin\varphi_2\ \ \sin\varphi_3]^T \tag{4.15}$$

$$\mathbf{s}_p(\Phi) \triangleq [\sin\varphi_1\ \ \sin(\varphi_2 + 2\pi/3)\ \ \sin(\varphi_3 - 2\pi/3)]^T \tag{4.16}$$

$$\mathbf{s}_n(\Phi) \triangleq [\sin\varphi_1\ \ \sin(\varphi_2 - 2\pi/3)\ \ \sin(\varphi_3 + 2\pi/3)]^T \tag{4.17}$$

In the phasor domain the x-sequences of the current signal are given by [2]

$$I_{x,r} = \frac{1}{3}[A_a\ A_b\ A_c]\mathbf{c}_x(\delta_a, \delta_b, \delta_c) \tag{4.18}$$

$$I_{x,i} = \frac{1}{3}[A_a\ A_b\ A_c]\mathbf{s}_x(\delta_a, \delta_b, \delta_c) \tag{4.19}$$

By using Eq. (4.5), and after some mathematical manipulations, it is concluded that [2]

$$\mathbf{c}_x(\delta_a, \delta_b, \delta_c) = [\frac{1}{A_aV_a}\ \ \frac{1}{A_bV_b}\ \ \frac{1}{A_cV_c}]^T \odot \Big(\mathbf{p} \odot \mathbf{c}_x(\theta_a, \theta_b, \theta_c) + \mathbf{q} \odot \mathbf{s}_x(\theta_a, \theta_b, \theta_c)\Big), \tag{4.20}$$

and

$$\mathbf{s}_x(\delta_a, \delta_b, \delta_c) = [\frac{1}{A_a V_a} \ \frac{1}{A_b V_b} \ \frac{1}{A_c V_c}]^T \Big(\mathbf{p} \odot \mathbf{s}_x(\theta_a, \theta_b, \theta_c) - \mathbf{q} \odot \mathbf{c}_x(\theta_a, \theta_b, \theta_c) \Big), \tag{4.21}$$

In the above equations the operator $\odot$ denotes the element-wise product. By putting Eq. (4.20) into Eq. (4.18) and Eq. (4.21) into Eq. (4.19), the following relationships are derived [2]

$$I_{x,r} = \mathbf{1}_3^T \Big(\mathbf{u}_{x,c} \odot \mathbf{p} + \mathbf{u}_{x,s} \odot \mathbf{q} \Big) \tag{4.22}$$

$$I_{x,i} = \mathbf{1}_3^T \Big(\mathbf{u}_{x,s} \odot \mathbf{p} - \mathbf{u}_{x,c} \odot \mathbf{q} \Big) \tag{4.23}$$

where $\mathbf{1}_3$ is the vector with all elements equal to 1. Moreover, [2]

$$\mathbf{u}_{x,c} = \frac{1}{3} [\frac{1}{V_a} \ \frac{1}{V_b} \ \frac{1}{V_c}]^T \odot \mathbf{c}_x(\theta_a, \theta_b, \theta_c), \tag{4.24}$$

$$\mathbf{u}_{x,s} = \frac{1}{3} [\frac{1}{V_a} \ \frac{1}{V_b} \ \frac{1}{V_c}]^T \odot \mathbf{s}_x(\theta_a, \theta_b, \theta_c). \tag{4.25}$$

The previous expressions are then simplified as [2]:

$$I_{x,r} = \mathbf{u}_{x,c}^T \mathbf{p} + \mathbf{u}_{x,s}^T \mathbf{q} \tag{4.26}$$

$$I_{x,i} = \mathbf{u}_{x,s}^T \mathbf{p} - \mathbf{u}_{x,c}^T \mathbf{q} \tag{4.27}$$

The above equations indicate that, the real and imaginary parts of the phasors I_x are linear functions of the aggregated powers, given by (4.5). Note that the vectors $\mathbf{p}$ and $\mathbf{q}$ follow a Gaussian distribution. Therefore, the phasors I_x are complex Gaussian random variables. If we take the expectation of Eqs. (4.26) and (4.27), then the mean values of the real and imaginary parts are derived as [2]

$$\mu_{x,r} = \mathbf{u}_{x,c}^T \bar{\mathbf{p}} + \mathbf{u}_{x,s}^T \bar{\mathbf{q}} \tag{4.28}$$

$$\mu_{x,i} = \mathbf{u}_{x,s}^T \bar{\mathbf{p}} - \mathbf{u}_{x,c}^T \bar{\mathbf{q}} \tag{4.29}$$

Similarly, the variances of the real and imaginary parts are found as [2]

$$\sigma_{x,r}^2 = \mathbb{E}\Big\{ (I_{x,r} - \mu_{x,r})(I_{x,r} - \mu_{x,r})^T \Big\} \tag{4.30}$$

$$\sigma_{x,i}^2 = \mathbb{E}\Big\{ (I_{x,i} - \mu_{x,i})(I_{x,i} - \mu_{x,i})^T \Big\} \tag{4.31}$$

Based on Eqs. (4.26) and (4.27), it is concluded that the variances are [2]:

$$\sigma^2_{x,r} = \mathbf{u}^T_{x,c}\mathbf{C}_P\mathbf{u}_{x,c} + \mathbf{u}^T_{x,s}\mathbf{C}_Q\mathbf{u}_{x,s} + \mathbf{u}^T_{x,c}\mathbf{C}_{PQ}\mathbf{u}_{x,s} + \mathbf{u}^T_{x,s}\mathbf{C}^T_{PQ}\mathbf{u}_{x,c} \tag{4.32}$$

$$\sigma^2_{x,i} = \mathbf{u}^T_{x,s}\mathbf{C}_P\mathbf{u}_{x,s} + \mathbf{u}^T_{x,c}\mathbf{C}_Q\mathbf{u}_{x,c} - \mathbf{u}^T_{x,s}\mathbf{C}_{PQ}\mathbf{u}_{x,c} - \mathbf{u}^T_{x,c}\mathbf{C}^T_{PQ}\mathbf{u}_{x,s} \tag{4.33}$$

As a result of interactions between random loads and DG systems, the real/reactive powers vary over the time. Hence, it is plausible to assume that the phasors of CSC at the main PCC can be modeled by time-series. The time-series of the phasors of CSC is composed of Gaussian processes.

4.3 Secondary Monitoring of Distributed Generation

The main concept behind DG monitoring is that the time-series of the phasors of CSC is pertinent to the temporal behavior of DG systems belonging to the microgrid. An illustration of the proposed secondary monitoring mechanism is given in Fig. 4.1. The phasors of CSC are acquired by a PMU at the main PCC, and then reported to the MGCC by data communications links. At the secondary control level, first a parameter estimator deduces a model for the time-series of the phasors of CSC using the received data. A decision making algorithm employs the estimated model to identify disconnection or connection of DG systems in real time. Once a change in DG is detected, a secondary control algorithm sends the new commands to local controllers via control links.

4.3.1 Time-Series Modeling of The Phasors of CSC at the Main PCC

Based on the stochastic analysis presented in section 4.2, it can be concluded that the phasors of CSC at the main PCC are correlated Gaussian random processes. The MGCC receives real-time information from the main PCC and models the time-series of the phasors of the currents as a vector autoregressive process [2]:

$$\mathbf{x}(k+1) = \mathbf{A}\mathbf{x}(k) + \mathbf{w}(k), \quad k = 0, 1, 2, ... \tag{4.34}$$

where

$$\mathbf{x}(k) \triangleq \Big[I_{p,r}(k)\ I_{p,i}(k)\ I_{n,r}(k)\ I_{n,i}(k)\ I_{z,r}(k)\ I_{z,i}(k) \Big]^T \tag{4.35}$$

denotes the vector of the actual phasors of the x-sequences of currents for the time k. The matrix $\mathbf{A} \in \mathbb{R}^{6\times 6}$ shows the transition matrix and the vector $\mathbf{w}(k) \in \mathbb{R}^6$ shows the process noise vector. Suppose that the vector $\mathbf{e}(k) \in \mathbb{R}^6$ denotes the data noise vector. It is supposed

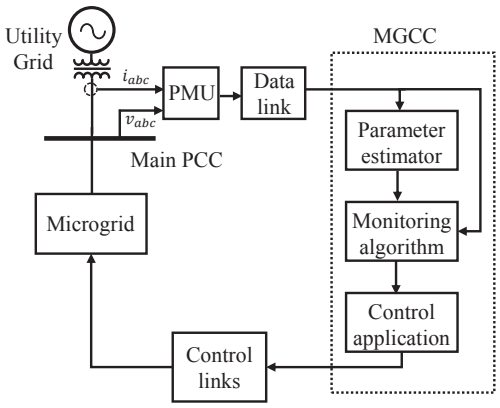

Figure 4.1 The concept of secondary monitoring and control by the MGCC in the hierarchical control structure [2]

that the data noise is independent of the process noise. The data vector is given by [2]

$$\mathbf{y}(k) = \mathbf{x}(k) + \mathbf{e}(k). \tag{4.36}$$

The process noise follows the Gaussian distribution with the following mean vector and covariance matrix [2]:

$$\mathbf{m} = \mathbb{E}\Big\{\mathbf{w}(k)\Big\} \tag{4.37}$$

$$\mathbf{Q} = \mathbb{E}\Big\{(\mathbf{w}(k) - \mathbf{m})(\mathbf{w}(k) - \mathbf{m})^T\Big\} \tag{4.38}$$

The data noise (which is a zero-mean random process) has a Gaussian probability density function (PDF) with the following covariance matrix [2]

$$\mathbf{R} = \mathbb{E}\Big\{\mathbf{e}(k)\mathbf{e}(k)^T\Big\}. \tag{4.39}$$

The vector $\mathbf{e}(k)$ is directly related to the performance of the PMU in terms of measuring the synchrophasors. Hence, $\mathbf{R}$ is *a priori* known covariance matrix. The stochastic analysis presented in section 4.2 reveals that:

- The mean of the process noise is not necessarily zero, i.e., $\mathbf{m} \neq \mathbf{0}$.
- The elements of the vectors $\mathbf{x}(k)$ are not generally zero-mean random variables.
- The process noises for different CSC can be correlated to each other, i.e., the matrix $\mathbf{Q}$ is not necessarily diagonal. The value of $\mathbf{Q}$ is a function of the covariance matrices $\mathbf{C}_P, \mathbf{C}_Q$, and $\mathbf{C}_{PQ}$.

- If the microgrid remains stable over the time, then the mean vector and the covariance matrix converge to fixed values. Moreover, the transition matrix for $\mathbf{x}(k)$ remains stable, i.e., $\max_i |\lambda_i| \leq 1$, $\lambda_i \in \mathrm{SP}(\mathbf{A})$.

4.3.2 Parameter Estimation

In order for the MGCC to have the model of the time-series of synchrophasors, the parameters $\mathbf{A}$, $\mathbf{Q}$, and $\mathbf{m}$ must be estimated. The online parameter estimators are preferred (in contrast with offline estimators) since they are more flexible and can adaptively extract information by processing the real-time data.

Definition 4.1: Dataset Update Time:
At the secondary control layer, the dataset update time denoted by T_s, is the time period between two successive arrivals of data vectors. In general, the dataset update time is larger than the reporting interval of the PMUs.

Algorithm 4.1 constructs the main PCC's dataset which updates its elements in accordance with Definition 4.1. The parameter N determines the size of the dataset.

Algorithm 4.1: Estimation Dataset for the Main PCC [2]

- Initialize: $k = 0$:
  Begin with $\mathcal{D}(0) = \{\underbrace{\mathbf{y}_0, \mathbf{y}_0, ..., \mathbf{y}_0}_{N \text{ elements}}\}$, where $\mathbf{y}_0 = [A_a \cos(\delta_a)\ A_a \sin(\delta_a)\ 0\ 0\ 0\ 0]^T$ is the initial data vector.

- Update: $\forall k \geq 1$:

  1. Obtain the data vector $\mathbf{y}(k)$ by reading the output of the data link at the time instant $t = kT_s$.
  2. Construct a temporary dataset $\tilde{\mathcal{D}}$ by removing the vector $\mathbf{y}(l|k-1)$ from $\mathcal{D}(k-1)$, where $\mathbf{y}(l|k-1) \in \mathcal{D}(k-1)$, $1 \leq l \leq N$ is the data vector whose measurement time tag is the earliest.
  3. Construct the complete dataset by appending $\mathbf{y}(k)$ to the temporary dataset:

$$\mathcal{D}(k) \triangleq \left\{\mathbf{y}_1, \mathbf{y}_2, ..., \mathbf{y}_N\right\} = \left\{\mathbf{y}(k), \tilde{\mathcal{D}}\right\} \tag{4.40}$$

After the estimation dataset for the main PCC is updated, the data vectors in $\mathcal{D}(k)$ are centered as [2]

$$\mathbf{y}'_i = \mathbf{y}_i - \frac{1}{N}\sum_{i=1}^{N}\mathbf{y}_i, \quad \mathbf{y}_i \in \mathcal{D}(k). \tag{4.41}$$

Based on the centered data, the transition matrix is estimated such that the forward prediction error is minimized for vector indices $i = 2, ..., N$. The following minimization problem is obtained [2]:

$$\hat{\mathbf{A}} = \arg\min_{\Theta} \frac{1}{N-1}\sum_{i=2}^{N} \parallel \mathbf{y}'_i - \Theta\mathbf{y}'_{i-1} \parallel^2 \tag{4.42}$$

If we solve the above minimization problem, then the least-squares estimate of the transition matrix is given by [2]

$$\hat{\mathbf{A}}(k) = \sum_{i=2}^{N} \frac{\mathbf{y}'_i \mathbf{y}'^T_{i-1}}{N-1} \left(\sum_{i=2}^{N} \frac{\mathbf{y}'_{i-1}\mathbf{y}'^T_{i-1}}{N-1} \right)^{-1} \tag{4.43}$$

Using (4.34), it is written [2]

$$\mathbf{x}(i+1) = \mathbf{A}^i\mathbf{x}(1) + \sum_{j=0}^{i-1} A^j\mathbf{w}(i-j). \tag{4.44}$$

It should be noted that $\mathbf{e}(k) \sim \mathcal{N}(0, \mathbf{R})$, hence, $\mathbb{E}\{\mathbf{y}(k)\} = \mathbb{E}\{\mathbf{x}(k)\}$. Assuming that the matrix $\mathbf{A}$ is stable (the expected value of $\mathbf{x}(k)$ converges), the mean $\mathbf{m}$ is calculated by [2]

$$\hat{\mathbf{m}}(k) = \left(\sum_{i=0}^{\infty} \hat{\mathbf{A}}^i(k) \right)^{-1} \sum_{i=1}^{N} \frac{\mathbf{y}_i}{N}. \tag{4.45}$$

Using Eqs. (4.34) and (4.36), it can be readily shown that [2]:

$$\mathbf{y}(i) - \mathbf{A}\mathbf{y}(i-1) = \mathbf{w}(i-1) + \mathbf{e}(i) - \mathbf{A}\mathbf{e}(i-1). \tag{4.46}$$

The random vectors $\mathbf{w}(i-1)$, $\mathbf{e}(i-1)$, and $\mathbf{e}(i)$ are independent, hence, the covariance matrix is estimated based on the estimate of the transition matrix and the sample means as follows

[2]:

$$\hat{\mathbf{Q}}(k) = -\mathbf{R} - \hat{\mathbf{A}}(k)\mathbf{R}\hat{\mathbf{A}}^T(k) + \frac{1}{N-1}\sum_{i=2}^{N}\left(\mathbf{y}_i - \hat{\mathbf{A}}(k)\mathbf{y}_{i-1}\right)\left(\mathbf{y}_i - \hat{\mathbf{A}}(k)\mathbf{y}_{i-1}\right)^T - \frac{1}{(N-1)^2}\left[\sum_{i=2}^{N}\left((\mathbf{y}_i - \hat{\mathbf{A}}(k)\mathbf{y}_{i-1}\right) \times \sum_{i=2}^{N}\left((\mathbf{y}_i - \hat{\mathbf{A}}(k)\mathbf{y}_{i-1}\right)^T\right] \tag{4.47}$$

Although the size of the estimation dataset is fixed (equal to N), however, it is updated every T_s seconds. Therefore, the proposed parameter estimator is adaptive and can effectively model time-varying aggregated powers at the main PCC.

4.3.3 Secondary Monitoring Algorithm

The procedure of DG monitoring based on the proposed model identification is explained in Algorithm 4.2. The output of this algorithm is the operational number of the microgrid which is defined according to Definition 4.2.

Definition 4.2: Operational Number:
The operational number of the microgrid, denoted by variable $\ell(k)$, is the estimated number of DG systems that are operational (connected to the network).

The constant N_{DG} denotes the number of DG systems that are deployed in the microgrid. The operational number always maintains the inequality $0 \leq \ell(k) \leq N_{DG}$. It is worth mentioning that, the MGCC triggers Algorithm 4.2 in a discrete-time manner, i.e., at the time instants $t = kT_s, \forall k > N$. The constant Γ is the deviation coefficient for event detection. The deviation coefficient and the size of the main PCC's dataset are two important parameters in the secondary DG monitoring. The optimal choice of theses parameters is explained in the next subsection.

Algorithm 4.2: Secondary DG Monitoring [2]:

For a given $\Gamma > 0$, $N > 0$ and $k > N$:

1. Obtain $\mathcal{D}(k)$ according to Algorithm 4.1.
2. Extract the PCC's parameters $\hat{\mathbf{A}}(k)$ and $\hat{\mathbf{m}}(k)$, based on $\mathcal{D}(k)$.

3. Calculate the forward prediction error as:

$$\varepsilon(k) = \mathbf{y}(k) - \hat{\mathbf{A}}(k-1)\mathbf{y}(u|k-1) - \hat{\mathbf{m}}(k-1), \tag{4.48}$$

where $\mathbf{y}(u|k-1) \in \mathcal{D}(k-1)$, $1 \leq u \leq N$ is the data vector whose measurement time tag is the latest.

4. Calculate the backward mean and standard deviation of norms as:

$$\mu(k) = \sum_{i=k-N}^{k-1} \frac{\|\varepsilon(i)\|}{N}, \tag{4.49}$$

$$\zeta(k) = \sqrt{\sum_{i=k-N}^{k-1} \frac{\|\varepsilon(i)\|^2}{N} - \mu(k)^2}. \tag{4.50}$$

5. Calculate the norm of the positive-sequence vector as:

$$\eta(k) = \|\mathbf{y}(k) \odot [1\ 1\ 0\ 0\ 0\ 0]^T\| \tag{4.51}$$

6. If $|\|\varepsilon(k)\| - \mu(k)| > \Gamma\zeta(k)$, then proceed to step 7, otherwise go to step 1 with time index $k+1$.

7. If $\eta(k) > \eta(k-1)$ & $\ell(k-1) \geq 1$, set $\ell(k) = \ell(k-1) - 1$.
If $\eta(k) < \eta(k-1)$ & $\ell(k-1) < N_{DG}$, set $\ell(k) = \ell(k-1) + 1$.
Otherwise, go to step 1 with time index $k+1$.

In contrast with load variations, sudden changes in DG are not predictable, a phenomenon that results in deviations from the one-step ahead predictions. Based on this premise, Algorithm 4.2 attempts to identify connection/disconnection of DG systems by comparing the norm of forward prediction error with its backward estimated mean values. It is assumed that the DG systems based on RES inject balanced currents, hence, the connection events are distinguishes from disconnection events by inspecting the norm of the positive-sequence component.

4.3.4 Performance Assessment of the Secondary DG Monitoring

Algorithm 4.2 relies on real-time data to determine the criterion for detection and decision making. This substantially improves robustness of the monitoring algorithm against variations of power consumption pattern. The accuracy of DG monitoring in terms of the operational number is crucial for high-level control and protection applications. Harsh data

noise degrades the model identification and thus lowers the reliability of DG monitoring. Moreover, DG systems that use RESs may result in random power fluctuations. The power fluctuations are detrimental to secondary DG monitoring in the sense that they decrease detectability of DG events.

The adverse impact of the previous phenomena manifests itself in the probability of false detection and probability of non-detection which are denoted by p_{fd} and p_{nd}, respectively. p_{fd} is the likelihood that a false disconnection/connection event is detected by the monitoring algorithm. p_{nd} shows the probability that a disconnection/connection event is not detected by the monitoring algorithm. In general, the optimal performance of the monitoring algorithm is achieved with the highest detection efficiency and reliability. Therefore, for a given size of the estimation dataset, the optimal value of the deviation coefficient can be found from the following equation [2]:

$$\Gamma^* = \arg\max_{\Gamma} \ (1 - p_{fd})(1 - p_{nd}). \tag{4.52}$$

It is worth mentioning that, $(1 - p_{fd})(1 - p_{nd})$ in Eq. (4.52) is the product of reliability and efficiency of detections, which can be translated to the accuracy of the estimated operational number. If this quantity is equal to unity, then the MGCC is capable of tracking all connection and disconnection events without any false alarm.

Solving Eq. (4.52) to find the maximum performance depends on a partial knowledge of power consumption by the microgrid loads. This knowledge can be obtained using either of the following load characterization methods:

- Offline knowledge: Offline methods process the recorded power consumption data and obtain empirical real/reactive power profiles for different buses. This knowledge is obtained during the design and planning of monitoring system.
- Online knowledge: Online methods collect information from smart metering devices and estimate the real/reactive power profiles [104]. This type of knowledge is almost real-time.

Online load characterization methods can be augmented to the proposed control/monitoring structure shown in Fig. 4.1. In this case, the MGCC is able to estimate the load variability by archiving and analyzing the smart metering data in real-time. In particular, the MGCC should extract the mean and variance of the real/reactive powers. Based on the derived statistics and the capacities of DG systems, the solution for Eq. (4.52) is obtained by using a

grid-search method. An advantage of using the online load characterization method is that, periodic and adaptive estimation of the monitoring parameters (N and Γ) are achieved. This improves the flexibility and efficiency of the DG monitoring system.

Synchrophasor data acquisition is subject to loss of clock reference or time synchronization, which result in reporting bad PMU data. Aside from renewable energy fluctuations and data impairments, bad synchrophasor data can deteriorate the performance of the secondary DG monitoring algorithm. Since the secondary DG monitoring algorithm depends on data extracted by a single PMU, it is crucial to filter out bad PMU data that may be reported from the main PCC. A sophisticated data validation algorithm, e.g., see [36], is able to detect bad data in real-time and replace them with the consistent data. It is also known that the measurement diversity provided by several PMUs can improve the quality of data conditioning [105]. Hence, the MGCC can prevent bad synchrophasor data from affecting the DG monitoring algorithm by employing diversity and validation methods in our proposed control/monitoring structure. The augmented structure reduces the probability of false detection and thus improves the reliability of secondary DG monitoring.

4.4 Real-Time DG Event Localization

The localization of DG events provides valuable information for real-time monitoring and reliable protection of microgrids. Generally, accurate localization of connection/disconnection events requires measurement diversity which comes at the cost of installing more measurement units in the network. By deploying PMUs at the power system nodes, the MGCC is able to find the location of the DG system that has been connected/disconnected. This important localization problem can be solved by using a local outlier detector which is explained in the sequel.

4.4.1 Local Outliers in Synchrophasor Datasets

Once the operational number of the microgrid changes, the MGCC should make decision about the location of the connected/disconnected DG system based on the received data from the PMUs. It should be highlighted that, the presence/absence of a DG system at some node affects the flow of power at the adjacent nodes. Therefore, one or more PMUs may sense such events in terms of changes in nodal voltage/current patterns. The detectability of changes in data patterns depends on the capacity and the location of the DG system with respect to the monitoring PMUs. However, upon a DG event, the reported synchrophasor data are likely to have outliers that can be detected. The following facts should be taken into account in detection of data outliers upon occurrence of a connection/disconnection event:

1. Synchrophasor datasets from different PMUs can simultaneously have outliers.

2. Renewable energy sources affect the features of synchrophasor datasets over the time.

It can be concluded that, the MGCC requires an adaptive identification algorithm to map the synchrophasor pattern changes to data outliers. The bottom line of the identification algorithm is that a degree of outlierness must be assigned to each detected outlier.

The local outlier factor (LOF) [106] and the local outlier probability (LOP) [107] are two concepts that can quantify the outlierness of a data point with respect to its dataset. In their seminal work, Breunig et al. developed a systematic approach for the LOF that assigns an density-based score to each data point [106]. The LOF method is based on the notions of k-distance (k is a positive integer) and reachability distance within neighborhoods of data points. In the LOF method, the choice of k is critical for proper scoring in different datasets. For example, a choice of k which is appropriate for a given synchrophasor dataset does not necessarily yield an accurate outlier scoring for another dataset. Moreover, the LOF method is basically designed for detection of outliers in clusters with uniform density. These drawbacks of the LOF method can also worsen the effect of data noise and may lead to unreliable detection results.

Kriegel et al. proposed the LOP concept which is a combination of density-based scoring with probabilistic concepts [107]. The LOP method is based on the notion of probabilistic distance of data points to their clusters. The main feature of the LOP method is that it includes a normalization in the probabilistic scoring of outlierness. Hence, the outlier detection becomes independent from the distribution of data. Moreover, the degree of outlierness is a number within the range $[0, 1]$ which can be interpreted as the likelihood of being an outlier. It turns out that, unlike the LOF method, the LOP method is noise tolerant and can be applied to different synchrophasor datasets. Motivated by this subtle point, we elaborate on the LOP concept in order to obtain reliable detection results in synchrophasor datasets.

4.4.2 Localization Based on the Concept of Local Outlier Probability

Suppose that N_{PMU} denotes the number of PMUs which are deployed within the microgrid (excluding the main PCC). Each PMU reports the phasors of the x-sequences of currents that flow into its associated power system bus. The observation nodes (or PMUs) are denoted by b_ν where $1 \leq \nu \leq N_{PMU}$. It should be underscored that, the PMUs may be deployed at buses which are not necessarily the local PCC of a DG system. However, to remove ambiguity from DG localization, the PMU placements should obey the condition 4.1.

Condition 4.1: Unambiguous DG Localization:
Localization of the connection/disconnection events is unambiguous if the path that connects the local PCC of a DG system to its nearest localizing PMU does not intersect with the similar path for another DG system.

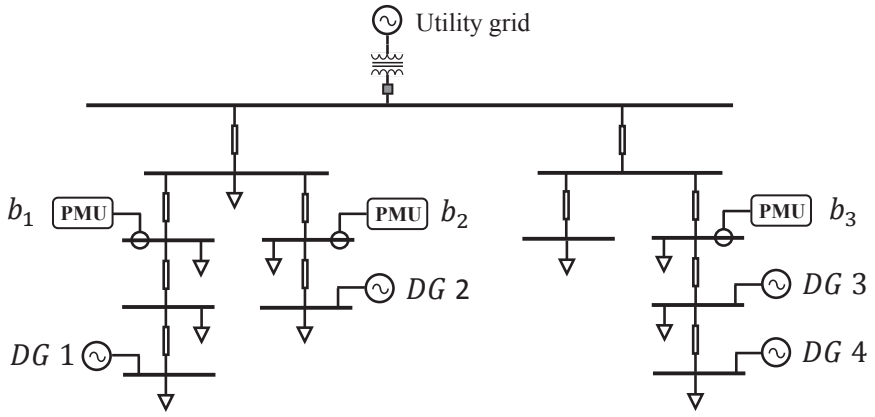

Figure 4.2 An illustration of ambiguity in localization for a radial microgrid with $N_{PMU} = 3$

Figure 4.2 shows an example of ambiguity in monitoring and localization of DG systems. This radial microgrid has four DG systems and three localizing PMUs. It is evident that, PMU b_1 is the nearest to DG 1, PMU b_2 is the nearest to DG 2, and PMU b_3 is the nearest to DG 3 and DG 4. Considering the graph of this microgrid, the path that connects the local PCC of DG 4 with PMU b_3 intersects with that of DG 3. Hence, DG Localization based on this PMU placement is not unambiguous.

Similar to (4.35), we represent data points in a six-dimensional Euclidean space

$$\mathbf{I}(k;b_\nu) \triangleq \Big[I_{p,r}(k;b_\nu)\ I_{p,i}(k;b_\nu)\ I_{n,r}(k;b_\nu)\ I_{n,i}(k;b_\nu)\ I_{z,r}(k;b_\nu)\ I_{z,i}(k;b_\nu) \Big]^T \tag{4.53}$$

In (4.53), $I_{x,r}(k;b_\nu)$ and $I_{x,i}(k;b_\nu)$ are the real and imaginary parts of the phasors of the x-sequences of currents that flow into node b_ν at time index k, respectively. The MGCC can use a mechanism similar to Algorithm 4.1 in order to construct a local dataset for each node. The local synchrophasor dataset for the node b_ν which is obtained at time index k is denoted by $\mathcal{D}(k;b_\nu)$ and is defined as in Definition 4.3.

Definition 4.3: Local Synchrophasor Dataset:
At the time index k, the local dataset of size N_L for the node b_ν is constructed as:

$$\mathcal{D}(k;b_\nu) \triangleq \Big\{\mathbf{I}(k-N_L+1;b_\nu), \mathbf{I}(k-N_L+2;b_\nu), ..., \mathbf{I}(k;b_\nu)\Big\} \tag{4.54}$$

It should be emphasized that, the update interval of the local dataset must equal the sample time for the main PCC dataset, i.e., T_s seconds. Next, we have the definition of distance between two data points that belong to the same local dataset:

Definition 4.4: Distance:
For a given node b_ν, the distance between two data points obtained at time indices k' and k'' is defined as:

$$d(k',k'';b_\nu) \triangleq \sqrt{[\mathbf{I}(k';b_\nu)-\mathbf{I}(k'';b_\nu)]^T[\mathbf{I}(k';b_\nu)-\mathbf{I}(k'';b_\nu)]} \tag{4.55}$$

Based on the concept of local dataset and Definition 4.4 for distance, the m-distance is defined as follows:

Definition 4.5: m-distance:
For a given local dataset $\mathcal{D}(k;b_\nu)$, the m-distance of the data point $\mathbf{I}(k';b_\nu) \in \mathcal{D}(k;b_\nu)$, denoted by $d_m(k';b_\nu)$, is defined as the distance between $\mathbf{I}(k';b_\nu)$ and its m-th nearest neighbor in $\mathcal{D}(k;b_\nu)$.

The above concepts allow us to define a context set for any data point, as explained in Definition 4.6.

Definition 4.6: Context set:
For a given local dataset $\mathcal{D}(k;b_\nu)$, the context set of the data point $\mathbf{I}(k'';b_\nu) \in \mathcal{D}(k;b_\nu)$,

denoted by $\mathcal{S}_m(k'';b_\nu)$, is composed of data points that satisfy the following relationship:

$$\mathcal{S}_m(k'';b_\nu) \triangleq \Big\{\mathbf{I}(k';b_\nu) \mid \mathbf{I}(k';b_\nu) \in \mathcal{D}(k;b_\nu), d(k',k'';b_\nu) \leq d_m(k'';b_\nu), k' \neq k''\Big\} \tag{4.56}$$

Algorithm 4.3 explains the procedure of DG localization based on the concept of LOP. In this algorithm, b_{ν_e} represents the monitoring node which is associated with the connection/disconnection event in the probabilistic sense. The constant λ and the operator erf(.) denote the significance level and the error function, respectively. The error function is numerically evaluated based on the following expression:

$$\text{erf}(x) = \frac{2}{\sqrt{\pi}} \int_0^x \exp(-y^2)dy \tag{4.57}$$

It is worth mentioning that the value of the significance level does not affect ranking of outliers in the local synchrophasor datasets. However, it does affect the likelihood that sudden load changes appear as outliers.

Algorithm 4.3: DG Localization Algorithm:

For a given $m > 0$, $\lambda > 0$, $1 \leq \nu \leq N_{PMU}$, and $k > N_L$:

1. Obtain the local dataset $\mathcal{D}(k;b_\nu)$
2. Extract all context sets $\mathcal{S}_m(k'';b_\nu)$ based on Eq. (4.56) and using the neighbor search method around every data point $\mathbf{I}(k'';b_\nu) \in \mathcal{D}(k;b_\nu)$
3. Calculate the standard distance for every data point $\mathbf{I}(k'';b_\nu) \in \mathcal{D}(k;b_\nu)$ as

$$\sigma_m(k'';b_\nu) = \sqrt{\frac{1}{\|\mathcal{S}_m(k'';b_\nu)\|} \sum_{k'} \Big(d^2(k',k'';b_\nu) \mid \mathbf{I}(k';b_\nu) \in \mathcal{S}_m(k'';b_\nu)\Big)} \tag{4.58}$$

4. Calculate the probabilistic local outlier factor (PLOF) as

$$\gamma(k'';b_\nu) = \frac{\sigma_m(k'';b_\nu)}{\frac{1}{\|\mathcal{S}_m(k'';b_\nu)\|} \sum_{k'} \Big(\sigma_m(k';b_\nu) \mid \mathbf{I}(k';b_\nu) \in \mathcal{S}_m(k'';b_\nu)\Big)} - 1 \tag{4.59}$$

5. Calculate the standard PLOF as

$$\alpha(k;b_\nu)=\sqrt{\frac{1}{\|\mathcal{D}(k;b_\nu)\|}\sum_{k'}\Big(\gamma^2(k';b_\nu)\mid \mathbf{I}(k';b_\nu)\in\mathcal{D}(k;b_\nu)\Big)} \tag{4.60}$$

6. Calculate the LOP

$$\beta(k'';b_\nu)=\max\left\{0,\operatorname{erf}\Big(\frac{\gamma(k'';b_\nu)}{\lambda\sqrt{2}\alpha(k;b_\nu)}\Big)\right\} \tag{4.61}$$

7. Localize the connection/disconnection event: Find the node index that shows the maximum LOP at the time index k:

$$\nu_e=\arg\max_{\nu}\ \beta(k;b_\nu) \tag{4.62}$$

In step 1 of Algorithm 4.3, the MGCC obtains N_{PMU} local datasets at the time instant $t=kT_s$. Assume that $\mathcal{D}(k;b_\nu)$ is the local dataset in which existence of an outlier is investigated. In step 2, a neighbor search method is used to extract N_L context sets for this dataset. In step 3, the standard distance of data points is calculated by finding the square root of the mean squared distance. In fact, $\sigma_m(k'';b_\nu)$ is the density around data point $\mathbf{I}(k'';b_\nu)$ based on its context set. The PLOF for data points is calculated in step 4. In (4.59), the estimated density $\sigma_m(k'';b_\nu)$ is centered and normalized by the average of the densities around all data points that belong to the context set $\mathcal{S}_m(k'';b_\nu)$.

Step 5 of Algorithm 4.3 calculates the standard PLOF based on the values of the normalized PLOFs for all data points in the dataset. Eq. (4.61) in step 6 maps the estimated PLOF into a number that lies in the interval $[0,1]$ and is interpreted as the LOP. If the value of $\beta(k'';b_\nu)$ is close to 0, then the data point $\mathbf{I}(k'';b_\nu)$ is located within a dense cluster and thus is not likely to be an outlier. The basic premise in Eq. (4.61) is that sufficiently large number of independent components are involved in the distances and thus the random PLOFs follow a Gaussian distribution. $\gamma(k'';b_\nu)\leq 0$ implies that data point $\mathbf{I}(k'';b_\nu)$ is not an outlier, and the $\max\{.,.\}$ operator is used to map such a PLOF to zero LOP. For $\gamma(k'';b_\nu)>0$, however, the error function in Eq. (4.61) shows the probability that the PLOF falls in the range $[-\gamma(k'';b_\nu),\gamma(k'';b_\nu)]$ with a significance λ.

The last step in Algorithm 4.3 identifies the location of the DG event. The localization is

based on the hypothesis that, if a connection/disconnection event is sensed by some monitoring PMUs at time index k, then the data points $\mathbf{I}(k; b_\nu)$ are outliers with respect to their associated dataset but with different scores. Therefore, in a probabilistic sense, the monitoring PMU which shows the largest LOP has the highest chance of being associated with the DG event.

4.5 Simulation Results

4.5.1 Network Simulation

The proposed DG monitoring algorithms are implemented in the IEEE 13-Bus network [108]. The single-line diagram of this distribution microgrid is illustrated in Fig. 4.3. The power circuit, monitoring PMUs, and the monitoring algorithms are simulated by MATLAB/Simulink. The short circuit power of the utility grid is 300 MVA and its short circuit ratio is equal to SCR = 7. The nominal voltage and the frequency of the microgrid are 15 kV and 60 Hz, respectively. Four DG systems driven by PV energy sources are deployed in the microgrid, i.e., $N_{DG} = 4$. The rated powers of DG systems are identical, and they are locally controlled with unity power factor by MPPT controllers. The monitoring PMU is deployed at bus 1 which is the main PCC of the microgrid. Four localizing PMUs ($N_{PMU} = 4$) are deployed at the following buses:

- Node b_1: PMU at bus 7
- Node b_2: PMU at bus 6
- Node b_3: PMU at bus 11
- Node b_4: PMU at bus 10

It can be concluded that the DG localization in this network is unambiguous.

The real/reactive powers of the loads are independent identically distributed. Table 4.2 shows the distribution of real and reactive powers of loads, where $\mathcal{U}[\alpha, \beta]$ denotes the uniform PDF over the interval $[\alpha, \beta]$. Table 4.2 gives the PDFs of powers for one statistically balanced scenario and two unbalanced scenarios with high/low degree of variability. The mean of real powers is 60 kW in both low and high variability profiles. However, the standard deviations of the real powers are 3.46 kW and 14.43 kW in the low and high variability profiles, respectively. The high variability profile in the unbalanced scenario is deliberately adopted to verify the performance of the DG monitoring approach under sudden load changes.

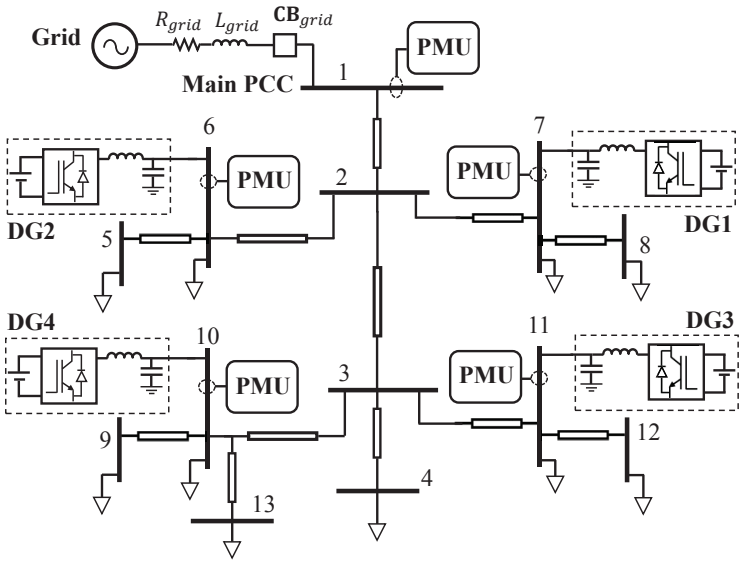

Figure 4.3 The single-line diagram of the test microgrid and the locations of DG systems and monitoring PMUs [2]

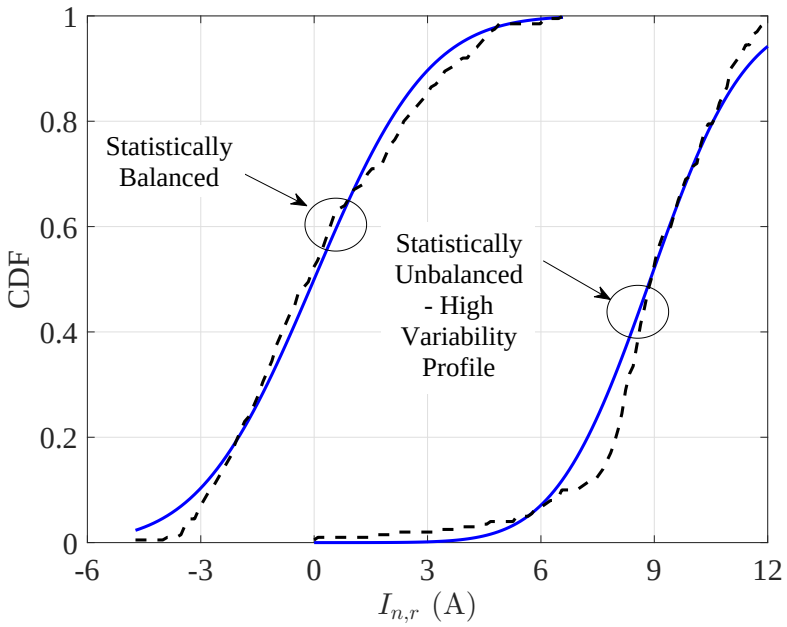

Figure 4.4 The simulated (dashed curves) and theoretical (solid curves) CDFs of $I_{n,r}(k)$ at the main PCC [2]

4.5.2 Monte Carlo Load Flow Simulations

The objective of Monte Carlo simulations is to numerically validate the stochastic analysis of the phasors of the CSC (presented in section 4.2) for the main PCC. To extract the actual

distributions of the phasors of the CSC, extensive load flow simulations are carried out with DG systems disconnected from the microgrid and negligible measurement noise. In each load flow simulation, the phasors of currents flowing into the main PCC are evaluated and stored for statistical analysis. Fig. 4.4 shows the CDFs of the real part of the phasor of the negative-sequence component. The solid and dashed curves indicate the actual CDF and the theoretical CDF of a Gaussian process, respectively. For the balanced scenario, the theoretical CDF is plotted with the mean $\mu_{n,r} = 0$, and standard deviation $\sigma_{n,r} = 2.37$. For the unbalanced scenario, the theoretical CDF has a mean $\mu_{n,r} = 8.9$ and a standard deviation $\sigma_{n,r} = 1.9$. It can be seen that the simulated CDFs match the theoretical CDFs in both scenarios. This observation corroborates the hypothesis that the synchrophasors of the CSC at the main PCC can be modeled as Gaussian processes.

4.5.3 Time-Domain Simulations

In the time-domain simulations, real/reactive power fluctuations due to operation of the DG systems are taken into account. PV variability is simulated by feeding realistic solar power data into the network. The solar power data are provided by NREL (integration studies dataset in the state of Georgia) [109]. Every 1 sec, a load is randomly selected and its real/reactive powers change in accordance with the unbalanced scenarios given in Table 4.2. Hence, the dataset update time at the secondary control layer is set as $T_s = 1$ sec. We adopt two daily scenarios with different spatio-temporal features of solar energy:

- Sunny day: clear sky condition with high degree of correlation between the powers of DG systems.
- Cloudy day: scattered clouds in the sky with low degree of correlation between the powers of DG systems

Figs. 4.5 (a) and (b) show the real powers generated by the DG systems in the aforementioned PV scenarios. It can be seen that, the highest degree of power variability occurs in the cloudy day. With respect to the secondary DG monitoring, the cloudy day represents a worst-case

Table 4.2 The distributions of the per-phase real/reactive powers of loads in different scenarios

	Statistically Balanced		Statistically Unbalanced (High Variability Profile)		Statistically Unbalanced (Low Variability Profile)	
	Active power (kW)	Reactive power (kVAr)	Active power (kW)	Reactive power (kVAr)	Active power (kW)	Reactive power (kVAr)
Phase A	$\mathcal{U}[0, 20]$	$\mathcal{U}[0, 5]$	$\mathcal{U}[20, 40]$	$\mathcal{U}[0, 20]$	$\mathcal{U}[28, 32]$	$\mathcal{U}[8, 12]$
Phase B	$\mathcal{U}[0, 20]$	$\mathcal{U}[0, 5]$	$\mathcal{U}[10, 30]$	$\mathcal{U}[0, 10]$	$\mathcal{U}[18, 22]$	$\mathcal{U}[3, 7]$
Phase C	$\mathcal{U}[0, 20]$	$\mathcal{U}[0, 5]$	$\mathcal{U}[5, 15]$	$\mathcal{U}[0, 5]$	$\mathcal{U}[8, 12]$	$\mathcal{U}[1, 5]$

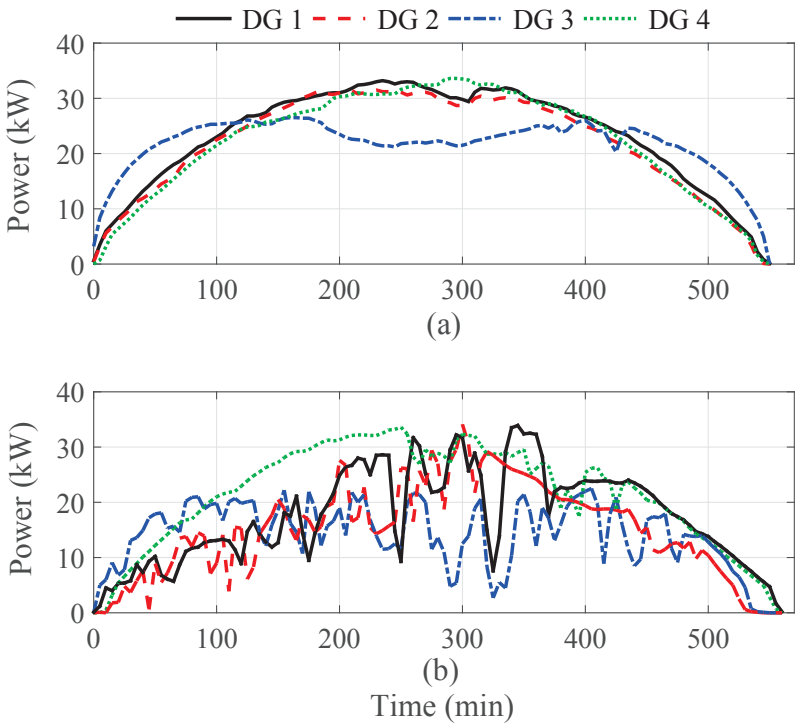

Figure 4.5 The per-phase real powers generated by DG systems in the period of one day: (a) Sunny day (b) Cloudy day [2]

scenario. It is worth mentioning that, the identical PV modules are departed enough so that they show different output patterns during cloudy day.

To assess tracking of DG events over the time, different connection and disconnection events occur according to the following sequence:

- $t = 150$ min: DG system 3 is disconnected form the microgrid.
- $t = 250$ min: DG system 4 is disconnected from the network.
- $t = 300$ min: DG system 3 reconnects with the microgrid.
- $t = 350$ min: DG system 4 reconnects with the network.

The time-domain simulation results for the sunny day are presented in Figs. 4.6-4.8. As shown in Fig. 4.6 (a), under the low variability profile, abrupt changes in the status of DG systems result in distinguishing peaks in the norm of forward prediction error. Note that under the low variability profile in the unbalanced scenario, the standard deviation of the real power of the loads is 3.46 kW. Therefore, the dispersion of the power absorbed by the loads is substantially less than the actual power of DG systems in the sunny day. As demonstrated in Fig. 4.6 (b), the DG monitoring algorithm updates the operational number of the microgrid

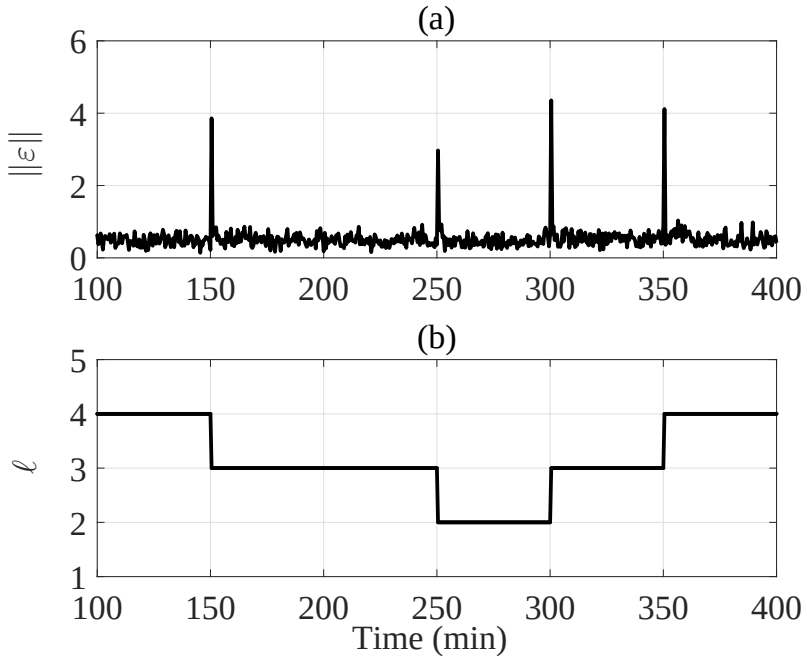

Figure 4.6 DG monitoring over the time in the unbalanced scenario with the low variability profile: $\mathbf{R} = 10^{-2}\mathbf{I}$, $N = 120$, $\Gamma = 4$ [2]

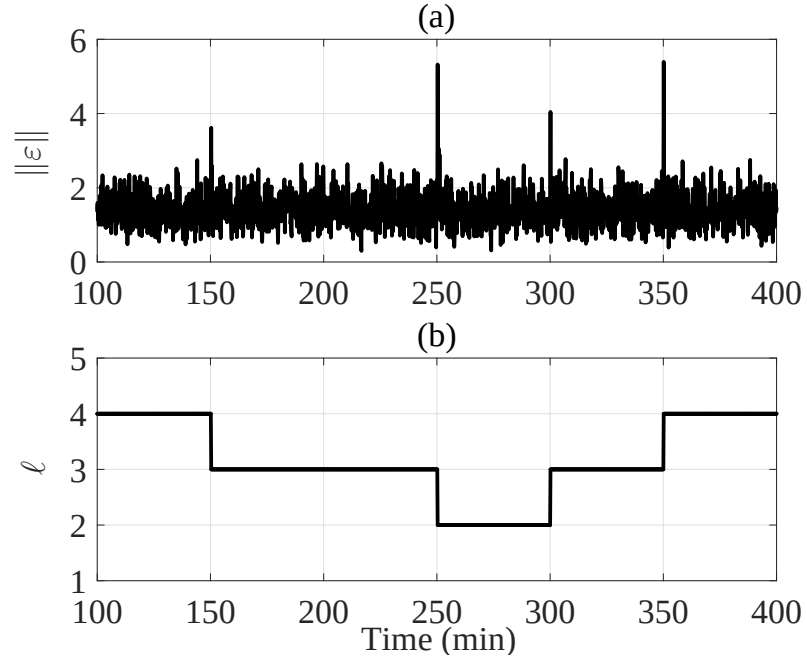

Figure 4.7 DG monitoring over the time in the unbalanced scenario with the high variability profile: $\mathbf{R} = 10^{-4}\mathbf{I}$, $N = 120$, $\Gamma = 4$ [2]

over the time.

The simulation results for the high variability load profile in the sunny day are presented in Figs. 4.7 and 4.8. By careful inspection of Fig. 4.7 (a) it can be concluded that significant load changes may lead to major deviations in the norm of forward prediction error. This observation is justified by the fact that, with the high variability profile, the standard deviation of the real power of the loads is 14.43 kW. Therefore, the dispersion of the real powers absorbed by the loads is comparable to the actual power of DG systems. Despite the abrupt changes in power consumption, the monitoring algorithm can prevent spurious events as can be seen in Fig. 4.7 (b). To elucidate the time-domain results, connection and disconnection events are detectable at the secondary control layers if the dispersion of the power consumed by local loads does not dominate over actual power of DG systems.

Fig. 4.8 demonstrates the negative impact of data noise under the high load variability profile. It can be seen that data noise along with a sudden load change at the time $t = 190$ min result in a false detection. Nevertheless, the two disconnection events at the times $t = 150$ min and $t = 250$ min and the connection event at $t = 300$ min are properly detected by the secondary monitoring algorithm. It is worth noting that, the connection of DG system 4 at the time $t = 350$ min is detectable, however, it is disregarded by the MGCC. This is due to the constraint that the operational number cannot surpass the total number of DG systems. By comparing the results shown in Figs. 4.8 and 4.6, it is concluded that the deleterious effect of noise in synchrophasor data is intensified by the high variability of loads. From the vantage point of the secondary DG monitoring, the worst case is related to the high dispersion of the load's powers and non-trivial data noise.

4.5.4 Performance Evaluation of Secondary DG Monitoring

Next, the performance the proposed secondary monitoring algorithm is assessed by extracting false alarms and non-detections in the test network. In order to numerically evaluate the statistical performance metrics, a large number of simulations are carried out. In each simulation, a DG system is randomly selected and then at a random time, belonging to the interval $[100, 500]$ min, it is disconnected from the microgrid. Fig. 4.9 depicts the probability that the secondary monitoring algorithm declares more than a false alarm in the daily scenarios. It can be seen that, it is important to properly set the size of the estimation dataset, N, in order to ensure a reliable DG monitoring. Furthermore, the DG monitoring algorithm gains higher robustness against synchrophasor noise by raising the value of the deviation coefficient, Γ. It is also worth noting that, the likelihood of a false alarm in the

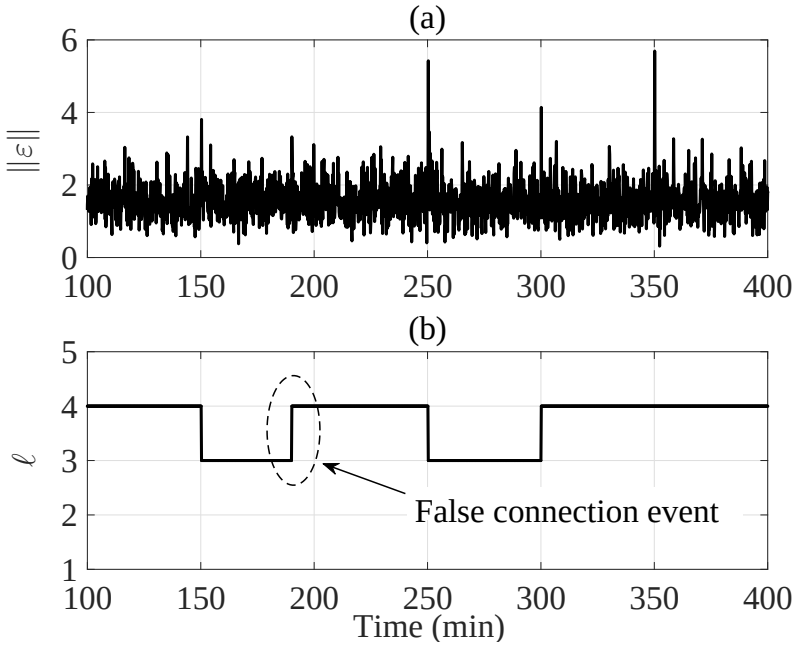

Figure 4.8 DG monitoring over the time in the unbalanced scenario with the high variability profile: $\mathbf{R} = 10^{-2}\mathbf{I}$, $N = 120$, $\Gamma = 4$ [2]

cloudy day is slightly greater in comparison with the sunny day. This observation implies that the operational number is prone to more errors under RES variability and non-trivial data noise.

The probability of non-detection versus different sizes of the estimation dataset is depicted in Fig. 4.10. It can be seen that, a proper size of the estimation dataset improves the accuracy of the parameter estimator and decreases the probability of non-detection. The monitoring algorithm is able to detect most of the disconnection/connection events in the sunny day. However, substantial renewable energy fluctuations in the cloudy can obscure DG disconnection/connection events and increase the probability of non-detection.

Figs. 4.11 and 4.12 show the efficiency of the monitoring algorithm for different values of the deviation coefficient. The simulation results given in Fig. 4.11 demonstrate the impact of load variability on DG monitoring. If the standard deviation of the real power of the loads is small enough, then the optimal value of the deviation coefficient results in the highest efficiency. Note that an efficiency equal to 100% means that the MGCC is capable of detecting all connection/disconnection events without false alarms. If the standard deviation of the real power of the loads increases, then the maximum efficiency which can be achieved is 93.4%.

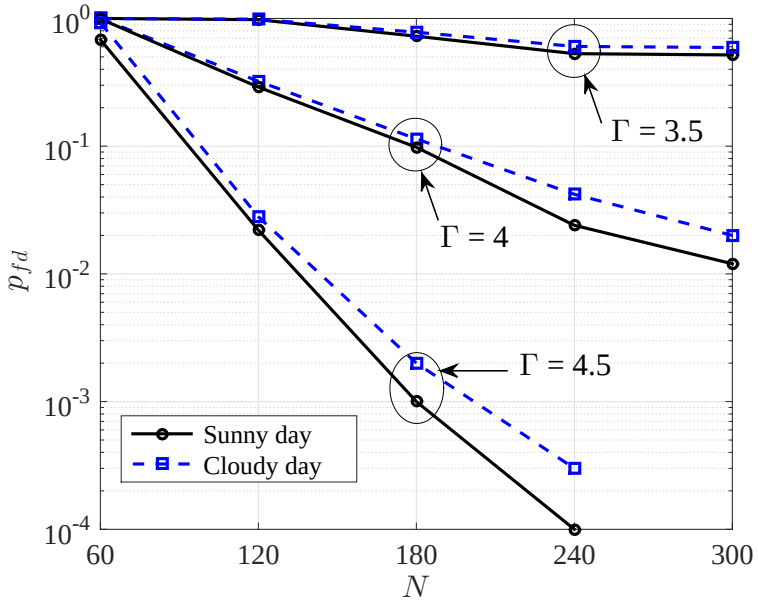

Figure 4.9 The probability of false detection vs. the size of estimation dataset: Unbalanced scenario with the high variability profile, $\mathbf{R} = 10^{-2}\mathbf{I}$ [2]

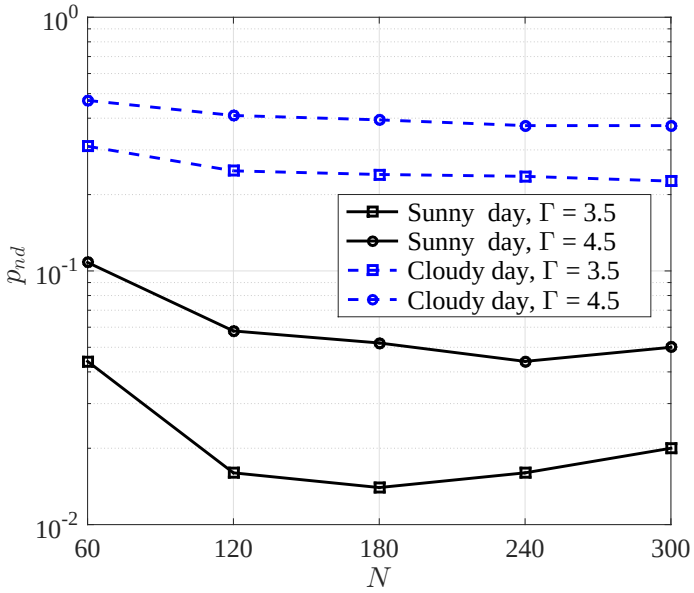

Figure 4.10 The probability of non-detection vs. the size of estimation dataset: Unbalanced scenario with the high variability profile, $\mathbf{R} = 10^{-3}\mathbf{I}$ [2]

This result reveals the extent in which the huge load changes can reduce the detectability of DG connection/disconnection events.

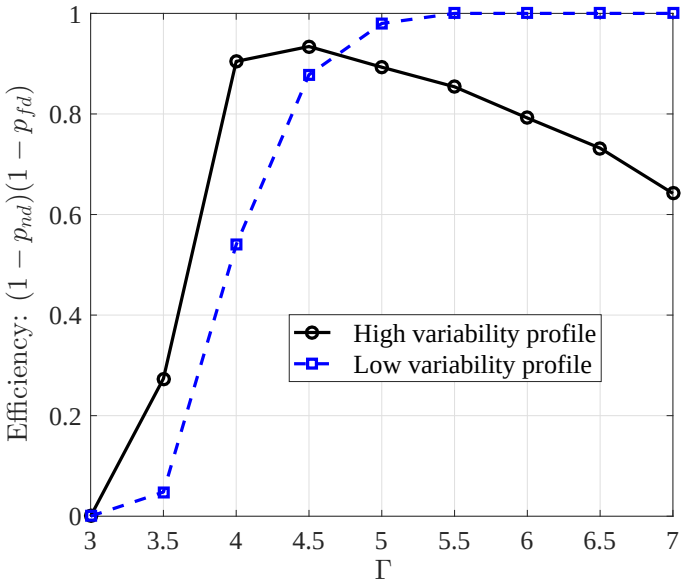

Figure 4.11 The efficiency of the monitoring algorithm as a function of the deviation coefficient: Sunny day, $\mathbf{R} = 10^{-2}\mathbf{I}$, $N = 180$ [2]

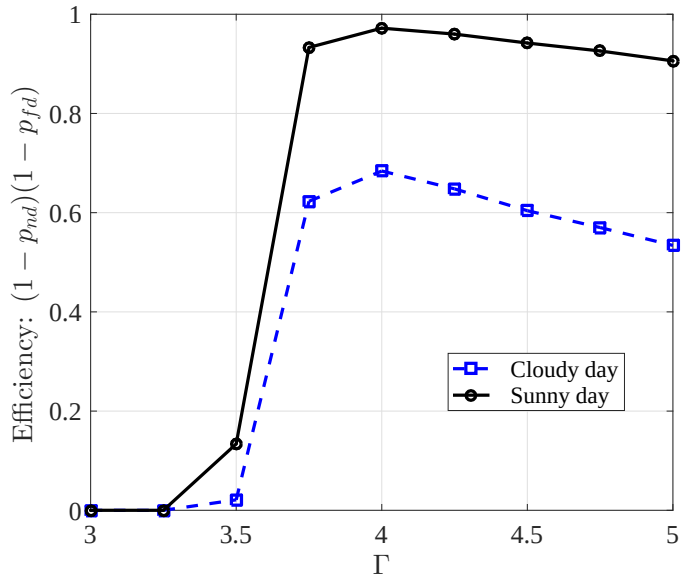

Figure 4.12 The efficiency of the monitoring algorithm as a function of the deviation coefficient: Unbalanced scenario with the high variability profile, $\mathbf{R} = 10^{-3}\mathbf{I}$, $N = 180$ [2]

Fig. 4.12 indicates how the solar energy fluctuations affect the efficiency of the monitoring algorithm. Note that the variance of the noise is decreased by 10 dB and the maximum

efficiency with the high load variability in the sunny day goes up to 97%. The result validates good robustness and high reliability of the monitoring algorithm in the presence of huge load changes and small-scale solar energy variations. The result shows that, the maximum efficiency which is achievable in the cloudy day with high load variability is 29% less than efficiency in the sunny day. In order to alleviate this problem, DS units can cooperate with DG systems to moderate solar energy fluctuations and recover the efficiency of DG monitoring in cloudy days [110].

4.5.5 DG Localization

The performance of the localization method (Algorithm 4.3) is investigated for the sunny day with the high variability profile in the unbalanced scenario. Unless otherwise stated, the localization algorithm employs the following parameters: $m = 20$, $\lambda = 6$, and $N_L = 120$.

Fig. 4.13 shows the values of LOP for the observation nodes when DG system 1 is disconnected at time 250 min. The LOP values are calculated at the detection time, i.e., when the secondary DG monitoring (Algorithm 4.2) changes the operational number of the microgrid. It can be seen that, the highest LOP is associated with the node b_1. This indicates that the disconnection of DG system 1 results in a distinguishing outlier in the local dataset of the node b_1. At this detection time, the LOPs for the observation nodes $b_2 - b_4$ are less than 0.2. Therefore, Algorithm 4.3 can localize the DG event by finding the maximum LOP among different observation nodes.

Fig. 4.14 demonstrates how the LOP for the observation node b_3 varies over the time. In this simulation, DG system 3 is disconnected at the time 150 min and then reconnects at the time 300 min. It can be seen that, the LOP is 0.9 and 0.99 at the time indices of disconnection and connection, respectively. Therefore, the disconnection and connection of DG system 3 are easily detectable. In addition to these time indices, there are three time indices that the LOP exceeds 0.6. These large LOP values are related to significant load changes at the buses 11 and 12 according to the high variability profile. The majority of LOP values in the time interval $[100, 350]$ min are less than 0.4.

Figs. 4.15 (a)-(d) compare the values of LOP for the observation nodes b_1-b_4, respectively. DG system 3 is disconnected at the time 150 min and then reconnects at the time 300 min and the significance level for outlier detection is decreased to $\lambda = 3$. Note that the LOP values for the observation node b_3 are 0.99 and 1 at the time indices of disconnection and connection, respectively. By comparing Fig. 4.15 (c) with Fig. 4.14 it turns out that the LOP of events

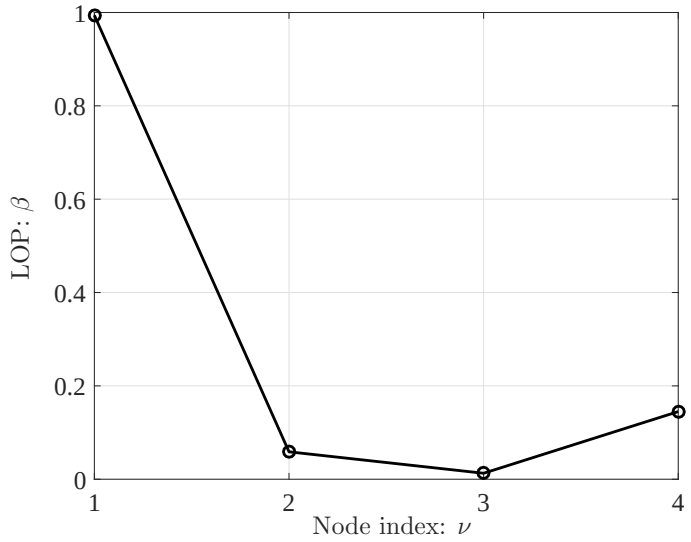

Figure 4.13 The LOPs for different observation nodes after disconnection of DG system 1

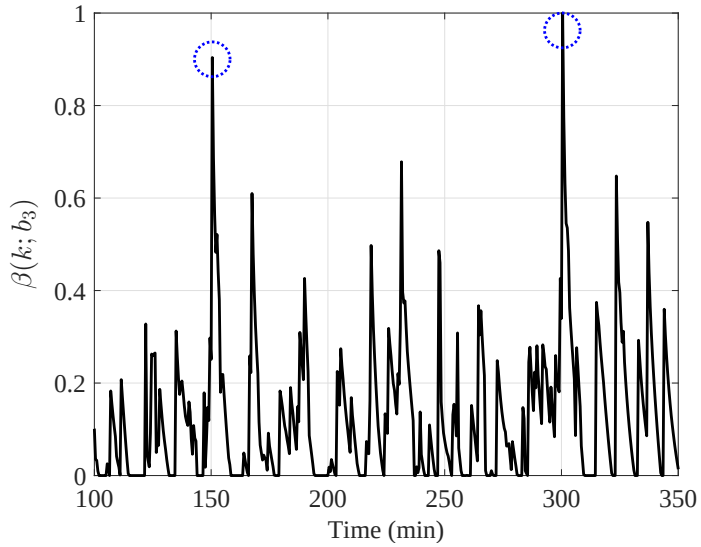

Figure 4.14 The values of LOP vs. time for the observation node b_3

are larger with smaller λ. In contrast with LOP values depicted in Fig. 4.14, the majority of LOP values are larger than 0.4. The results shown in Figs. 4.15 (a)-(d) reveal that, the disconnection/connection events are completely detectable by Algorithm 4.3. In fact, the LOP values for the node b_3 are remarkably larger than the LOP for the other observation nodes at the detection time indices. These simulation results substantiate the effectiveness of the proposed algorithm in terms of identifying DG events within the microgrid.

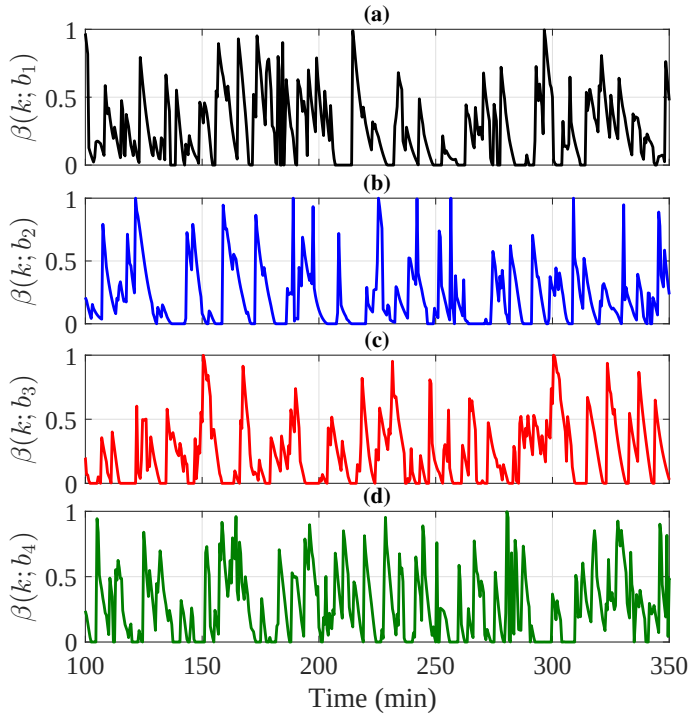

Figure 4.15 The comparison between the LOPs of different observation nodes: $\lambda = 3$

4.6 Conclusion

Adaptive model-based, and probabilistic methods for secondary monitoring of DG events are developed. By adopting our proposed algorithms, the MGCC can reliably estimate the number of operational DG systems and find the location of the systems that have changed their status. It was shown that the phasors of the CSC at the main PCC can be modeled as complex Gaussian random variables. Afterward, a least-square parameter estimator extracts the model of the phasors of the CSC. The monitoring algorithm employs the extracted model to evaluate the forward prediction errors and detect disconnection/connection events. Simulation results revealed that the proposed monitoring algorithm can properly update the detection threshold based on the previously received data. In light of this flexibility, it can reliably track the operational number of the microgrid over the time. It was shown that, the LOP method can be applied on local synchrophasor datasets in order to detect the outliers that stem from DG connection/disconnection events. When the operational number of the microgrid changes, the location of the DG events is identified by finding the maximum LOP among different observation nodes.

CHAPTER 5 COORDINATED PROTECTION AND SECONDARY CONTROL

Unlike conventional energy networks, smart grids include different technologies and integrated systems that necessitate coordination. In particular, secondary control systems should cooperate with protection systems in order to improve power quality while protecting power system components. The cooperation between protection and control systems is vital for reliable operation of distribution networks. This chapter elaborates on a new approach for backup protection and secondary control of DG systems in ADNs. The backup protection is accomplished by a centralized fault detection method which processes synchronized data in real-time. In the presence of DG systems, faults must be detected within a critical time, otherwise the post-fault stability of network is jeopardized. The primary objective of the fault detector is to identify faults which are not detected by local relays within a tolerance time. The fault detection triggers a secondary control algorithm that makes decision about the optimal setpoints of DG systems. The secondary controller (SC), which has access to archived synchrophasor datasets, calculates the real/reactive power disturbances after the fault. The proposed approach is called *coordinated protection and secondary control* which leverages restoration of voltage and frequency in the islanded part of the network. The coordination between protection and control functionalities is achievable by accounting tor the response time of the protective devices and the communications delays. The proposed mechanism is a promising method for reliable and adaptive protection that ultimately leads to improved situational awareness in ADNs.

5.1 Introduction

As discussed in Chapter 1, ADNs will employ a large number of DG systems, renewable sources, and metering/electronic devices. The power exchange in such networks is bidirectional which implies that the power can be delivered to consumers even when the network operates in the islanded mode (disconnected from the utility grid). However, the high penetration of DG systems results in new challenges in terms of hierarchical control and protection against faults [111, 112, 113].

From the network control vantage point, DG systems are classified as slave and master systems [114]. The master DG systems stabilize the voltage/frequency and are controlled as voltage source in the islanded operation mode [114, 115]. The slave DG systems are typically controlled as current source and generate real/reactive power based on the setpoints according

to a centralized/distributed control strategy. The presence of different types of DG systems in the network may result in protection issues. Short-circuit current variability, relay failure in fault clearance, and subsequent stability concerns are among the major issues that may take place in ADNs [90, 116]. The isolation of a faulty line leads to transition of a portion of the network into the islanded operation mode. The islanded subnetwork employs master/slave strategy or a droop control strategy to stabilize voltage/frequency and maintain the power quality in the acceptable range [117, 118].

5.1.1 Literature Review

Communication systems can be effectively used by hierarchical control and protection applications [119]. By virtue of communications, digital relays and IEDs are able to send and receive information and change their protection settings according to the conditions of the network [120, 121]. A communication-based relaying strategy for fast fault isolation is introduced in [122]. Based on this protection method, the network is divided into different sections for rapid restoration of power and minimal service outage. In [123], a communication-based over-current relaying method is proposed for radial distribution networks. This protection scheme requires installation of directional over-current relays at the two ends of the line. The communications systems transfer inter-tripping and blocking signals in order to isolate faults that lie in the primary protection zones of relays [123].

Protection and control schemes that account for the impact of DG systems in microgrids are discussed in [124] and [125]. The paper written by Ustun et al. [124] deals with a central protection method based on the IEC 61850 standard. Their proposed method facilitates detection of the fault current direction by updating the protection settings of the relays. In this method, the central unit should monitor the microgrid's operation mode, the status of DG systems, and the nominal current values [124]. It is known that synchronous machine-based and inverter-based DG systems can remarkably affect the microgrid stability in the fault-triggered islanded mode [125]. The authors in [125] point out that, the fault isolation time must be less than a critical value to ensure post-fault stability. Specifically, the critical isolation time depends on three factors: the loads, the control mode of DG systems (real/reactive power or voltage/frequency control), and the network control scheme (master/slave or droop-based).

Recently, synchrophasor data analysis is used for detection of faults in transmission lines [126, 61]. Identification of the faulty branch and estimation of the fault location is discussed in [126]. The fault location is estimated through the fast Fourier transform (FFT) of equiva-

lent voltage phase angles at different nodes. The authors in [61] develop a wide-area backup protection method for transmission lines. The line faults are detected based on the processing of the zero- and positive-sequence components of currents that flow into the faulty zone. The authors also propose an optimization model in order to determine the minimum number of PMUs required for their backup protection system [61].

A remarkable setback in the previously mentioned methods is that the time requirements of post-fault stability are not taken into account in the detection process. Specifically, if the network configuration undergoes some changes, e.g., by sudden connection/disconnection of DG systems, then the conventional protection methods may clear the faulty line after the critical isolation time. The late isolation of fault can jeopardize the post-fault stability of voltage/frequency in the islanded subnetwork. Another shortcoming of the existing methods is that the impacts of fault detection time and communication delays are not fully analyzed. It should be stresses that, these delays may lead to loss of coordination between protection and fault-triggered control of DG systems.

5.1.2 Contributions

In this chapter, a versatile approach is proposed which improves adaptive backup protection and centralized control systems. At the secondary control layer, a central unit receives synchrophasor data from different PMUs and identifies faults in accordance with the post-fault stability requirements. The protection and control functionalities are performed based on the processing of synchrophasor datasets and exchange of protective/control signals. A decision making algorithm finds the post-fault setpoints of real/reactive powers of DG systems that belong to the islanded subnetwork. The setpoints of DG systems are calculated by considering communication delays between the local controllers and the SC.

This chapter has two main contributions which are summarized as follows:

1. Adaptive backup protection: The proposed approach isolates line faults in a critical clearance time. This way the detector ensures the post-fault stability and improves smooth transition into the islanded operation mode. Moreover, a request-reply mechanism is devised to localize faulty segment in real-time. Spatio-temporal analysis of voltage magnitude and frequency data empowers the central detector to distinguish faults from grid disconnection events.

2. Enhanced fault-triggered control: A decision making algorithm solves a quadratic minimization problem in order to determine the post-fault reference powers of DG systems.

The decision making algorithm minimizes the total control effort and mitigates the adverse effect of communication delays. An exponential cost factor is assigned to a DG system which has a communication delay greater than the protection response time. The control mechanism is coordinated with the protective actions by transmitting control commands at the proper times.

The simulation results confirm that the proposed approach improves reliability of protection and also facilitates post-fault voltage/frequency recovery in ADNs.

5.1.3 List of Symbols

Table 5.1 lists the symbols and their descriptions which are used throughout this chapter.

5.2 Line Protection

As described in Section 2.3 PMUs, PDCs, and data communication links are the main components of synchrophasor networks. Assume that a local synchrophasor network is employed by a distribution network. The PMUs are sources of information that are connected to the local PDC via data communication links. The local PDC provides synchrophasor datasets for the secondary/central control unit of the distribution network.

The procedure of coordinated backup protection and secondary control is depicted in Fig. 5.1. As illustrated in this figure, the SC communicates with the local PDC, the digital relays, and the local controllers of DG systems. In this approach, the SC is responsible for timely detection of potential faults and management of DG systems. Moreover, the SC should coordinate control of DG systems with the critical protective actions.

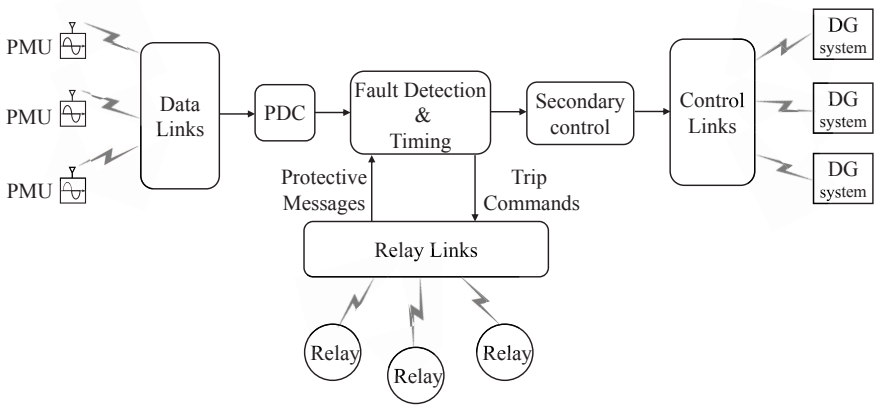

Figure 5.1 The concept of coordinated protection and control based on synchrophasor data processing in distribution grids [3]

Table 5.1 List of symbols in coordinated protection and control system

Symbol	Description
t	Time
k	Discrete time index
x	Either of the phases A,B,C
$\Delta V_x(k)$	Mean magnitude deviation for phase x
$\Delta f(k)$	Mean frequency deviation
f_n	Nominal frequency
$V_{x,n}(b_i)$	Nominal voltage magnitude of phase x of observation node b_i
$\delta_f(k)$	Range of frequency data
τ_{pmu}	PMU processing time
τ_{pdc}	PDC processing time
τ_{dat}	Time delay in the communications of synchrophasor data
F_r	Reporting rate of PMUs
τ_{ldd}	Largest data delay
$N_f(k)$	Frequency disturbance counter
$N^+_{V,x}(k)$	Over-voltage disturbance counter in phase x
$N^-_{V,x}(k)$	Under-voltage disturbance counter in phase x
δ_{il}	Islanding band
$\bar{I}_x(k; b_i, b_j)$	Normalized magnitude of the current of phase $x$in the edge (b_i, b_j)
e_{fl}	Faulty edge
T_{fl}	Fault tolerance time
T_{il}	Islanding tolerance time
Γ_f	Threshold of frequency disturbance
$\Gamma^+_{V,x}$	Threshold of over-voltage disturbance
$\Gamma^-_{V,x}$	Threshold of under-voltage disturbance
ΔP_x	Perturbation in real power
ΔQ_x	Perturbation in reactive power
k_{fl}	Fault detection index
$(P^\star_{x,i}, Q^\star_{x,i})$	Setpoint of real/reactive powers of phase x before the fault
$(P^{\star\star}_{x,i}, Q^{\star\star}_{x,i})$	Setpoint of real/reactive powers of phase x after the fault
T_{cb}	Operation time of circuit breakers
τ_{rel}	Communication delay in relay links
η	Increment constant
$T_{h,i}$	Hold times
$\tau_{ctl,i}$	Communication delay in control links

Assume that L PMUs are deployed at the distribution network and the synchrophasor data are reported at a rate of F_r fps. Under the normal (grid-connected) operation mode, the set of PMUs are represented by an undirected graph as $\mathcal{M} = (\mathcal{B}, \mathcal{E})$. The set of vertices

is denoted by $\mathcal{B} = \{b_0, b_1, ..., b_{L-1}\}$, and the set of edges is represented by $\mathcal{E}$. Each PMU is associated with a unique observation node (vertex) of the graph, $b_i \in \mathcal{B}$, and each edge $e_i \in \mathcal{E}$ represents a pair of adjacent observation nodes. The following conventions are used throughout this chapter:

- The vertex with the lowest index, b_0, represents the main PCC of the network
- Each edge is associated with two contiguous buses of the network

After isolation of the faulty line, the portion of the network which operates in the normal (grid-connected) mode is associated with a subgraph $\mathcal{M}_{gm} = (\mathcal{B}_{gm}, \mathcal{E}_{gm})$. The islanded portion of the network can potentially operate under the islanded mode and is associated with a subgraph $\mathcal{M}_{im} = (\mathcal{B}_{im}, \mathcal{E}_{im})$. Suppose that $e_{fl} \in \mathcal{E}$ is the faulty edge, i.e., the line segment incurring the fault. The subgraphs $\mathcal{M}_{gm}$ and $\mathcal{M}_{im}$ are determined by removing the edge e_{fl} from the network graph. Accordingly, the end vertices of the faulty edge will belong to the sets $\mathcal{B}_{gm}$ and $\mathcal{B}_{im}$. Similarly, the DG systems within the network can be divided into two groups. $\mathcal{G}_{im}$ and $\mathcal{G}_{gm}$ indicate the sets of DG systems that belong to the islanded and grid-connected subnetworks, respectively.

The SC has the knowledge of the type, location, and the rated power of the DG systems. Hence, it needs to find the faulty edge in order to infer the subgraphs $\mathcal{M}_{gm}$ and $\mathcal{M}_{im}$, and the DG sets $\mathcal{G}_{gm}$ and $\mathcal{G}_{im}$. An example of subgraphs of a radial ADN is shown in Fig. 5.2. In this

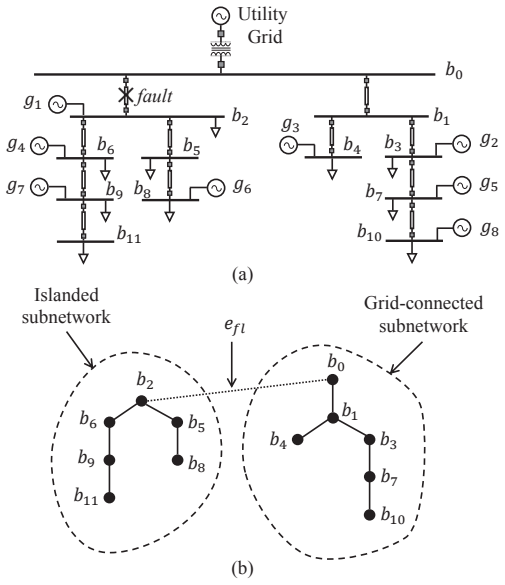

Figure 5.2 An example of formation of subnetworks due to a fault between buses b_0 and b_2

network, the edge (b_0, b_2) incurs a line fault and thus the DG sets are $\mathcal{G}_{gm} = \{g_2, g_3, g_5, g_8\}$ and $\mathcal{G}_{im} = \{g_1, g_4, g_6, g_7\}$.

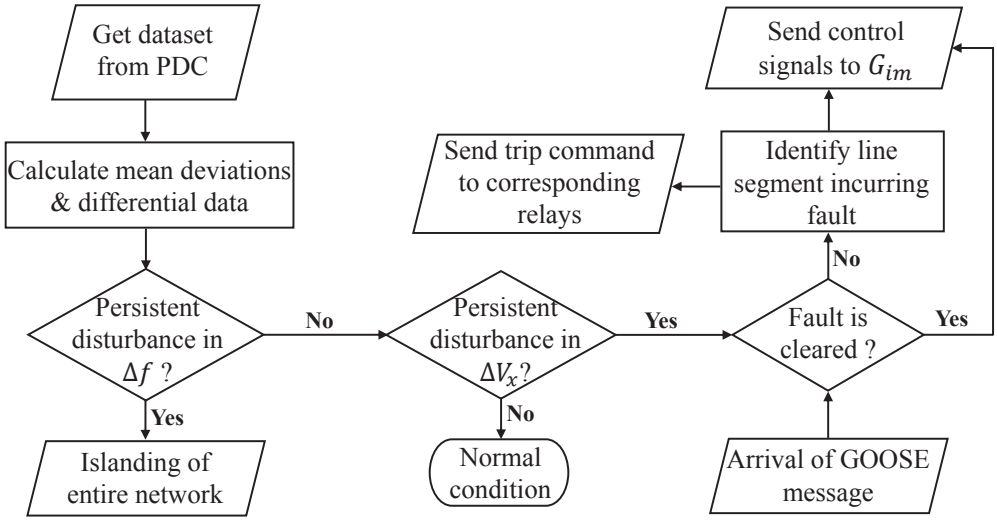

Figure 5.3 The flowchart of centralized fault identification [3]

Fig. 5.3 shows the functional flowchart of the proposed detection approach in smart distribution networks. In this chapter, the variable x represents either of the phases A,B,C:

$$x \in \{A, B, C\}$$

Suppose that $f(k; b_i)$, $V_x(k; b_i)$ and $\theta_x(k; b_i)$ denote the frequency, voltage magnitude and phase angle reported from the phase x of the node b_i at the time index k, respectively. Based on the synchrophasor dataset for the time index k, the SC calculates the mean magnitude and frequency deviations as [3]:

$$\Delta V_x(k) = \frac{1}{L} \sum_{i=0}^{L-1} \Big(V_x(k; b_i) - V_{x,n}(b_i) \Big), \tag{5.1}$$

$$\Delta f(k) = \frac{1}{L} \sum_{i=0}^{L-1} \Big(f(k; b_i) - f_n \Big), \tag{5.2}$$

In the above equations, f_n denotes the nominal frequency, and $V_{x,n}(b_i)$ shows the nominal voltage magnitude of the phase x of the observation node b_i. If the distribution network operates in off-nominal conditions then the mean magnitude/frequency deviation given by Eqs. (5.1) and (5.2) will change which can undermine the performance of the fault detector and the SC. To solve this problem the disturbance detector system is necessary. The disturbance detection system in Chapter 3 is designed to detect off-nominal conditions as fast and

reliable as possible.
As discussed in Subsection 2.3.1, the data conveyed by the synchrophasor dataset have identical measurement time. This allows the SC to measure the range of frequency data at the time index k [3]

$$\delta_f(k) \triangleq \max_i \Big\{ f(k; b_i) \Big\} - \min_i \Big\{ f(k; b_i) \Big\}, \quad b_i \in \mathcal{B} \tag{5.3}$$

A reliable fault detector should be able to differentiate faults from grid disconnection events. To this aim, it is necessary to analyze the temporal correlations in synchrophasor datasets. It should be noted that, PMUs employ parameter estimators as described in Section 3.2. This implies that when the network undergoes a transition, coupling between the estimated phasors and the frequency data is likely. Therefore, a line fault that inherently affects the phasor data can also have impacts on the frequency data. In this case, the frequency data may exhibit deviations from normal values. Basically, the system frequency is a network-wide parameter [127]. However, under the impact of faults, the frequency data reported from different observation nodes may not be consistent (assuming noiseless measurements). Therefore, the SC may observe disturbances in the reported magnitude data as well as incongruous disturbances in the reported frequency data. It is thus crucial to cope with false islanding alarms, and ensure reliability of fault detection over the entire network.

Now let t_{fl} denote the time instant that a line fault occurs in the work. Moreover, suppose that the data links in the local synchrophasor network are lossless, i.e., there is no packet dropout. As a consequence of the fault, the SC receives a series of magnitude disturbance data with a time latency. In this setting, the first synchrophasor dataset that conveys magnitude/frequency disturbance is received with a delay upper bounded by [3]:

$$\tau_{ldd} = \frac{1}{F_r} + \tau_{pmu} + \tau_{dat} + \tau_{pdc}, \tag{5.4}$$

In Eq. 5.4, τ_{pmu} and τ_{pdc} are the PMU and the PDC processing times, respectively. The parameter τ_{dat} represents the time delay in the communications of synchrophasor data. The value of τ_{dat} depends on the data communication links. The SC can take advantage of the time tags embedded in synchrophasor data packets and estimate the value of τ_{dat}. It is therefore cogent to suppose that the value of the data communication delay is constant during the detection interval, and is *a priori* known by the SC. In general, faults can occurs randomly at any time between two consecutive data reporting instants. Based on this fact, $1/F_r$ in Eq. 5.4 indicates the largest delay in the reporting of disturbance data. From the vantage point of centralized protection, Eq. (5.4) gives the worst case of delay in fault detection.

It is known that, the conventional protection systems may not isolate faults in a timely manner. This issue is likely to arise when high-capacity DG systems affect short-circuit currents [90], [116]. In this case, a backup protection scheme should detect faults within the proper time. Algorithm 5.1 explains the steps involved in the centralized detection of faults based on synchrophasor data processing. Basically, this algorithm employs three disturbance counters, namely, $N^{-}_{V,x}(k)$, $N^{+}_{V,x}(k)$, and $N_f(k)$. These counters are updated upon arrival of synchrophasor datasets and are used to identify persistent voltage/frequency disturbances.

In Algorithm 5.1, the parameter δ_{il} denotes the islanding band. The islanding band is a detection parameter that defines an upper limit for the range of frequency data expressed in Eq. 5.3. The values of $\delta_f(k)$ are compared with the islanding band to verify congruous disturbances in the reported frequency data. If the instantaneous range of frequency data remains below this band, then an islanding event can be potentially the source of the observed disturbances.

The variable $\bar{I}_x(k; b_i, b_j)$ in Algorithm 5.1 denotes the normalized magnitude of the current of phase x that flows into the edge (b_i, b_j) at time k. This parameter is calculated as [3]:

$$\bar{I}_x(k; b_i, b_j) = \frac{I_x(k; b_i, b_j)}{I_{x,n}(k; b_i, b_j)}, \quad (b_i, b_j) \in \mathcal{E} \tag{5.5}$$

In the above equation, $I_x(k; b_i, b_j)$ and $I_{x,n}(k; b_i, b_j)$ denote the reported and the nominal current magnitudes of the edge (b_i, b_j), respectively. The SC obtains the value of $I_x(k; b_i, b_j)$ by means of a request-and-reply mechanism. The SC first sends a request message to the local relays associated with the edge (b_i, b_j). Upon reception of the request message, the relays reply their instantaneously measured current. It is worth noting that, the SC has *a priori* knowledge of the nominal current magnitudes for each edge.

Algorithm 5.1: Centralized Fault Detection [3]

For $k = 0$:
Initialize $N^{-}_{V,x}(0) = N^{+}_{V,x}(0) = N_f(0) = 0$.
For $k > 0$:

1) Calculate $\Delta V_x(k)$, and $\Delta f(k)$ based on (5.1) and (5.2), and update disturbance counters:

$$N^-_{V,x}(k) = \max\left(N^-_{V,x}(k-1) + \text{sgn}\Big(\Gamma^-_{V,x} - \Delta V_x(k)\Big), 0\right) \tag{5.6}$$

$$N^+_{V,x}(k) = \max\left(N^+_{V,x}(k-1) + \text{sgn}\Big(\Delta V_x(k) - \Gamma^+_{V,x}\Big), 0\right) \tag{5.7}$$

$$N_f(k) = \max\left(N_f(k-1) + \text{sgn}\Big(|\Delta f(k)| - \Gamma_f\Big), 0\right) \tag{5.8}$$

2) Differentiate islanding events from faults:
Proceed to islanding alarm if either of the conditions (C-I) and (C-II) is met, otherwise go to step 3.

- **Condition (C-I)**: Persistent over-voltage disturbance:

$$\begin{cases} N^+_{V,x}(k)/F_r + \tau_{ldd} \geq T_{il} & \text{for at least one value of } x \\ N^-_{V,x}(k)/F_r + \tau_{ldd} < T_{fl} & \text{for the rest of values of } x \end{cases}$$

- **Condition (C-II)**: Persistent frequency disturbance:

$$\begin{cases} N_f(k)/F_r + \tau_{ldd} \geq T_{il} \\ \delta_f(k) \leq \delta_{il} \end{cases}$$

3) Detect fault:
If one of the conditions (C-III), (C-IV), (C-V) is satisfied, then set the detection index as $k_{fl} = k$ and proceed to step 4. Otherwise, go to step 1 with time index $k+1$.

- **Condition (C-III)**: Single-phase fault:

$$\begin{cases} N^-_{V,x}(k)/F_r + \tau_{ldd} \geq T_{fl}, & \text{for exactly one value of } x \\ \Delta V_x(k) > 0, & \text{for the other two values of } x \end{cases}$$

- **Condition (C-IV)**: Two-phase fault:

$$\begin{cases} N^-_{V,x}(k)/F_r + \tau_{ldd} \geq T_{fl}, & \text{for two values of } x \\ \Delta V_x(k) > 0, & \text{for the other value of } x \end{cases}$$

- **Condition (C-V)**: Three-phase fault:

$$N^{-}_{V,x}(k)/F_r + \tau_{ldd} \geq T_{fl}, \quad \text{for all values of } x$$

4) Identify faulty edge:
Identify the edge incurring the fault based on the values of the normalized fault currents:

$$e_{fl} = \arg\max_{(b_i,b_j)\in\mathcal{E}} \sum_{x|\Delta V_x(k_{fl})<0} \bar{I}_x(k_{fl}; b_i, b_j) \tag{5.9}$$

5) Trigger secondary protection & control:
Send trip command to the relays protecting the edge e_{fl}.

---

* sgn(.) is the sign function.

The constants T_{fl} and T_{il} in Algorithm 5.1 represent the fault and the possible islanding tolerance times, respectively. The constant $\Gamma^{-}_{V,x} < 0$ is the threshold of under-voltage disturbance. The constants $\Gamma^{+}_{V,x} > 0$ and $\Gamma_f > 0$ are the thresholds of over-voltage and frequency disturbance for verification of islanding events, respectively. As discussed in Chapter 4, the SC can employ elaborate data processing methods to track the presence/absence of DG systems over the time. Based on the knowledge of the operational DG systems and types of loads, the SC decides about the proper value of the fault tolerance. In this approach, the backup protection scheme satisfies the requirements of voltage/frequency stability after the fault clearance.

The frequency/voltage disturbance thresholds for fault detection are determined during the network design stage. Once the locations and the rated capacities of DG systems are known, islanding simulations are carried out to determine the islanding band δ_{il} and thresholds Γ_f, and $\Gamma^{+}_{V,x}$. It should be highlighted that, some transients due to switching, lightning, etc. can entail observable disturbances in the frequency data reported from some nodes. In this regard, Eqs. (5.1) and (5.2) attenuate the impact of such transient disturbances by averaging the deviations over all observation nodes. Hence, islanding events are verified only if such transients last longer than the islanding tolerance time. It is worth mentioning that, line faults which have very low impedance result in significant under-voltages that are observable at most of the nodes. The extent of the voltage drop varies among different observation nodes, however, the under-voltage remarkably affects the mean magnitude deviation expressed in Eq. 5.2. Fault studies/simulations are useful for finding the proper value of $\Gamma^{-}_{V,x}$ provided

that the DG systems operate at their maximum power.

Step 2 of Algorithm 5.1 verifies possible islanding events by monitoring persistent over-voltages or frequency excursions. Particularly, Condition (C-I) investigates disturbance in the form of over-voltage in at least one phase with the other phases showing normal conditions. Condition (C-II) analyzes the features of frequency data across the entire network. Upon disconnection of the network from the utility grid, the frequency data reported from observation nodes differ from the nominal frequency. The occurrence of islanding translates into congruous and persistent deviation of frequency data. This means that $\delta_f(k)$ remains in the islanding band, and the mean frequency deviation oversteps the threshold Γ_f. It should be noted that, the data extraction by PMUs is generally sensitive to the amplitude of the input voltage signals. Line faults significantly affect the voltage amplitude which in turn may result in incongruous frequency deviations. In this case, step 3 of Algorithm 5.1 proceeds to the fault verification if $\delta_f(k)$ goes beyond the islanding band. The SC detects a line fault if at least one phase shows persistent under-voltage, and the other (healthy) phases show increased voltage magnitude. In step 4 of Algorithm 5.1, the SC first acquires the magnitudes of fault currents by sending request messages to the relays via relay links. Afterward, the faulty segment is detected by searching for the edge which has the largest total normalized current. In step 5, trip commands are sent to the relays associated with the edge e_{fl} and the secondary control for $\mathcal{G}_{im}$ is triggered. This procedure is similar to direct transfer trip (DTT) scheme in which remote circuit breakers are tripped upon reception of the trip command [116]

It is worth mentioning that, the SC receives a generic object oriented substation event (GOOSE) message from the local protection system if the relays detect the fault before the tolerance time is elapsed [128], [129]. This allows the SC to determine the DG systems that belong to the islanded subnetwork and perform the DG management properly. Different steps in Algorithm 5.1 are devised such that the fault detector can differentiate faults from other events in a timely manner. In what follows, the response of the SC to a fault and the DG management procedure are discussed.

5.3 Secondary Control of Islanded Subnetwork

Assume that the SC identifies a fault on the edge $e_{fl} = (b_l, b_m)$ (through a GOOSE message or Algorithm 5.1). Fig. 5.4 shows the single-line model of the faulty segment which is connected to a load with impedance $Z_{x,l,m}$. The line impedances, that are denoted by Z_l and Z_m, are assumed to be fixed and known by the SC, and the shunt admittance is ignored. Moreover, suppose that the observation node b_l is closer to the b_0 (the main PCC)

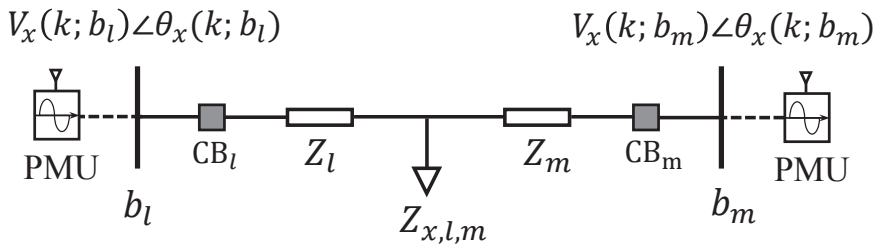

Figure 5.4 Single-phase model of the edge (b_l, b_m): Z_l and Z_m are the line impedances, $Z_{x,l,m}$ denotes the load impedance [3]

than the observation node b_m. Upon fault detection, the associated circuit breakers CB_l, CB_m operate and thus the grid-connected and islanded subnetworks are created. After this protective action is performed, the observation nodes b_l and b_m belong to the sets $\mathcal{B}_{gm}$ and $\mathcal{B}_{im}$, respectively.

One of the main functionalities of the SC is to maintain reliable operation of the network and ensure economic power exchange with the utility grid. Hence, the SC should mitigate the impact of faults on the power quality and minimize the power outage. To this aim, a control mechanism is triggered by the SC that ensure power delivery for the islanded subnetwork. The primary objective of the fault-triggered control scheme is to manage the DG systems that belong to $\mathcal{G}_{im}$ by updating their setpoints. In this method, the hierarchical droop-based control of the islanded subnetwork starts with minimal power mismatch between sources and consumers. In the islanded subnetwork, load sharing and voltage/frequency stability are achieved by a hierarchical droop control method [127], [118]. This secondary control approach results diminishes post-fault transients and improves restoration of voltage/frequency for the islanded subnetwork.

The isolation of the faulty edge e_{fl} results in changes in the real/reactive power exchanged at the node b_m. These power changes are calculated as [3]:

$$\Delta P_x = \Re\mathfrak{e}\left\{\frac{-Z^*_{x,l,m}V_mV_l^* + (Z_l^* + Z^*_{x,l,m})|V_m|^2}{Z_l^*Z_m^* + (Z_l^* + Z_m^*)Z^*_{x,l,m}}\right\} \tag{5.10}$$

$$\Delta Q_x = \Im\mathfrak{m}\left\{\frac{-Z^*_{x,l,m}V_mV_l^* + (Z_l^* + Z^*_{x,l,m})|V_m|^2}{Z_l^*Z_m^* + (Z_l^* + Z_m^*)Z^*_{x,l,m}}\right\} \tag{5.11}$$

where,

$$V_l = V_x(\nu; b_l) \exp\Big(j\theta_x(\nu; b_l)\Big), \tag{5.12}$$

$$V_m = V_x(\nu; b_m) \exp\Big(j\theta_x(\nu; b_m)\Big), \tag{5.13}$$

$$\nu = k_{fl} - \lceil T_{fl} F_r \rceil \tag{5.14}$$

The operator $\lceil y \rceil$ shows the nearest integer number that is larger than or equal to y. According to the above formulations, $\Delta P_x < 0$ ($\Delta Q_x < 0$) implies that the real (reactive) power flows from the grid-connected portion into the prospective islanded portion of the network. Once the faulty edge is detected, the SC can easily evaluate these important parameters by requesting access to the previously archived datasets in the local PDC .

Suppose that $g_{im,i} \in \mathcal{G}_{im}$ represents the i^{th} DG system that belongs to the islanded subnetwork, $1 \leq i \leq \| \mathcal{G}_{im} \|$, and $\| \mathcal{G}_{im} \| \geq 1$. Let $(P^{\star}_{x,i}, Q^{\star}_{x,i})$ denote the setpoint of real/reactive powers of phase x of $g_{im,i}$ immediately before the fault instant, i.e., when the network operates normally. Furthermore, suppose that $S_{\max,i}$ (VA) shows the maximum per-phase power of the DG system $g_{im,i}$. After detection of a faulty edge, the SC decides about the new setpoints for the DG set $\mathcal{G}_{im}$. The decision making process minimizes the total control effort and compensates for lack/excess of real/reactive powers in the islanded subnetwork. This decision making process is expressed as the minimization problem $\mathcal{P}$ with non-linear constraints for each phase, Eqs. (5.15)-(5.19) [3]. In the control problem $\mathcal{P}$, the positive number $\zeta_i > 0$ indicates the cost factor for the secondary control of the DG system $g_{im,i}$. The solution of the decision making problem $\mathcal{P}$ are found by means of an iterative trust-region method [130].

$$\mathcal{P}: \underset{\{(P_{x,i}, Q_{x,i})\}}{\text{Minimize}} \sum_{i=1}^{\|\mathcal{G}_{im}\|} \zeta_i \Big((P_{x,i} - P^{\star}_{x,i})^2 + (Q_{x,i} - Q^{\star}_{x,i})^2 \Big) \tag{5.15}$$

subject to:

$$\Delta P_x + \sum_{i=1}^{\|\mathcal{G}_{im}\|} P_{x,i} - P^{\star}_{x,i} = 0, \tag{5.16}$$

$$\Delta Q_x + \sum_{i=1}^{\|\mathcal{G}_{im}\|} Q_{x,i} - Q^{\star}_{x,i} = 0, \tag{5.17}$$

$$P^2_{x,i} + Q^2_{x,i} \leq S^2_{\max,i}, \quad i = 1, 2, ..., \| \mathcal{G}_{im} \| \tag{5.18}$$

$$P_{x,i} \geq 0, \qquad i = 1, 2, ..., \| \mathcal{G}_{im} \| \tag{5.19}$$

Communication links are employed to transfer control commands between the SC and the local controllers of DG systems. The TCP is deemed to be a reliable data communications protocol for these control links [124]. As discussed in Section 3.3, the TCP-based control links can impose communication delays. The communication delay is a probabilistic parameter of the networked control systems which varies in a known range [131]. Moreover, different control links may lead to different delays in the arrival of control signals at DG systems. It is concluded that the efficacy of the DG management mechanism depends on the communication delays. The SC is able to assess the expected value of communication delays by inspecting the acknowledgment signals in the control links. The variations of delays can be compensated by adapting the cost factors before solving the problem $\mathcal{P}$ as explained in the sequel.

Suppose that $\tau_{ctl,i}$ indicate the average communication delay in the control link between the SC and the local controller of the DG system $g_{im,i}$. From a networked control perspective, local controllers that are expected to receive commands with larger delays have higher control costs. Moreover, the SC should estimate the total time needed for the fault clearance to properly coordinate between the protection and the control of DG systems in $\mathcal{G}_{im}$. The mechanism of secondary control for the islanded subnetwork is explained in Algorithm 5.2. In this algorithm, $(P^{\star\star}_{x,i}, Q^{\star\star}_{x,i})$ are the solutions of the control problem $\mathcal{P}$ which show the optimal post-fault setpoints.

In step 3 of Algorithm 5.2, first the feasibility of droop-based islanded control for the DG set $\mathcal{G}_{im}$ is verified. If the total power demanded by loads is higher than the total capacity of DG systems in the islanded subnetwork, then a load shedding mechanism is invoked [**?** 132]. The SC triggers the load shedding in order to decrease the power consumption in the islanded subnetwork. The cost factors for secondary control of $\mathcal{G}_{im}$ are determined in step 4 of Algorithm 5.2. Equations (5.21) and (5.22) are exponential models that adjust the cost factors based on the average communication delays in control links, and the increment constant η. According to this model, the cost factors exponentially rise if control commands are likely to be applied later than the fault clearance instant.

In the proposed approach, the fault clearance time depends on two important parameters that are related to time, namely T_{cb} and τ_{rel}. T_{cb} represents the required time for the operation of the circuit breakers. τ_{rel} is the total communication delay in two-way signal communications between the relays and the SC. It should be noted that, the operation time of the circuit

breakers is a fixed parameter of the protection system, and is thus is assumed to be known by the SC. Here, a basic assumption is that the operation time of the circuit breakers is larger than the delay in relay links, i.e., $\tau_{rel} \leq T_{cb}$.

Algorithm 5.2: Secondary Control of $\mathcal{G}_{im}$ [3]

1. Calculate ΔP_x and ΔQ_x for all values of $x \in \{A, B, C\}$.

2. Calculate the total pre-fault powers for $\mathcal{G}_{im}$:

$$P_x^\star = \sum_{i=1}^{\|\mathcal{G}_{im}\|} P_{x,i}^\star, \quad Q_x^\star = \sum_{i=1}^{\|\mathcal{G}_{im}\|} Q_{x,i}^\star \tag{5.20}$$

3. If condition (C-VI) is satisfied, then proceed to the load shedding mechanism for the islanded subnetwork. Otherwise, go to step 4.

$$\textbf{(C-VI)} : \sqrt{(P_x^\star - \Delta P_x)^2 + (Q_x^\star - \Delta Q_x)^2} > \sum_{i=1}^{\|\mathcal{G}_{im}\|} S_{\max,i}$$

4. If the fault is detected by the central detector, then set the cost factors as

$$\zeta_i = \begin{cases} 1 & \tau_{ctl,i} \leq \tau_{rel} + T_{cb} \\ e^{\eta\left(\tau_{ctl,i} - \tau_{rel} - T_{cb}\right)} & \text{o.w.} \end{cases} \tag{5.21}$$

   If the fault is detected by local relays, then use

$$\zeta_i = \begin{cases} 1 & \tau_{ctl,i} \leq T_{cb} - \tau_{rel} \\ e^{\eta\left(\tau_{ctl,i} + \tau_{rel} - T_{cb}\right)} & \text{o.w.} \end{cases} \tag{5.22}$$

5. Based on the calculated cost factors in step 4, solve the problem $\mathcal{P}$ for each phase and obtain $(P_{x,i}^{\star\star}, Q_{x,i}^{\star\star})$.

6. If the fault is detected by the central detector, then calculate the hold times by:

$$T_{h,i} = \max\left(\tau_{rel} + T_{cb} - \tau_{ctl,i}, 0\right) \tag{5.23}$$

   If the fault is detected by local relays, then use:

$$T_{h,i} = \max\left(T_{cb} - \tau_{rel} - \tau_{ctl,i}, 0\right) \tag{5.24}$$

After the hold time $T_{h,i}$ is elapsed, send $(P^{\star\star}_{x,i}, Q^{\star\star}_{x,i})$ to the system $g_{im,i}$.

The SC should make decision about the time instant that the post-fault setpoints of real/reactive powers should be transfered to the local controllers. This time coordination is translated into transmission of some control commands with some delay. In other words, the signal communications start after a known hold time, denoted by $T_{h,i}$, is elapsed. The time coordination between protective actions and the management of DG systems in $\mathcal{G}_{im}$ is accomplished in step 6 of Algorithm 5.2. The hold times for coordination can be estimated based on the mean communication delay in the control links and the fault detection case (local or centralized). In this step, Eqs. (5.23) and (5.24) attempt to apply the new setpoints of DG systems after the fault clearance. According to this timing method, the DG set $\mathcal{G}_{im}$ is not likely to inject further power in the presence of the fault.

A basic assumption in Eqs. (5.21) and (5.22) is that the DG systems in the islanded subnetwork have equal response times. However, depending on their types and the technology, DG systems may have different response times upon arrival of control commands. DG systems which have larger response time require more time to change their output powers. In this case, an effective method is to associate higher cost factors to the DG systems with slower response. Therefore, the cost factors should be determined according to the total control delay. The total control delay is the sum of the control link delay and the relative response delay of the DG systems.

It should be highlighted that, the focus of this chapter is on fault-triggered management of DG systems in ADNs. In the context of hierarchical control, it is plausible to assume that the operating DG systems can receive setpoint commands from the SC. However, the proposed approach can be easily generalized to networks with both controllable and uncontrollable DG systems. To this aim, the decision making problem $\mathcal{P}$ is solved only for those DG systems which are able to receive commands from the SC. Since the real/reactive power disturbances $(\Delta P_x, \Delta Q_x)$ are found through real-time synchrophasor data, the structure of Algorithm 5.2 is not affected by the presence of uncontrollable DG systems in the network.

5.4 Simulation Results

5.4.1 Network Simulation

The proposed approach for coordinated backup protection and control of DG systems is implemented for the IEEE 34-bus distribution network with the circuit diagram shown in Fig.

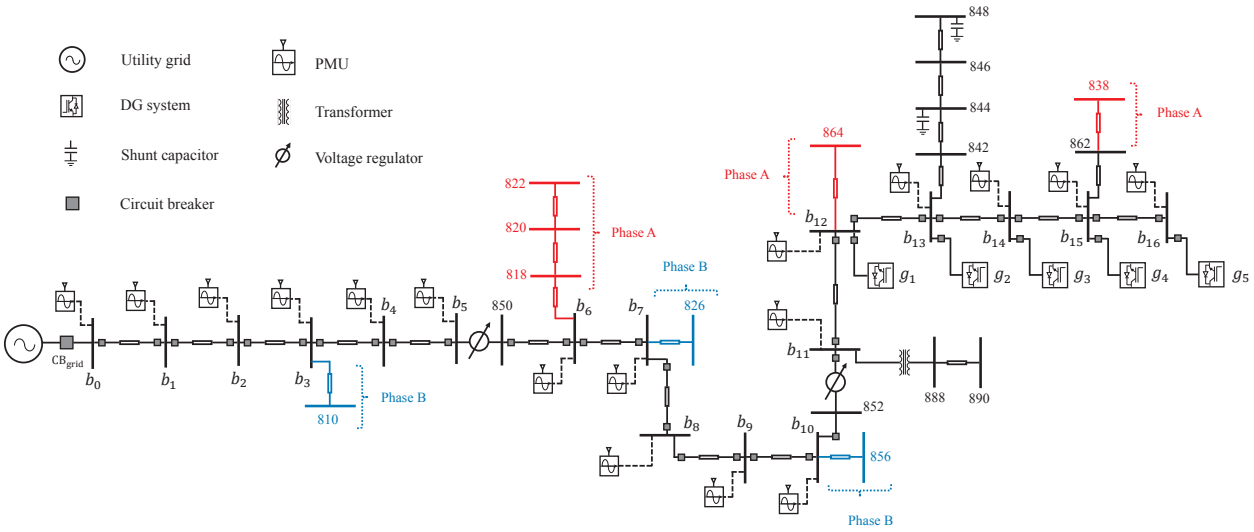

Figure 5.5 The IEEE 34-bus distribution network with DG systems, circuit breakers, and distributed PMUs [3]

5.5. The nominal system frequency is $f_n = 60$ Hz, and the nominal voltage is 24.9 kV. As shown in this figure, 17 PMUs are deployed across the main feeder and the edges belong to the set $\mathcal{E} = \{(b_i, b_{i+1}), i = 0, 1, ..., 15\}$. The parameter estimator employed by the PMUs is the UTSP (as detailed in chapter 3). A local PDC collects the synchrophasor data from the PMUs and feeds the datasets to the SC. The communications delays in the synchrophasor network are identical, and unless otherwise stated, the fault detector and the SC parameters are given in Table 5.2. As illustrated in Fig. 5.5, five inverter-based DG systems, namely $g_1 - g_5$, are connected to the observation nodes $b_{12} - b_{16}$, respectively. The inverter-based DG systems operate under balanced condition, in the current control mode, and with unity power factor. Table 5.3 gives the real powers (before the fault instant) and the per-phase capacities of DG systems.

Over-current relays are deployed in each segments of the main feeder to protect the network against line faults. The protection settings of the over-current relays are in accordance with the extremely inverse trip characteristics [133]. The circuit breakers operate after 3 cycles from arrival of the trip command. The Electromagnetic Transients Program EMTP-RV simulates the electrical part of the network and the data acquisition by PMUs. A MATLAB module is employed for solving the decision making problem $\mathcal{P}$ and management of DG systems. Different time-domain and statistical simulations are carried out for performance evaluation of the coordinated protection and control scheme.

Table 5.2 The values of parameters for centralized fault detection simulations

Parameter	Description	Value
t_f	Fault instant	1 sec
F_r	Reporting rate of PMUs	120 fps
τ_{pmu}	PMU processing time	15 msec
τ_{pdc}	PDC processing time	2 msec
τ_{dat}	Delay in synchrophasor data communications	5 msec
T_{cb}	The operation time of circuit breakers	50 msec
τ_{rel}	Delay in transfer of trip & GOOSE messages	5 msec
T_{fl}	The fault tolerance time	200 msec
Γ_f	The threshold of frequency disturbance	0.1 Hz
$\Gamma^{+}_{V,x}$	The threshold of over-voltage disturbance	0.1 p.u
$\Gamma^{-}_{V,x}$	The threshold of under-voltage disturbance	-0.2 p.u
η	The increment constant in exponential model	0.1 msec^{-1}
δ_{il}	The islanding band	1 Hz

Table 5.3 The real/reactive powers of inverter-based DG systems under the normal condition

DG system: g_i	$S_{\max,i}$ (kVA)	$P^{\star}_{x,i}$ (kW)	$Q^{\star}_{x,i}$ (kVAr)
g_1	150	10	0
g_2	120	10	0
g_3	100	10	0
g_4	90	10	0
g_5	70	10	0

5.4.2 Differentiating Faults From Islanding Events

Figs. 5.6 (a)-(c) show the simulation results when the entire network becomes isolated from the utility grid at time $t = 1$ sec. After the islanding moment, the mean frequency deviation exceeds the disturbance threshold Γ_f and thus the frequency disturbance counter increases with the arrival of data at the SC. The instantaneous range of frequency data versus the time is demonstrated in Fig. 5.6 (c). It is evident that $\delta_f(k)$ shows small-scale frequency perturbations that tend to settle around zero. It is seen that, the instantaneous range of frequency data falls below the islanding band δ_{il}. It can be concluded that the frequency disturbances are both persistent and congruous. These results satisfy the condition (C-II) in Algorithm 5.1 which is related to an islanding event.

Figs. 5.7 (a)-(c) demonstrate the simulation results in the case of a three-phase fault close to the main PCC. As can be seen in this figure, this particular fault entails incongruous deviations in the frequency data, and the frequency disturbance counter rises. However,

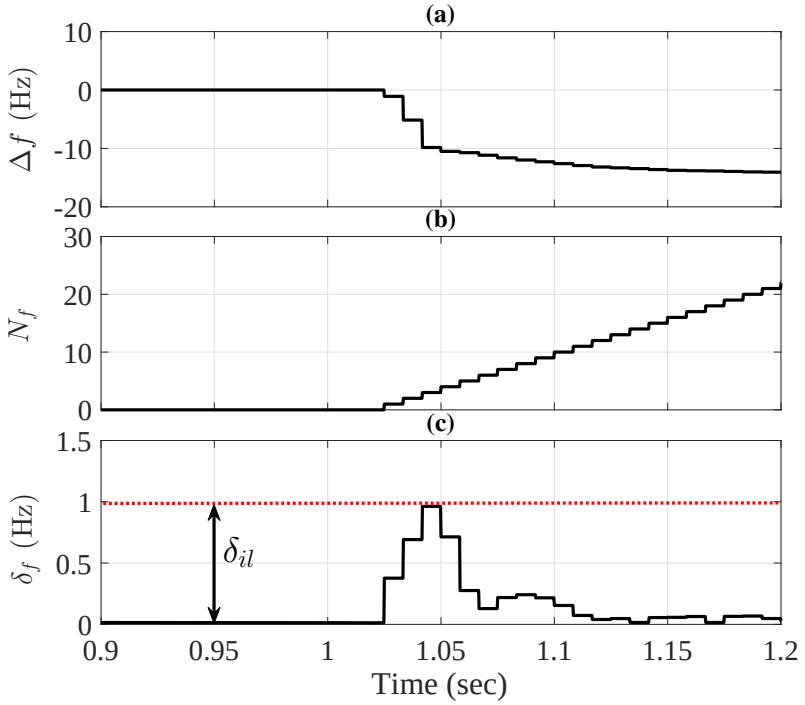

Figure 5.6 Persistent disturbance in the frequency data when the entire network becomes isolated from the utility grid at time $t = 1$ sec. (a): The mean frequency deviation, (b): The frequency disturbance counter, (c): The instantaneous range of frequency data [3]

unlike the islanding case, the instantaneous range of frequency data oversteps the islanding band. Hence, the frequency disturbances are not persistent and congruous in the case of this fault. Therefore, step 3 of Algorithm 5.1 investigates the occurrence of a fault within the network. The presented simulation results validate the effectiveness of the developed backup protection scheme. By comparing Figs. 5.6 and 5.7 in turns out that the faults can be distinguished from the islanding events by inspecting spatio-temporal features of synchrophasor data.

5.4.3 Statistical Analysis of Fault Data

Tables 5.4 and 5.5 present the statistics of voltage magnitude and frequency data when random faults occur across the main feeder. The obtained statistics give insight into the variation patterns of the reported synchrophasor data with respect to minimum, maximum and mean values. A large number of simulations have been run to extract the statistics of reported data in the presence of different types of faults. In each run, first an edge is randomly chosen and then a specified fault occurs on that edge at the fault time t_{fl}. Afterward, the frequency and voltage magnitude data which are archived by the local PDC are processed. A time window (which begins at the fault instant) with the length of 200 msec is used for statistical

analysis. For a given fault type, the mean values of reported data are calculated by averaging the archived data over all observation nodes.

The statistics shown in Table 5.4 indicate that nearly all observation nodes report sensible voltage drops in the faulty phases. The voltage magnitude data associated with the healthy phases show some temporary perturbations, but the mean values are higher than the nominal values. The results summarized in Table 5.5 demonstrate the important features of frequency data reported after the faults occur. For single-phase faults, the reported frequency data tend to incur temporary (trivial) disturbances and as it was expected, the mean value is approx-

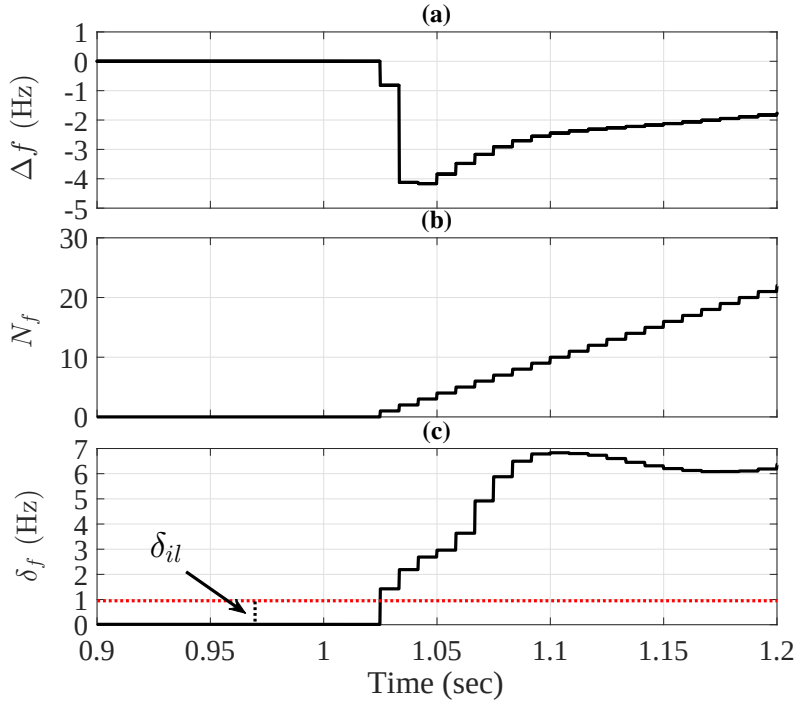

Figure 5.7 Incongruous disturbances in the frequency data when a three-phase fault occurs between nodes b_2 and b_3 at time $t = 1$ sec. (a): The mean frequency deviation, (b): The frequency disturbance counter, (c): The instantaneous range of frequency data [3]

Table 5.4 The statistics of reported voltage magnitude data for different types of faults

Fault Type	Voltage Magnitude (p.u.)								
	Phase A			Phase B			Phase C		
	Min	Max	Mean	Min	Max	Mean	Min	Max	Mean
Single-phase Fault (Phase A-Ground)	0.0002	1.0079	0.3618	0.9177	1.1819	1.0732	0.9133	1.1160	1.0347
Two-phase Fault (Phases A-B-Ground)	0.0002	1.0080	0.3726	0.0013	1.0100	0.3716	0.3111	2.1971	1.0759
Three-phase Fault (Phases A-B-C-Ground)	0.0000	1.0080	0.3540	0.0000	1.0100	0.3632	0.0000	1.0056	0.3523

imately equal to f_n. In the case of two- and three-phase faults, however, the disturbances carried by the frequency data can be significant. It is evident that the minimum and maximum values of reported frequency data are likely to deviate from the nominal value. It is worth mentioning that, the negligible amplitude of voltage signals that are measured at some nodes may influence the estimation of instantaneous frequency. Three-phase faults are severe contingencies that result in incongruous disturbances in reported frequency data, e.g., the mean of frequency data is 2.345 Hz less than the nominal value. The results for three-phase faults clarify the incongruous frequency disturbances by comparing the maximum value of the frequency data with their minimum value. These incongruous frequency disturbances are discernible when the range of frequency data does not remain within the islanding band. Algorithm 5.1 uses this detection strategy to differentiate legitimate faults from islanding events.

Table 5.5 The statistics of reported frequency data for different types of faults

Fault Type	Frequency (Hz)		
	Min	Max	Mean
Single-phase Fault (Phase A-Ground)	59.2301	62.4417	60.0246
Two-phase Fault (Phases A-B-Ground)	34.1950	86.4769	60.0323
Three-phase Fault Phases A-B-C-Ground)	52.9431	60.9863	57.6550

5.4.4 Time-Domain Scenario I: Fault Detection by Local Relays

In the first time-domain scenario, a single-phase fault occurs in the phase A of the edge (b_{13}, b_{14}). In this test, the local over-current relays identify the fault at $t = 1.173$ sec, and the detection time is less than the fault tolerance time. Therefore, the fault is locally detected by over-current relays and a GOOSE message is received by the SC at $t = 1.178$ sec. The detection index for this case is thus equal to $k_{fl} = 140$.

Fig. 5.8 shows the frequency data reported from three nodes in the network. This illustrative result reveals that the frequency data reported from different observation nodes are not necessarily identical in the presence of the fault. This figure also shows that the first dataset that conveys disturbances is received by the SC at the time $t = 1.025$ sec. This means that if the fault occurs at $t_{fl} = 1$ sec, then the data communication delay is 25 msec. It should be underscored that, the largest data delay in this synchrophasor network is $\tau_{ldd} = 30.3$ msec (calculated based on Eq. (5.4)). The mean frequency deviation and the frequency disturbance counter versus the time are plotted in Fig. 5.9. It can be seen that, N_f begins

counting at the time $t = 1.025$ sec, however, it decreases to zero after an interval of $6/F_r$. The return of this counter to zero indicates that the frequency disturbances are not persistent in the presence of this single-phase fault.

After the GOOSE message is received by the SC, the faulty edge is identified as $e_{fl} = (b_{13}, b_{14})$. In this scenario, the islanded subnetwork is associated with the DG set $\mathcal{G}_{im} = \{g_{im,1} = g_3, g_{im,2} = g_4, g_{im,3} = g_5\}$. Since the fault is detected by the local relays in a timely manner, the response time of the protection system is equal to 45 msec. The SC uses Eq. (5.22) to calculate the exponential cost factors for decision making. The performance of the SC in terms of post-fault voltage recovery in scenario I is demonstrated in Fig. 5.10. Fig. 5.10 (a) shows the voltage signal provided that the communication delays in control links are all equal to 40 msec (smaller than the protection response time). The islanded subnetwork experience the voltage signal shown in Fig. 5.10 (b) when the delay of control signals for DGs g_4 and g_5 increases to 100 msec (larger than the protection response time). Regardless of the higher communication delay, the SC can successfully manage DG systems and the voltage signal is quickly restored. This result confirms that, the use of exponential cost factors in the control problem $\mathcal{P}$ can effectively compensate for the delay spread of control links. Finally, Fig. 5.10 (c) shows the voltage signal in islanded subnetwork when the delays of control links are not taken into account in the decision making problem $\mathcal{P}$. It is concluded that, the SC

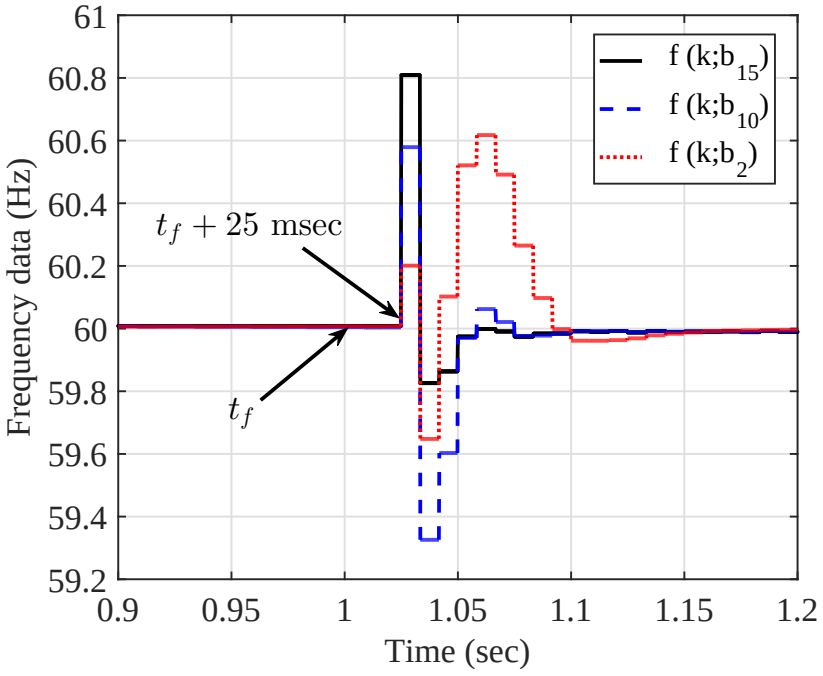

Figure 5.8 The Frequency data of three nodes in scenario I [3]

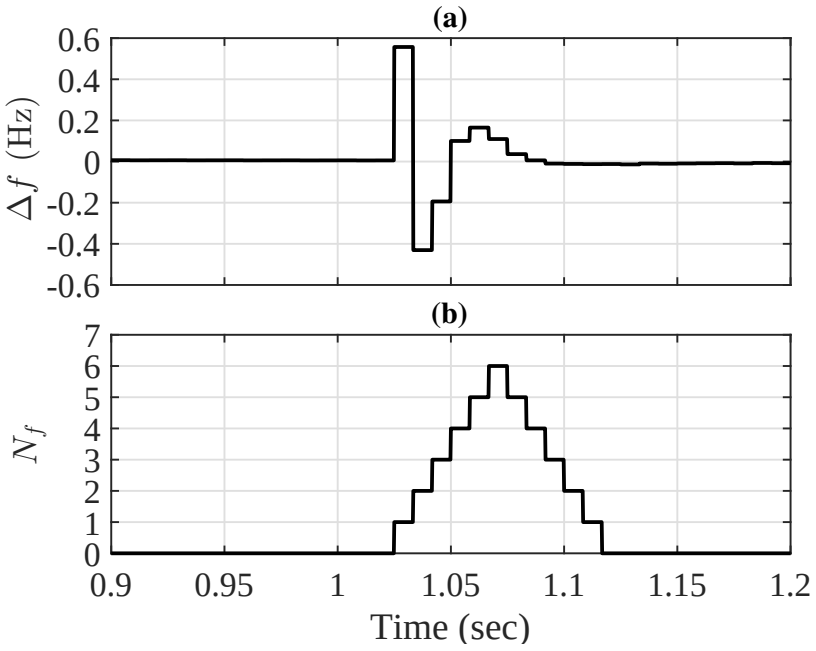

Figure 5.9 Temporary disturbance in the frequency data when the network is subject to line fault in scenario I. (a) The mean frequency deviation, (b) The frequency disturbance counter [3]

can maintain the balance of power after the fault clearance, although higher communication delays result in slower voltage restoration.

It should be noted that, the reported frequency data are estimates of the actual frequency in the islanded subnetwork, however, they are useful in evaluation of the post-fault transients. Figs. 5.11 (a)-(c) illustrate the average values of frequency data, denoted by $\bar{f}$, in Scenario I. The values of $\bar{f}$ for the islanded subnetwork are calculated based on the following equation [3]

$$\bar{f}(k) = \frac{1}{\parallel \mathcal{G}_{im} \parallel} \sum_{\mathcal{B}_{im}} f(k; b_i), \quad \mathcal{B}_{im} = \{b_{14}, b_{15}, b_{16}\}$$

A quick frequency restoration is achieved when the delays are smaller than the protection response time, as shown in Fig. 5.11 (a). A comparison between Fig. 5.11 (b) and (c) again confirms that the proposed decision making algorithm counteracts the negative effect of communication delays if they surpass the protection response time. The numerical results demonstrated in Figs. 5.10 and 5.11 corroborate the advantages of cooperation between the local protection systems and the SC for fast and reliable voltage/frequency recovery in the islanded subnetwork.

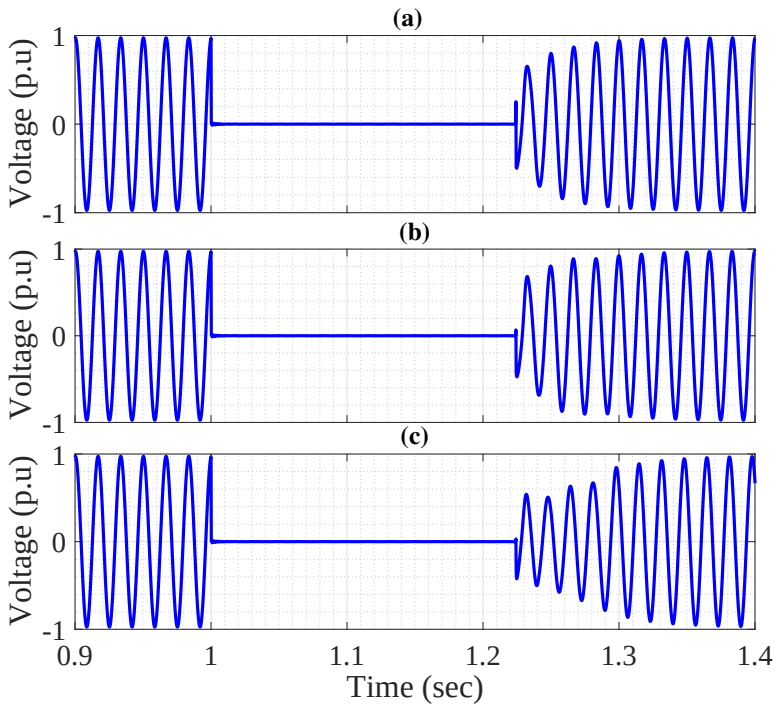

Figure 5.10 The voltage waveform of phase A of observation node b_{16} in scenario I: (a) $\tau_{ctl,1} = \tau_{ctl,2} = \tau_{ctl,3} = 40$ msec, (b) $\tau_{ctl,1} = 40, \tau_{ctl,2} = \tau_{ctl,3} = 100$ msec, with exponential cost factors (c) $\tau_{ctl,1} = 40, \tau_{ctl,2} = \tau_{ctl,3} = 100$ msec, with unity cost factors $\zeta_i = 1$ [3]

5.4.5 Time-Domain Scenario II: Centralized Fault Detection

In this scenario, a line-to-ground fault occurs in the phase A of the edge (b_8, b_9), and the over-current relays detect the fault at the time $t = 1.242$ sec. Hence, in this case, the detection time of the local protection system (242 msec) is longer than the fault tolerance time. Therefore, the fault should be identified by the SC and the protective messages are sent to the relays associated with the faulty edge. The detection index in this scenario is found as $k_{fl} = 143$ and the faulty edge can be identified through Eq. (5.9). Algorithm 5.1 can localize the faulty edge by detecting the edge that exhibits the largest normalized fault current, as shown in Fig. 5.12.

Figs. 5.13 (a) and (d) indicate that the line fault in this case yields persistent under-voltage disturbances in the phase A. As it is clear in Figs. 5.13 (b) and (c), the healthy phases (B and C) show positive values of mean magnitude deviation. The result shown in Fig. 5.13 (d) reveals that the SC can detect the fault as soon as the magnitude disturbance counter, $N^{-}_{V,A}$, equals 21 at the time $t = 1.192$ sec. These simulation results demonstrate that when the local protection system is not fast enough, the proposed backup protection scheme properly

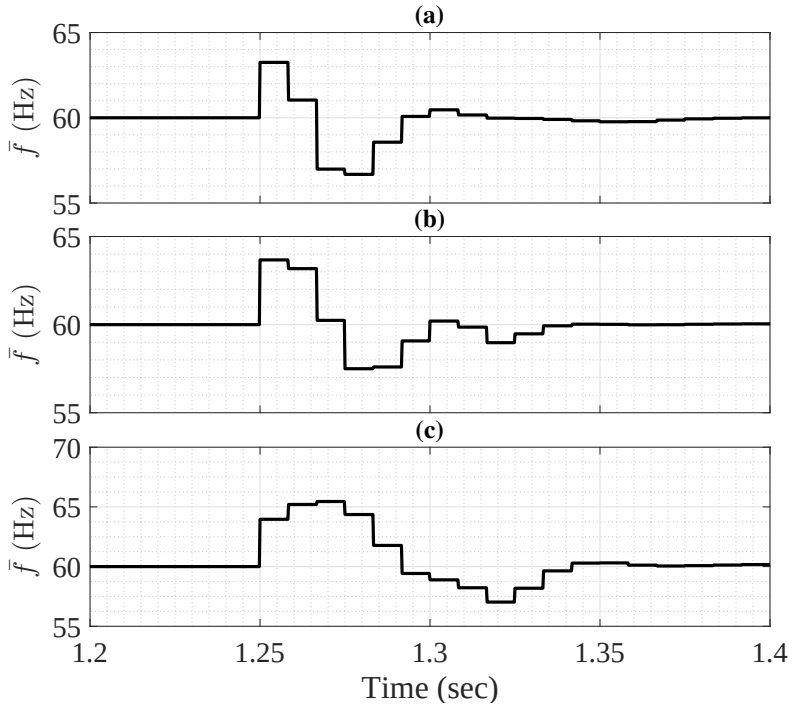

Figure 5.11 The average values of frequency data after isolation of fault in scenario I: (a) $\tau_{ctl,1} = \tau_{ctl,2} = \tau_{ctl,3} = 40$ msec, (b) $\tau_{ctl,1} = 40, \tau_{ctl,2} = \tau_{ctl,3} = 100$ msec, with exponential cost factors (c) $\tau_{ctl,1} = 40, \tau_{ctl,2} = \tau_{ctl,3} = 100$ msec, with unity cost factors $\zeta_i = 1$ [3]

detects the fault within the fault tolerance time .

Figs. 5.14 (a) and (b) show the voltages of phase B versus time in Scenario II. In this case, the DG set of the islanded subnetwork is $\mathcal{G}_{im} = \{g_{im,i}\} = \{g_1, ..., g_5\}$ and the delays associated with their control links are: $\tau_{ctl,1} = 60$ msec, $\tau_{ctl,2} = 80$ msec, $\tau_{ctl,3} = 100$ msec, $\tau_{ctl,4} = 70$ msec, and $\tau_{ctl,5} = 120$ msec. It is evident that the communication delays in control links are larger than the response time of the protection system, which is equal to 55 msec. By ignoring the delays of the control links the cost factors for all DG systems are unity. Hence, the delay dispersion of links is not taken into account in decision making problem and the post-fault voltages exhibit more distortions as shown in Fig. 5.14 (a). However, Fig. 5.14 (b) confirms that the voltage of the islanded subnetwork incurs fewer distortions by using the exponential cost model and including the delays of control links in the problem $\mathcal{P}$.

Fig. 5.15 shows the optimal post-fault apparent powers that the decision maker determined for different DG systems in the islanded subnetwork. It is seen that, if the dispersion of delays in control links are not taken into account, then a uniform power allocation is decided for the the DG set $\mathcal{G}_{im}$. In this particular case, the post-fault apparent powers of all DG

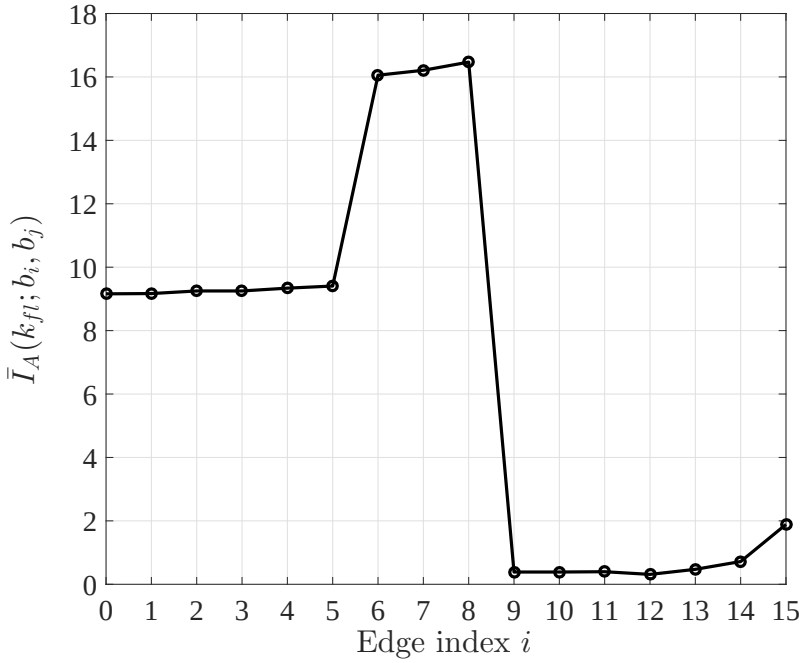

Figure 5.12 The normalized fault currents in Scenario II: $k = k_{fl}$ [3]

systems are 49 kVA. By using the exponential cost factors in the decision making process a non-uniform power allocation is obtained, which is tailored to the communications and capacity constraints of DG systems. As shown in Fig. 5.14 (b), DG system g_1 which has the shortest communications delay generates power near its rated power. This adaptive power allocation improves the response of the DG systems to the fault isolation event.

5.4.6 Scenario III: Fault in the Presence of Machine-Based DG Systems

In this time-domain scenario, the fault isolation and secondary control mechanisms are investigated in the presence of a machine-based DG in addition to the inverter-based DG systems. The conventional machine-based DG is a synchronous machine with rated power of 300 kVA. This DG system is connected to the observation node b_{10} via a step-up transformer with delta-wye connections and 13.8 kV to 24.9 kV voltage ratings. The faulty segment is the edge (b_8, b_9) which incurs a three-phase fault at the time instant $t_f = 1$ sec. The communication delays in the control links of the machine- and inverter-based DG systems are equal to 40 msec. In this scenario, if the fault tolerance time of the backup protection is 200 msec, then the local over-current protection system detects the fault at $t = 1.166$ sec. Under this circumstance, the SC receives a GOOSE message at $t = 1.171$ sec.

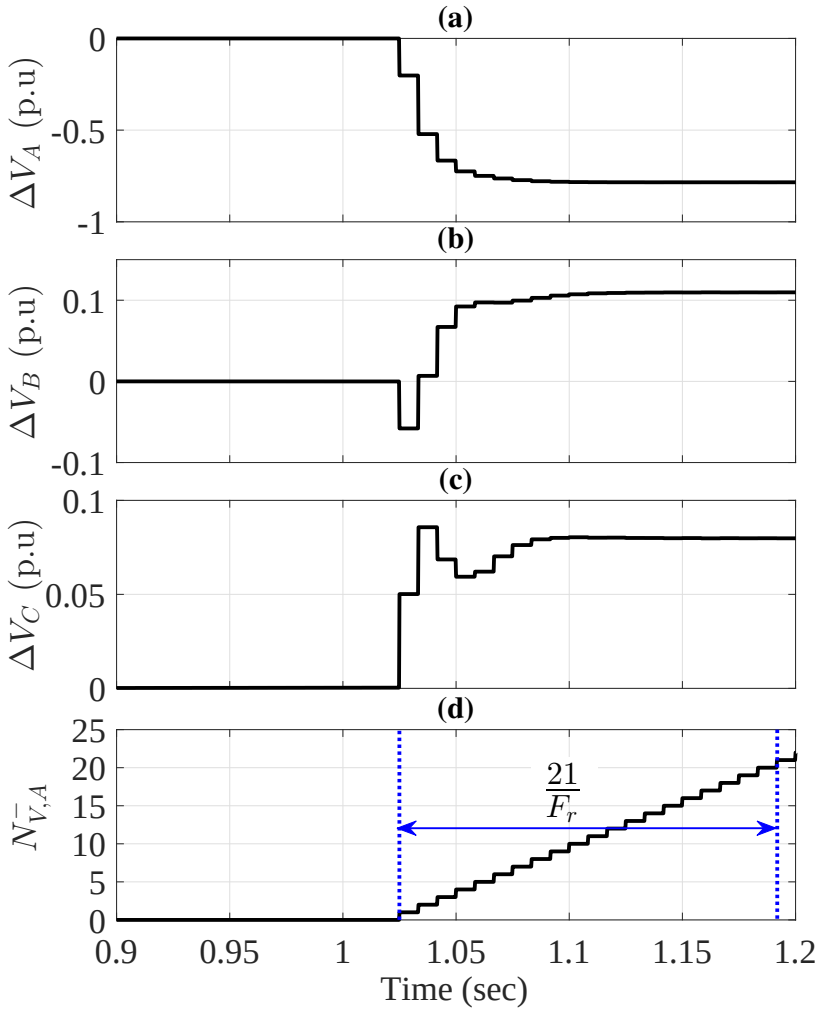

Figure 5.13 Persistent magnitude disturbance in scenario II: (a)-(c) The mean magnitude deviation for phases A-C, (d): The magnitude disturbance counter for phase A [3]

Fig. 5.16 (a) illustrates the voltage magnitude data versus time when the fault detection is carried out by over-current relays. In this case, the slower response of conventional machine-based DG system is ignored in the decision making problem. The result shown in Fig. 5.16 (a) reveal that the isolation of the fault entails post-fault voltage distortions that gradually disappear in the presence of the conventional machine-based DG system. This poor performance can be justified by the fact that the DG management by the SC is not tailored to the actual post-fault DG conditions in the islanded subnetwork.

The post-fault voltage distortions can be significantly diminished by decreasing the fault tolerance time and including the relative response time of the machine-based DG system, as shown in Fig. 5.16 (b). In this test, the fault tolerance time is reduced to 30 msec

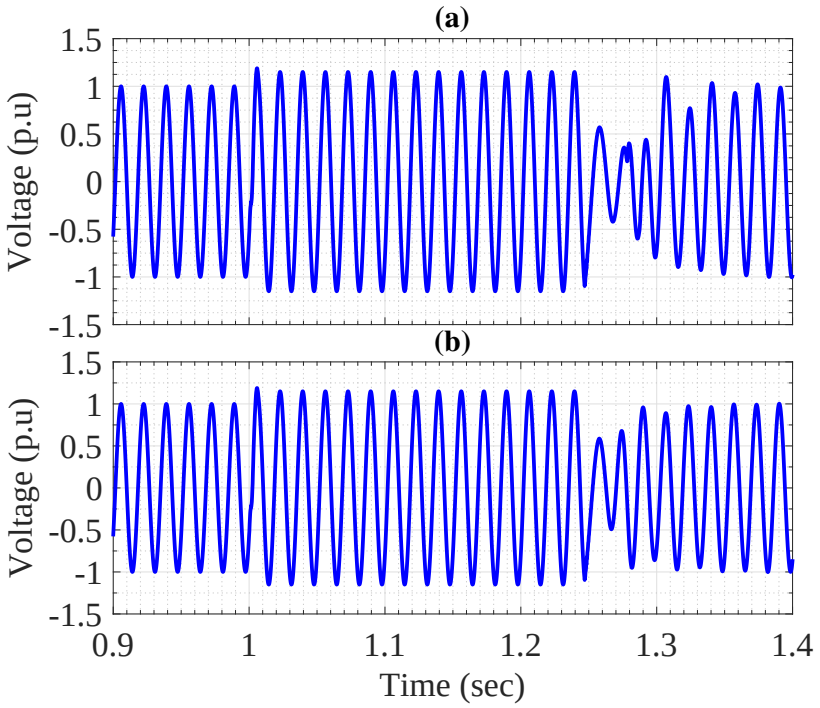

Figure 5.14 The voltage waveform of phase B of observation node b_{13} in scenario II: (a) With unity cost factors $\zeta_i = 1$, (b) With exponential cost factors given by (5.21) [3]

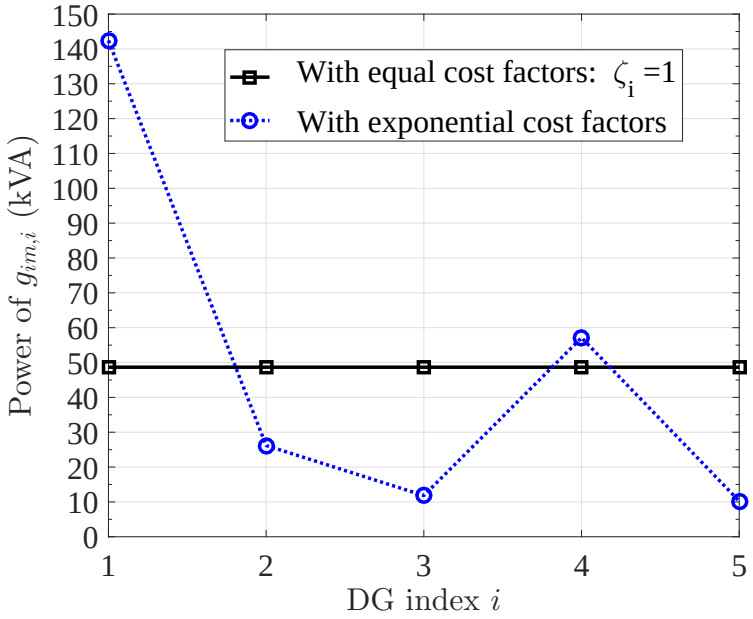

Figure 5.15 The post-fault apparent powers for phase B at different DG systems in Scenario II [3]

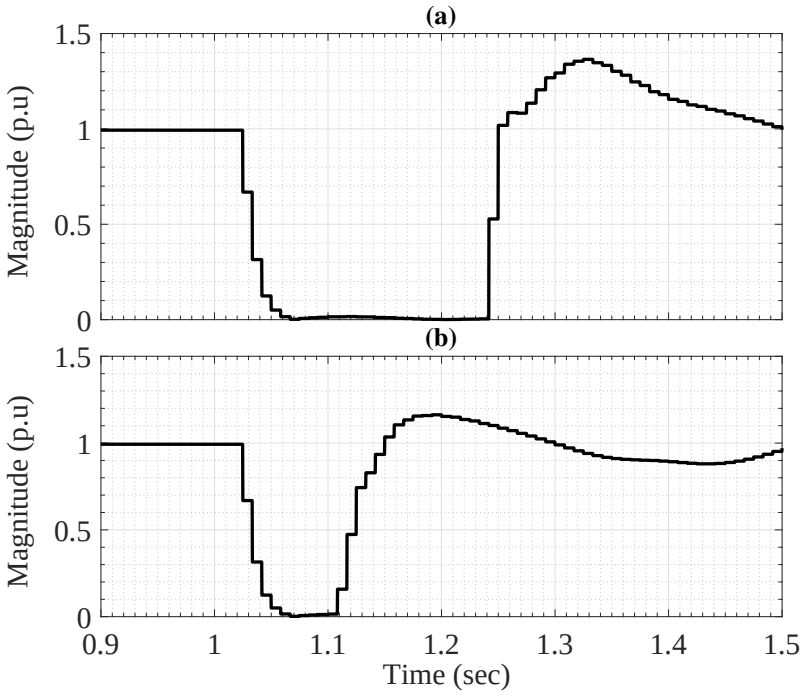

Figure 5.16 The magnitude data reported from phase A of the node b_{10} in Scenario III: (a) Detection by over-current relays with tolerance time $T_{fl} = 200$ msec (b) Centralized detection with tolerance time $T_{fl} = 30$ msec [3]

and the total control delays are calculated based on the response times of the DG systems. The cost factors for control of inverter-based DG systems were less than the cost factor assigned to the machine-based DG system. Fig. 5.16 (b) clearly shows that, in contrast with over-current relays, the central fault detector isolates the fault within a short time. This faster fault isolation allows for better response of DG systems in the islanded subnetwork. However, the magnitude of voltage still shows small-scale distortions which emanate from the machine-based DG system. The aforementioned results corroborate the effectiveness of the developed approach for reliable backup protection and adaptive control of both machine- and inverter-based DG systems.

5.5 Conclusion

The detection of line faults within the permissible fault tolerance time is one of the advanced techniques for adaptive protection and control of smart grids. This chapter develops a new approach for coordinated backup protection and secondary control of DG systems. A low-complexity fault detection algorithm is proposed which identifies faults through processing of synchrophasor datasets and communications with local relays. The proposed fault detector

discriminates islanding events from faults and ensures fault isolation according the post-fault stability requirements. Synchronized with the fault detector, a decision making algorithm finds the post-fault setpoints of real/reactive powers of DG systems in the islanded subnetwork. The response time of relays, the capacity of DG systems, and the communication delays are taken into account in the solving the secondary control problem. The EMTP simulation results confirmed that the coordinated protection and control approach can reliably clear different types of faults within the fault tolerance time. The proposed approach leads to fast voltage/frequency recovery in modern distribution grids. The proposed method can be extended to case of ADNs with responsive loads, i.e., loads equipped with controllers and smart meters. In this context, loads are communicating with different agents so that they can participate in voltage and frequency regulation of the network.

CHAPTER 6 CONCLUSION AND RECOMMENDATIONS

6.1 Thesis Summary

This thesis develops synchrophasor data analytics that leverage event-triggered control and protection applications for smart grids. The thesis paves the way for more intelligent and resilient power systems by elaborating on disturbance/event detection based on processing of synchrophasor datasets. It is mentioned that, advanced control and communication technologies along with renewable energy sources will be incorporated in smart grids. Moreover, synchrophasor technology and its important role in data-centric control and protection schemes are discussed. A data processing framework is introduced which is composed of three building blocks: data acquisition, data analytics, and high-level applications. Data acquisition deals with extraction of signals, information, and behavioral messages from the components of the grid. Different sources of information (e.g., PMUs, IEDs, smart meters, etc.) and different types of data impairments (e.g., noise, delay, and unpredictable loss of data) are discussed. Techniques and algorithms that analyze the acquired data are the analytics which improve control and protection functionalities. Resource management, situational awareness, hierarchical control, and backup protection are among the high-level applications. The main contributions of the thesis which are related to the synchrophasor data analytics are summarized as follows:

1. Reliable disturbance detection:
A new structure for centralized detection of voltage/frequency disturbances in microgrids is developed. In this structure, the MGCC detects subtle deviations of the voltage/frequency in both grid-connected and islanded modes. It is shown that, the MGCC can employ a local PDC (equipped with an interpolative data concentration algorithm) in order to counteract severe noise and data loss in communications links. The overall detection structure deals with noisy and intermittent synchrophasor data, however, it can decrease the average detection time by exploiting the measurement diversity. The reliability of the detection structure is evaluated in terms of the probability of false detection which may occur due to noise. In the low and moderate SNR regions, the performance of the centralized monitoring system is superior when compared with that of local detectors. It is shown that, false detections can be suppressed at the cost of larger average detection time.

2. Monitoring of DG systems:
An adaptive model-based method for monitoring of DG systems detects presence and ab-

sence of DG systems in microgrids/ADNs. By analyzing synchrophasor datasets, the MGCC can estimate the number of operational DG systems and find the location of DG connection/disconnection events. For the main PCC, a least-square parameter estimator extracts the model of the phasors of the CSC (time-series of Gaussian random processes). Based on the extracted model, a monitoring algorithm evaluates the forward prediction error to detect disconnection/connection events. The monitoring algorithm properly updates the detection threshold based on the previously received data. Therefore, the MGCC is able to reliably track the operational number of the microgrid over the time. Random fluctuations of PV sources along with sudden load changes can reduce the efficiency of the DG monitoring. DS units can smooth the fluctuations in solar energy and thus leverage the performance of the DG monitoring. By deploying more PMUs in the network, local synchrophasor datasets are reported to the MGCC. The data outliers that stem from DG events are detectable by means of the LOP method and the local datasets. The location of the DG events is identified by finding the maximum LOP among different local datasets.

3. Coordinated protection and control:
An approach for coordinated backup protection and secondary control of DG systems is developed. A low-complexity fault detection algorithm identifies line faults by processing of synchrophasor datasets and communications with local relays. The fault detector distinguishes between faults and islanding events by simultaneous monitoring of frequency and voltage data. The fault detector in conjunction with the DG monitoring unit ensure that the post-fault stability requirements are met. A decision making algorithm determines the post-fault reference points of real/reactive powers of DG systems in the islanded portion of the network. The response time of protective devices, the capacity of DG systems, and the communication delays are taken into account in the decision making process. This synergy of backup protection and secondary control leads to fast recovery of voltage/frequency in smart distribution grids.

The analytical algorithms and mechanisms presented in this thesis aid researchers and engineers in developing intelligent control and protection systems for smart grids. In particular, secondary and tertiary control of microgrids, adaptive and backup protection, and online resource management are directly empowered by the synchrophasor data analytics. The computer simulation results confirm the effectiveness of the proposed methods for real-life scenarios. Finally, the thesis, given its cross-disciplinary contributions serves as an initial step towards advanced grid technologies.

6.2 List of Publications

The research outcomes of this PhD project are as follows:

1) Younes Seyedi, Houshang Karimi, and Josep M. Guerrero, "Centralized disturbance detection in smart microgrids with noisy and intermittent synchrophasor data," IEEE Transactions on Smart Grid, Early Access, DOI: 10.1109/TSG.2016.2539947

2) Younes Seyedi, Houshang Karimi, and Santiago Grijalva, "Distributed generation monitoring for hierarchical control applications in smart microgrids," IEEE Transactions on Power Systems, vol. 32, no. 3, pp. 2305-2314, May 2017

3) Younes Seyedi, and Houshang Karimi, "Coordinated protection and control based on synchrophasor data processing in smart distribution networks," IEEE Transactions on Power Systems, Early Access, DOI: 10.1109/TPWRS.2017.2708662

4) Reza Pourramezan, Younes Seyedi, Houshang Karimi, Guchuan Zhu, and Michel Mont-Briant, "Design of an Advanced Phasor Data Concentrator for Monitoring of Distributed Energy Resources in Smart Microgrids," IEEE Transactions on Industrial Informatics, Early Access, DOI: 10.1109/TII.2017.2697438

5) Younes Seyedi, and Houshang Karimi, "Design of networked protection systems for smart distribution grids: A data-driven approach," IEEE PES General Meeting, July 2017, Chicago, IL, USA, Accepted

6) Younes Seyedi, Houshang Karimi, and Santiago Grijalva "A new probabilistic approach for localization of distributed generation events in active distribution networks," In preparation

6.3 Future Works

This research opens a window into state-of-the-art topics that can be pursued in future studies. Some of the related topics are suggested and briefly described below:

1. Integrated simulation platform for smart grid:
Conventional power system components can be accurately modeled and analyzed by sophisticated software and real-time simulators. However, incorporation of synchrophasor networks and advanced metering devices into the grid requires integrated simulation methodologies.

An integrated simulation platform can significantly facilitate analysis and testing of intelligent control and protection applications. new simulation approaches should be developed which account for the interactions between power systems components and synchrophasor networks.

2. Networked protection systems:

Hierarchical and backup protection systems essentially operate based on the exchange of signals, data, and protective messages. If these systems rely on shared communication media, then they may suffer from challenges and issues regarding reliability. In particular, loss of data due to communication/device failure and loss of synchronization due to time delays. Networked protection systems should be designed in order to overcome the aforementioned issues. New mechanisms must be developed to ensure robustness of the communication-based protection schemes. Networked protection systems rely on communication systems to improve protection capabilities.

If a dedicated communication medium is employed for control and protection systems, then deterministic QoS can be achieved. However, there are different types of technologies which can be used for networked protection applications such as optical communications, wireless LANs, cellular networks and power line communications. Further studies are still needed for the qualified choice of communication technology. The required QoS and the cost should also be assessed to ensure a high level of performance while minimizing the cost.

3. Data security in smart grid:

Smart grids belong to the broader class of cyber-physical systems where computer-based algorithms are tightly integrated with data networks and physical systems. As discussed in this thesis, analytics, decision making, and event detection are important features of smart power systems. In view of the above facts, data security is of crucial importance for the power grid safety and reliability. For instance, new approaches are necessary for detection of malicious attacks on synchrophasor data streams. These attacks may inject misleading information into synchrophasor networks. Therefore, PMUs and PDCs should employ screening and validation algorithms in order to discard illegitimate data and prevent them from reaching control and protection applications.

REFERENCES

[1] Y. Seyedi, H. Karimi, and J. Guerrero, "Centralized disturbance detection in smart microgrids with noisy and intermittent synchrophasor data," *IEEE Transactions on Smart Grid*, Early Access, DOI: 10.1109/TSG.2016.2539947, 2016.

[2] Y. Seyedi, H. Karimi, and S. Grijalva, "Distributed generation monitoring for hierarchical control applications in smart microgrids," *IEEE Transactions on Power Systems*, vol. 32, no. 3, pp. 2305–2314, May 2017.

[3] Y. Seyedi and H. Karimi, "Coordinated protection and control based on synchrophasor data processing in smart distribution networks," *IEEE Transactions on Power Systems*, Early Access, DOI: 10.1109/TPWRS.2017.2708662 2017.

[4] The North American Electric Reliability Corporation. Nerc president's top priority issues for bulk power system reliability – january 7, 2011. [Online]. Available: http://www.NERC.com

[5] J. Mahseredjian, S. Dennetire, L. Dub, B. Khodabakhchian, and L. Grinlajoie, "On a new approach for the simulation of transients in power systems," *Electric Power Systems Research*, vol. 77, no. 11, pp. 1514–1520, Sep 2007.

[6] MathWorks. Simulink - simulation and model-based design. [Online]. Available: https://www.mathworks.com/

[7] R. Pourramezan, Y. Seyedi, H. Karimi, G. Zhu, and M. Mont-Briant, "Design of an advanced phasor data concentrator for monitoring of distributed energy resources in smart microgrids," *IEEE Transactions on Industrial Informatics*, Early Access, DOI:10.1109/TII.2017.2697438, 2017.

[8] F. Li, W. Qiao, H. Sun, H. Wan, J. Wang, Y. Xia, Z. Xu, and P. Zhang, "Smart transmission grid: Vision and framework," *IEEE Transactions on Smart Grid*, vol. 1, no. 2, pp. 168–177, Sept 2010.

[9] C. H. Lo and N. Ansari, "Decentralized controls and communications for autonomous distribution networks in smart grid," *IEEE Transactions on Smart Grid*, vol. 4, no. 1, pp. 66–77, March 2013.

[10] A. P. S. Meliopoulos, G. Cokkinides, R. Huang, E. Farantatos, S. Choi, Y. Lee, and X. Yu, "Smart grid technologies for autonomous operation and control," *IEEE Transactions on Smart Grid*, vol. 2, no. 1, pp. 1–10, March 2011.

[11] R. A. Gupta and M. Y. Chow, "Networked control system: Overview and research trends," *IEEE Transactions on Industrial Electronics*, vol. 57, no. 7, pp. 2527–2535, July 2010.

[12] J. M. Guerrero, M. Chandorkar, T. L. Lee, and P. C. Loh, "Advanced control architectures for intelligent microgrids - part i: Decentralized and hierarchical control," *IEEE Transactions on Industrial Electronics*, vol. 60, no. 4, pp. 1254–1262, April 2013.

[13] D. E. Olivares, A. Mehrizi-Sani, A. H. Etemadi, C. A. Cañizares, R. Iravani, M. Kazerani, A. H. Hajimiragha, O. Gomis-Bellmunt, M. Saeedifard, R. Palma-Behnke, G. A. Jiménez-Estévez, and N. D. Hatziargyriou, "Trends in microgrid control," *IEEE Transactions on Smart Grid*, vol. 5, no. 4, pp. 1905–1919, 2014.

[14] J. M. Guerrero, J. C. Vasquez, J. Matas, L. G. de Vicuna, and M. Castilla, "Hierarchical control of droop-controlled AC and DC microgrids - A general approach toward standardization," *IEEE Transactions on Industrial Electronics*, vol. 58, no. 1, pp. 158–172, Jan 2011.

[15] X. Lu, J. M. Guerrero, K. Sun, J. C. Vasquez, R. Teodorescu, and L. Huang, "Hierarchical control of parallel ac-dc converter interfaces for hybrid microgrids," *IEEE Transactions on Smart Grid*, vol. 5, no. 2, pp. 683–692, 2014.

[16] Y. A. R. I. Mohamed and A. A. Radwan, "Hierarchical control system for robust microgrid operation and seamless mode transfer in active distribution systems," *IEEE Transactions on Smart Grid*, vol. 2, no. 2, pp. 352–362, 2011.

[17] H. Gharavi and B. Hu, "Scalable synchrophasors communication network design and implementation for real-time distributed generation grid," *IEEE Transactions on Smart Grid*, vol. 6, no. 5, pp. 2539–2550, Sept 2015.

[18] "Use of IEC 61850 to transmit synchrophasor information according to IEEE c37.118," *IEC TR 61850-90-5:2012*, 2012.

[19] A. von Meier, D. Culler, A. McEachern, and R. Arghandeh, "Micro-synchrophasors for distribution systems," in *ISGT 2014*, Feb 2014, pp. 1–5.

[20] B. Pinte, M. Quinlan, and K. Reinhard, "Low voltage micro-phasor measurement unit (μpmu)," in *2015 IEEE Power and Energy Conference at Illinois (PECI)*, Feb 2015, pp. 1–4.

[21] X. Chen, K. J. Tseng, and G. Amaratunga, "State estimation for distribution systems using micro-synchrophasors," in *2015 IEEE PES Asia-Pacific Power and Energy Engineering Conference (APPEEC)*, Nov 2015, pp. 1–5.

[22] Power Sensors Limited. Ultra precise synchro-phasors measurements. [Online]. Available: http://www.powersensorsltd.com

[23] J. D. L. Ree, V. Centeno, J. S. Thorp, and A. G. Phadke, "Synchronized phasor measurement applications in power systems," *IEEE Transactions on Smart Grid*, vol. 1, no. 1, pp. 20–27, June 2010.

[24] "IEEE standard for synchrophasor measurements for power systems," *IEEE Std C37.118.1-2011 (Revision of IEEE Std C37.118-2005)*, pp. 1–61, Dec 2011.

[25] I. Kamwa, A. K. Pradhan, and G. Joos, "Adaptive phasor and frequency-tracking schemes for wide-area protection and control," *IEEE Transactions on Power Delivery*, vol. 26, no. 2, pp. 744–753, April 2011.

[26] P. Romano and M. Paolone, "Enhanced interpolated-DFT for synchrophasor estimation in FPGAs: Theory, implementation, and validation of a PMU prototype," *IEEE Transactions on Instrumentation and Measurement*, vol. 63, no. 12, pp. 2824–2836, Dec 2014.

[27] M. Karimi-Ghartemani, M. Mojiri, A. Safaee, J. A. Walseth, S. A. Khajehoddin, P. Jain, and A. Bakhshai, "A new phase-locked loop system for three-phase applications," *IEEE Transactions on Power Electronics*, vol. 28, no. 3, pp. 1208–1218, March 2013.

[28] M. Karimi-Ghartemani, B. T. Ooi, and A. Bakhshai, "Application of enhanced phase-locked loop system to the computation of synchrophasors," *IEEE Transactions on Power Delivery*, vol. 26, no. 1, pp. 22–32, Jan 2011.

[29] M. Karimi-Ghartemani and H. Karimi, "Processing of symmetrical components in time-domain," *IEEE Transactions on Power Systems*, vol. 22, no. 2, pp. 572–579, May 2007.

[30] I. Kamwa, S. R. Samantaray, and G. Joos, "Compliance analysis of pmu algorithms and devices for wide-area stabilizing control of large power systems," *IEEE Transactions on Power Systems*, vol. 28, no. 2, pp. 1766–1778, May 2013.

[31] C. kong Wong, I. tak Leong, C. san Lei, J. tao Wu, and Y. duo Ham, "A novel algorithm for phasor calculation based on wavelet analysis [power system analysis]," in *2001 Power Engineering Society Summer Meeting. Conference Proceedings (Cat. No.01CH37262)*, vol. 3, July 2001, pp. 1500–1503 vol.3.

[32] P. Banerjee and S. C. Srivastava, "A subspace-based dynamic phasor estimator for synchrophasor application," *IEEE Transactions on Instrumentation and Measurement*, vol. 61, no. 9, pp. 2436–2445, Sept 2012.

[33] J. A. de la O Serna, "Synchrophasor estimation using Prony's method," *IEEE Transactions on Instrumentation and Measurement*, vol. 62, no. 8, pp. 2119–2128, Aug 2013.

[34] "IEEE standard for synchrophasor data transfer for power systems," *IEEE Std C37.118.2-2011 (Revision of IEEE Std C37.118-2005)*, pp. 1–53, Dec 2011.

[35] "IEEE guide for phasor data concentrator requirements for power system protection, control, and monitoring," *IEEE Std C37.244-2013*, pp. 1–65, May 2013.

[36] K. D. Jones, A. Pal, and J. S. Thorp, "Methodology for performing synchrophasor data conditioning and validation," *IEEE Transactions on Power Systems*, vol. 30, no. 3, pp. 1121–1130, May 2015.

[37] W. Zheng, H. Ma, and X. He, "Modeling, analysis, and implementation of real time network controlled parallel multi-inverter systems," in *Proceedings of The 7th International Power Electronics and Motion Control Conference*, vol. 2, June 2012, pp. 1125–1130.

[38] Q. Shafiee, C. Stefanovic, T. Dragicevic, P. Popovski, J. C. Vasquez, and J. M. Guerrero, "Robust networked control scheme for distributed secondary control of islanded microgrids," *IEEE Transactions on Industrial Electronics*, vol. 61, no. 10, pp. 5363–5374, Oct 2014.

[39] A. K. Singh, R. Singh, and B. C. Pal, "Stability analysis of networked control in smart grids," *IEEE Transactions on Smart Grid*, vol. 6, no. 1, pp. 381–390, Jan 2015.

[40] S. Sivaranjani and D. Thukaram, "A networked control systems perspective for wide-area monitoring control of smart power grids," in *2013 IEEE Innovative Smart Grid Technologies-Asia (ISGT Asia)*, Nov 2013, pp. 1–6.

[41] S. Wang, X. Meng, and T. Chen, "Wide-area control of power systems through delayed network communication," *IEEE Transactions on Control Systems Technology*, vol. 20, no. 2, pp. 495–503, March 2012.

[42] N. R. Chaudhuri, D. Chakraborty, and B. Chaudhuri, "An architecture for FACTS controllers to deal with bandwidth-constrained communication," *IEEE Transactions on Power Delivery*, vol. 26, no. 1, pp. 188–196, Jan 2011.

[43] A. A. A. Radwan and Y. A. R. I. Mohamed, "Networked control and power management of AC/DC hybrid microgrids," *IEEE Systems Journal*, pp. 1–12, 2014.

[44] J. Zhang, G. Welch, G. Bishop, and Z. Huang, "A two-stage kalman filter approach for robust and real-time power system state estimation," *IEEE Transactions on Sustainable Energy*, vol. 5, no. 2, pp. 629–636, April 2014.

[45] J. Du, S. Ma, Y. C. Wu, and H. V. Poor, "Distributed hybrid power state estimation under PMU sampling phase errors," *IEEE Transactions on Signal Processing*, vol. 62, no. 16, pp. 4052–4063, Aug 2014.

[46] E. Ghahremani and I. Kamwa, "Local and wide-area PMU-based decentralized dynamic state estimation in multi-machine power systems," *IEEE Transactions on Power Systems*, vol. 31, no. 1, pp. 547–562, Jan 2016.

[47] J. Zhao, G. Zhang, K. Das, G. N. Korres, N. M. Manousakis, A. K. Sinha, and Z. He, "Power system real-time monitoring by using PMU-based robust state estimation method," *IEEE Transactions on Smart Grid*, vol. 7, no. 1, pp. 300–309, Jan 2016.

[48] J. Liu, J. Tang, F. Ponci, A. Monti, C. Muscas, and P. A. Pegoraro, "Trade-offs in PMU deployment for state estimation in active distribution grids," *IEEE Transactions on Smart Grid*, vol. 3, no. 2, pp. 915–924, June 2012.

[49] N. Kashyap, S. Werner, Y. F. Huang, and T. Riihonen, "Power system state estimation under incomplete PMU observability- A reduced-order approach," *IEEE Journal of Selected Topics in Signal Processing*, vol. 8, no. 6, pp. 1051–1062, Dec 2014.

[50] N. H. Abbasy and H. M. Ismail, "A unified approach for the optimal PMU location for power system state estimation," *IEEE Transactions on Power Systems*, vol. 24, no. 2, pp. 806–813, May 2009.

[51] B. Gou and R. G. Kavasseri, "Unified PMU placement for observability and bad data detection in state estimation," *IEEE Transactions on Power Systems*, vol. 29, no. 6, pp. 2573–2580, Nov 2014.

[52] J. Qi, K. Sun, and W. Kang, "Optimal pmu placement for power system dynamic state estimation by using empirical observability gramian," *IEEE Transactions on Power Systems*, vol. 30, no. 4, pp. 2041–2054, July 2015.

[53] S. Dasgupta, M. Paramasivam, U. Vaidya, and V. Ajjarapu, "Real-time monitoring of short-term voltage stability using PMU data," *IEEE Transactions on Power Systems*, vol. 28, no. 4, pp. 3702–3711, Nov 2013.

[54] S. G. Ghiocel, J. H. Chow, G. Stefopoulos, B. Fardanesh, D. Maragal, B. Blanchard, M. Razanousky, and D. B. Bertagnolli, "Phasor-measurement-based state estimation for synchrophasor data quality improvement and power transfer interface monitoring," *IEEE Transactions on Power Systems*, vol. 29, no. 2, pp. 881–888, March 2014.

[55] Y. Wu, M. Musavi, and P. Lerley, "Synchrophasor-based monitoring of critical generator buses for transient stability," *IEEE Transactions on Power Systems*, vol. 31, no. 1, pp. 287–295, Jan 2016.

[56] A. Kaci, I. Kamwa, L. A. Dessaint, and S. Guillon, "Synchrophasor data baselining and mining for online monitoring of dynamic security limits," *IEEE Transactions on Power Systems*, vol. 29, no. 6, pp. 2681–2695, Nov 2014.

[57] A. Shaik and P. Tripathy, "Development of phasor estimation algorithm for P-class PMU suitable in protection applications," *IEEE Transactions on Smart Grid*, DOI:10.1109/TSG.2016.2582342 2016.

[58] C.-S. Chen, C.-W. Liu, and J.-A. Jiang, "A new adaptive PMU based protection scheme for transposed/untransposed parallel transmission lines," *IEEE Transactions on Power Delivery*, vol. 17, no. 2, pp. 395–404, Apr 2002.

[59] N. A. Al-Emadi, A. Ghorbani, and H. Mehrjerdi, "Synchrophasor-based backup distance protection of multi-terminal transmission lines," *IET Generation, Transmission Distribution*, vol. 10, no. 13, pp. 3304–3313, 2016.

[60] S. V. Muddebihalkar and G. N. Jadhav, "Analysis of transmission line current differential protection scheme based on synchronized phasor measurement," in *2015 Conference on Power, Control, Communication and Computational Technologies for Sustainable Growth (PCCCTSG)*, Dec 2015, pp. 21–25.

[61] M. K. Neyestanaki and A. M. Ranjbar, "An adaptive pmu-based wide area backup protection scheme for power transmission lines," *IEEE Transactions on Smart Grid*, vol. 6, no. 3, pp. 1550–1559, May 2015.

[62] M. Biswal, S. M. Brahma, and H. Cao, "Supervisory protection and automated event diagnosis using PMU data," *IEEE Transactions on Power Delivery*, vol. 31, no. 4, pp. 1855–1863, Aug 2016.

[63] J. Zare, F. Aminifar, and M. Sanaye-Pasand, "Synchrophasor-based wide-area backup protection scheme with data requirement analysis," *IEEE Transactions on Power Delivery*, vol. 30, no. 3, pp. 1410–1419, June 2015.

[64] R. Leelaruji and L. Vanfretti, "Utilizing synchrophasor-based protection systems with VSC-HVDC controls to mitigate voltage instability," in *2012 IEEE International Conference on Power System Technology (POWERCON)*, Oct 2012, pp. 1–6.

[65] M. M. Hyder, R. H. Khan, K. Mahata, and J. Y. Khan, "A predictive protection scheme based on adaptive synchrophasor communications," in *2013 IEEE International Conference on Smart Grid Communications (SmartGridComm)*, Oct 2013, pp. 762–767.

[66] S. Sagiroglu, R. Terzi, Y. Canbay, and I. Colak, "Big data issues in smart grid systems," in *2016 IEEE International Conference on Renewable Energy Research and Applications (ICRERA)*, Nov 2016, pp. 1007–1012.

[67] C. S. Lai and L. L. Lai, "Application of big data in smart grid," in *2015 IEEE International Conference on Systems, Man, and Cybernetics*, Oct 2015, pp. 665–670.

[68] H. Jiang, K. Wang, Y. Wang, M. Gao, and Y. Zhang, "Energy big data: A survey," *IEEE Access*, vol. 4, pp. 3844–3861, 2016.

[69] J. Hu and A. V. Vasilakos, "Energy big data analytics and security: Challenges and opportunities," *IEEE Transactions on Smart Grid*, vol. 7, no. 5, pp. 2423–2436, Sept 2016.

[70] X. He, Q. Ai, R. C. Qiu, W. Huang, L. Piao, and H. Liu, "A big data architecture design for smart grids based on random matrix theory," *IEEE Transactions on Smart Grid*, vol. 8, no. 2, pp. 674–686, March 2017.

[71] X. Fang, S. Misra, G. Xue, and D. Yang, "Smart grid - the new and improved power grid: A survey," *IEEE Communications Surveys Tutorials*, vol. 14, no. 4, pp. 944–980, 2012.

[72] H. Mahmood and J. Jiang, "Modeling and control system design of a grid connected vsc considering the effect of the interface transformer type," *IEEE Transactions on Smart Grid*, vol. 3, no. 1, pp. 122–134, 2012.

[73] E. O. Schweitzer, D. Whitehead, G. Zweigle, and K. G. Ravikumar, "Synchrophasor-based power system protection and control applications," in *2010 63rd Annual Conference for Protective Relay Engineers*, March 2010, pp. 1–10.

[74] "IEEE guide for design, operation, and integration of distributed resource island systems with electric power systems," *IEEE Std 1547.4-2011*, pp. 1–54, July 2011.

[75] H. H. Zeineldin, "A q-f droop curve for facilitating islanding detection of inverter-based distributed generation," *IEEE Transactions on Power Electronics*, vol. 24, no. 3, pp. 665–673, March 2009.

[76] H. Laaksonen, "Advanced islanding detection functionality for future electricity distribution networks," *IEEE Transactions on Power Delivery*, vol. 28, no. 4, pp. 2056–2064, Oct 2013.

[77] S. Li and X. Wang, "Monitoring disturbances in smart grids using distributed sequential change detection," in *2013 5th IEEE International Workshop on Computational Advances in Multi-Sensor Adaptive Processing (CAMSAP)*, Dec 2013, pp. 432–435.

[78] M. Sumner, A. Abusorrah, D. Thomas, and P. Zanchetta, "Real time parameter estimation for power quality control and intelligent protection of grid-connected power electronic converters," *IEEE Transactions on Smart Grid*, vol. 5, no. 4, pp. 1602–1607, July 2014.

[79] K. El-Arroudi, G. Joos, I. Kamwa, and D. T. McGillis, "Intelligent-based approach to islanding detection in distributed generation," *IEEE Transactions on Power Delivery*, vol. 22, no. 2, pp. 828–835, April 2007.

[80] H. Karimi, A. Yazdani, and R. Iravani, "Negative-sequence current injection for fast islanding detection of a distributed resource unit," *IEEE Transactions on Power Electronics*, vol. 23, no. 1, pp. 298–307, Jan 2008.

[81] A. V. Oppenheim and R. W. Schafer, *Discrete-time signal processing*, 3rd ed. Prentice Hall, 2009.

[82] A. Papoulis and S. U. Pillai, *Probability, Random Variables, and Stochastic Processes*, 4th ed. McGraw-Hill, 2002.

[83] T. Khalifa, A. Abdrabou, K. Naik, M. Alsabaan, A. Nayak, and N. Goel, "Split- and aggregated-transmission control protocol (sa-tcp) for smart power grid," *IEEE Transactions on Smart Grid*, vol. 5, no. 1, pp. 381–391, Jan 2014.

[84] X. Song, Z. Sahinoglu, and J. Guo, "Transient disturbance detection for power systems with a general likelihood ratio test," in *2013 IEEE International Conference on Acoustics, Speech and Signal Processing*, May 2013, pp. 2839–2843.

[85] J. T. Bialasiewicz, "Renewable energy systems with photovoltaic power generators: Operation and modeling," *IEEE Transactions on Industrial Electronics*, vol. 55, no. 7, pp. 2752–2758, July 2008.

[86] S. M. Ashabani and Y. A. r. I. Mohamed, "New family of microgrid control and management strategies in smart distribution grids - analysis, comparison and testing," *IEEE Transactions on Power Systems*, vol. 29, no. 5, pp. 2257–2269, Sept 2014.

[87] M. Kezunovic, L. Xie, and S. Grijalva, "The role of big data in improving power system operation and protection," in *2013 IREP Symposium Bulk Power System Dynamics and Control - IX Optimization, Security and Control of the Emerging Power Grid*, Aug 2013, pp. 1–9.

[88] J. M. Guerrero, J. C. Vasquez, J. Matas, L. G. de Vicuna, and M. Castilla, "Hierarchical control of droop-controlled ac and dc microgrids - a general approach toward standardization," *IEEE Transactions on Industrial Electronics*, vol. 58, no. 1, pp. 158–172, Jan 2011.

[89] O. Palizban and K. Kauhaniemi, "Secondary control in ac microgrids challenges and solutions," in *2015 International Conference on Smart Cities and Green ICT Systems (SMARTGREENS)*, May 2015, pp. 1–6.

[90] G. Antonova, M. Nardi, A. Scott, and M. Pesin, "Distributed generation and its impact on power grids and microgrids protection," in *2012 65th Annual Conference for Protective Relay Engineers*, April 2012, pp. 152–161.

[91] W. K. A. Najy, H. H. Zeineldin, and W. L. Woon, "Optimal protection coordination for microgrids with grid-connected and islanded capability," *IEEE Transactions on Industrial Electronics*, vol. 60, no. 4, pp. 1668–1677, April 2013.

[92] D. Y. Zheng and Z. Zhou, "Hierarchical protection control system of smart substations," *J. Mod. Power Syst. Clean Energy*, vol. 2, no. 3, pp. 282–288, September 2014.

[93] A. Souza, E. M. Lourenço, and A. S. Costa, "Real-time monitoring of distributed generation through state estimation and geometrically-based tests," in *2010 IREP Symposium Bulk Power System Dynamics and Control - VIII (IREP)*, Aug 2010, pp. 1–8.

[94] Y. Wang, X. Ma, and J. Malcolm, "Enhancing condition monitoring of distributed generation systems through optimal sensor selection," in *IECON 2013 - 39th Annual Conference of the IEEE Industrial Electronics Society*, Nov 2013, pp. 7610–7616.

[95] D. Issicaba, A. S. Costa, and J. L. Colombo, "Real-time monitoring of points of common coupling in distribution systems through state estimation and geometric tests," *IEEE Transactions on Smart Grid*, vol. 7, no. 1, pp. 9–18, Jan 2016.

[96] R. Jingding, C. Yanbo, and Z. Lihua, "Discussion on monitoring scheme of distributed generation and micro-grid system," in *2011 4th International Conference on Power Electronics Systems and Applications*, June 2011, pp. 1–6.

[97] K.-R. Shih and S.-J. Huang, "Application of a robust algorithm for dynamic state estimation of a power system," *IEEE Transactions on Power Systems*, vol. 17, no. 1, pp. 141–147, Feb 2002.

[98] L. Zanni, S. Sarri, M. Pignati, R. Cherkaoui, and M. Paolone, "Probabilistic assessment of the process-noise covariance matrix of discrete kalman filter state estimation of active distribution networks," in *2014 International Conference on Probabilistic Methods Applied to Power Systems (PMAPS)*, July 2014, pp. 1–6.

[99] G. C. Paap, "Symmetrical components in the time domain and their application to power network calculations," *IEEE Transactions on Power Systems*, vol. 15, no. 2, pp. 522–528, May 2000.

[100] M. He and J. Zhang, "A dependency graph approach for fault detection and localization towards secure smart grid," *IEEE Transactions on Smart Grid*, vol. 2, no. 2, pp. 342–351, June 2011.

[101] G. Valverde, A. T. Saric, and V. Terzija, "Stochastic monitoring of distribution networks including correlated input variables," *IEEE Transactions on Power Systems*, vol. 28, no. 1, pp. 246–255, Feb 2013.

[102] R. Singh, B. C. Pal, and R. A. Jabr, "Statistical representation of distribution system loads using gaussian mixture model," *IEEE Transactions on Power Systems*, vol. 25, no. 1, pp. 29–37, Feb 2010.

[103] A. Bracale, P. Caramia, G. Carpinelli, A. R. D. Fazio, and P. Varilone, "A bayesian-based approach for a short-term steady-state forecast of a smart grid," *IEEE Transactions on Smart Grid*, vol. 4, no. 4, pp. 1760–1771, Dec 2013.

[104] E. J. Palacios-García, Y. Guan, M. Savaghebi, J. C. Vásquez, J. M. Guerrero, A. Moreno-Munoz, and B. S. Ipsen, "Smart metering system for microgrids," in *IECON 2015 - 41st Annual Conference of the IEEE Industrial Electronics Society*, Nov 2015, pp. 289–294.

[105] M. B. D. C. Filho, J. C. S. de Souza, and M. A. R. Guimaraens, "Enhanced bad data processing by phasor-aided state estimation," *IEEE Transactions on Power Systems*, vol. 29, no. 5, pp. 2200–2209, Sept 2014.

[106] M. M. Breunig, H. P. Kriegel, R. T. Ng, and J. Sander, "LOF: identifying density-based local outliers," in *ACM Sigmod Record*, May 2000, pp. 93–104.

[107] H. P. Kriegel, P. Kroger, E. Schubert, and A. Zimek, "LoOP: local outlier probabilities," in *18th ACM Conference on Information and Knowledge Management*, Nov 2009, pp. 1649–1652.

[108] W. H. Kersting, "Radial distribution test feeders," *IEEE Transactions on Power Systems*, vol. 6, no. 3, pp. 975–985, Aug 1991.

[109] NREL. Solar power data for integration studies datasets. [Online]. Available: http://www.nrel.gov/

[110] M. J. E. Alam, K. M. Muttaqi, and D. Sutanto, "Mitigation of rooftop solar pv impacts and evening peak support by managing available capacity of distributed energy storage systems," *IEEE Transactions on Power Systems*, vol. 28, no. 4, pp. 3874–3884, Nov 2013.

[111] X. Su, M. A. S. Masoum, and P. J. Wolfs, "Multi-objective hierarchical control of unbalanced distribution networks to accommodate more renewable connections in the smart grid era," *IEEE Transactions on Power Systems*, vol. 31, no. 5, pp. 3924–3936, Sept 2016.

[112] J. C. Kim, S. M. Cho, and H. S. Shin, "Advanced power distribution system configuration for smart grid," *IEEE Transactions on Smart Grid*, vol. 4, no. 1, pp. 353–358, March 2013.

[113] L. Jin, R. Kumar, and N. Elia, "Model predictive control-based real-time power system protection schemes," *IEEE Transactions on Power Systems*, vol. 25, no. 2, pp. 988–998, May 2010.

[114] J. A. P. Lopes, C. L. Moreira, and A. G. Madureira, "Defining control strategies for microgrids islanded operation," *IEEE Transactions on Power Systems*, vol. 21, no. 2, pp. 916–924, May 2006.

[115] J. Rocabert, A. Luna, F. Blaabjerg, and P. Rodríguez, "Control of power converters in ac microgrids," *IEEE Transactions on Power Electronics*, vol. 27, no. 11, pp. 4734–4749, Nov 2012.

[116] E. O. Schweitzer, D. Finney, and M. V. Mynam, "Applying radio communication in distribution generation teleprotection schemes," in *2012 65th Annual Conference for Protective Relay Engineers*, April 2012, pp. 310–320.

[117] I. P. Nikolakakos, H. H. Zeineldin, M. S. El-Moursi, and N. D. Hatziargyriou, "Stability evaluation of interconnected multi-inverter microgrids through critical clusters," *IEEE Transactions on Power Systems*, vol. 31, no. 4, pp. 3060–3072, July 2016.

[118] Y. S. Kim, E. S. Kim, and S. I. Moon, "Frequency and voltage control strategy of standalone microgrids with high penetration of intermittent renewable generation systems," *IEEE Transactions on Power Systems*, vol. 31, no. 1, pp. 718–728, Jan 2016.

[119] S. Brahma, "Advancements in centralized protection and control within a substation," *IEEE Transactions on Power Delivery*, vol. 31, no. 4, pp. 1945–1952, Aug 2016.

[120] H. M. Zeineldin, H. H. Sharaf, and E. El-Saadany, "Protection coordination for microgrids with grid-connected and islanded capabilities using dual setting directional overcurrent relays," *IEEE Transactions on Smart Grid*, 2016.

[121] L. Che, X. Zhang, and M. Shahidehpour, "Communication-assisted hierarchical protection strategy for high-reliability microgrids," in *2015 IEEE Power Energy Society General Meeting*, July 2015, pp. 1–5.

[122] S. Turner, "High-speed communication-assisted tripping and sectionalizing for distribution systems," in *2012 65th Annual Conference for Protective Relay Engineers*, April 2012, pp. 129–136.

[123] V. C. Nikolaidis, E. Papanikolaou, and A. S. Safigianni, "A communication-assisted overcurrent protection scheme for radial distribution systems with distributed generation," *IEEE Transactions on Smart Grid*, vol. 7, no. 1, pp. 114–123, Jan 2016.

[124] T. S. Ustun, C. Ozansoy, and A. Zayegh, "Modeling of a centralized microgrid protection system and distributed energy resources according to IEC 61850-7-420," *IEEE Transactions on Power Systems*, vol. 27, no. 3, pp. 1560–1567, Aug 2012.

[125] A. H. K. Alaboudy, H. H. Zeineldin, and J. Kirtley, "Microgrid stability characterization subsequent to fault-triggered islanding incidents," *IEEE Transactions on Power Delivery*, vol. 27, no. 2, pp. 658–669, April 2012.

[126] P. Gopakumar, M. J. B. Reddy, and D. K. Mohanta, "Transmission line fault detection and localisation methodology using pmu measurements," *IET Generation, Transmission Distribution*, vol. 9, no. 11, pp. 1033–1042, 2015.

[127] C. Ahumada, R. Cárdenas, D. Sáez, and J. M. Guerrero, "Secondary control strategies for frequency restoration in islanded microgrids with consideration of communication delays," *IEEE Transactions on Smart Grid*, vol. 7, no. 3, pp. 1430–1441, May 2016.

[128] A. Apostolov and B. Vandiver, "Iec 61850 goose applications to distribution protection schemes," in *2011 64th Annual Conference for Protective Relay Engineers*, April 2011, pp. 178–184.

[129] M. S. Almas and L. Vanfretti, "A hybrid synchrophasor and goose-based power system synchronization scheme," *IEEE Access*, vol. 4, pp. 4659–4668, 2016.

[130] J. Nocedal and S. Wright, *Numerical optimization*. Springer Verlag, 2006.

[131] S. Sonmez, S. Ayasun, and C. O. Nwankpa, "An exact method for computing delay margin for stability of load frequency control systems with constant communication delays," *IEEE Transactions on Power Systems*, vol. 31, no. 1, pp. 370–377, Jan 2016.

[132] J. Tang, J. Liu, F. Ponci, and A. Monti, "Adaptive load shedding based on combined frequency and voltage stability assessment using synchrophasor measurements," *IEEE Transactions on Power Systems*, vol. 28, no. 2, pp. 2035–2047, May 2013.

[133] G. Benmouyal, M. Meisinger, J. Burnworth, W. A. Elmore, K. Freirich, P. A. Kotos, P. R. Leblanc, P. J. Lerley, J. E. McConnell, J. Mizener, J. P. de Sa, R. Ramaswami, M. S. Sachdev, W. M. Strang, J. E. Waldron, S. Watansiriroch, and S. E. Zocholl, "IEEE standard inverse-time characteristic equations for overcurrent relays," *IEEE Transactions on Power Delivery*, vol. 14, no. 3, pp. 868–872, Jul 1999.